HYPHENATION OF ANALYTICAL TECHNIQUES TO SINGLE CELL CAPILLARY ELECTROPHORESIS-MASS SPECTROMETRY

BY

MARINA CATHERINE PHILIP

DISSERTATION

Submitted in partial fulfillment of the requirements
for the degree of Doctor of Philosophy in Chemistry
in the Graduate College of the
University of Illinois at Urbana-Champaign, 2020

Urbana, Illinois

Doctoral Committee:

Professor Jonathan V. Sweedler, Chair
Professor Andrew A. Gewirth
Assistant Professor Hee-Sun Han
Professor Peter M. Yau

ABSTRACT

Single cell chemical analysis pushes the limits of analytical measurements. Small volumes, large dynamic range, and chemical complexity all contribute to the analytical challenge of investigating single cell biology. To comprehensively study single cell chemistry, technologies require low limits of detection, accurate quantitation, confident identity assignment, and ability to process complex chemical mixtures. Heterogeneity in nucleic acids, proteins, peptides, metabolites, lipids, and more result in functionally significant differences between cells within the same tissue. Mass spectrometry (MS) has emerged as an effective tool for single cell chemical analysis because of its versatility, sensitivity, and ability to distinguish analytes in complex samples. Different MS approaches have various advantages and disadvantages for chemical analysis; for instance, matrix-assisted laser desorption ionization (MALDI)-MS enables rapid analysis but suffers in quantitation, whereas capillary electrophoresis–electrospray ionization (CE–ESI)-MS has low limits of detection and quantitative capabilities, but is comparatively low-throughput. Additionally, each method tends to be better suited for different chemical classes. Improvements in technology are constantly evolving to address the limitations of individual MS analyses, yet they tend to be limited in at least one dimension.

This thesis describes a strategy to bridge the gap between the advantages and disadvantages of orthogonal analytical techniques by performing multiple measurements on the same single cell. By taking advantage of material left behind after a sample isolation or analysis, we can expand chemical coverage of single cell analysis, confidently classify cell types, and correlate different chemical classes within the same cell. Our approach uses a liquid microjunction (LMJ) extraction probe which extracts chemical content from a single cell off a microscope slide. We describe the assembly, operation, and validation of the LMJ probe as a strategy for performing optically guided

single cell MALDI-MS profiling followed by CE–ESI-MS metabolite profiling. The first demonstrated application of the device is the analysis of single cells from rat pancreatic islets of Langerhans, which perform the canonical glucose-regulating function of the pancreas. Each cell type within islets of Langerhans are defined by the peptide hormone complement contained therein (*e.g.* α cells contain glucagon, β cells contain insulin), and cells can be rapidly profiled and classified by their peptide content with MALDI-MS. By screening cells prior to extraction, we can specifically target only the cells of interest for lower-throughput CE–ESI-MS analysis. After MALDI-MS profiling, we use the LMJ probe to extract metabolites directly from the microscope slide for follow-up CE–ESI-MS metabolite profiling.

After validating the LMJ probe, we further apply the technology to different chemical measurements and biological systems. First, we describe application of the probe to CE–ESI-MS metabolite profiling of single rat cerebral neurons and astrocytes. The gold standard in biological differentiation and classification of neurons and astrocytes is immunocytochemistry (ICC), where cells must be fixed and crosslinked for antibody incubation, which precludes follow-up MS analysis. To circumvent this limitation, we extract metabolite content from the cell with the LMJ probe prior to ICC. The neuron and astrocyte markers we selected are a transmembrane protein and structural protein, respectively, which remain adhered to the microscope slide after extraction. Thus, we can profile cells with CE–ESI-MS and later classify them as neurons or astrocytes after ICC to correlate chemical content with cell type.

Second, we applied LMJ extraction to RNA, which has potential applications in both MS and transcriptomics, a powerful tool for gene extrusion profiling. We designed a biphasic extraction addition to the LMJ probe to enable RNA extraction from buccal ganglia from *Aplysia californica* with simultaneous delivery of an aqueous and organic phase. The biphasic extraction

reduces the number of preprocessing steps, preventing sample loss, and successfully extracts suitable amounts of RNA for MS analysis.

Finally, we applied field-amplified sample injection (FASI) to our CE–ESI-MS system to improve limits of detection by 100-fold for single cell analysis. FASI is typically of limited use in MS applications because it favors the injection of ionic salts into the capillary, which causes ion suppression at the electrospray interface. We addressed this by incorporating a desalting step into the sample preparation, which preserved metabolite material while precipitating interfering salts. We expect this addition to our CE–ESI-MS toolkit to enable greater metabolite detection and identifications in our single cell analyses.

ACKNOWLEDGEMENTS

I have many to thank for supporting me over the past five years. First, I must thank Prof. Jonathan Sweedler for the opportunity to work in his lab and granting me the freedom to develop as a scientist. Under his leadership, I was able to work on projects I cared about and follow my passions, for which I am grateful. I would also like to thank my committee, Prof. Andrew Gewirth, Prof. Hee-Sun Han, and Prof. Peter Yau for their support and guidance. I am also grateful to many members of the Sweedler group for their collaboration, mentorship, and companionship during my time here. I was fortunate enough to work closely with Dr. Troy Comi, Dr. Hsiao-Wei Liao, Dr. Elizabeth Neumann, Dr. Joanna Ellis, Dr. Kevin Clark, Shannon Murphy, Zoe Tian, Carolyn Oh, and Cindy Lee. Thank you for lending me your ear, your advice, and your help. Elizabeth and Jo, you are some of the best scientists and bravest women I know. I couldn't have asked better friends to go through this with, and I'm so proud of us for making it across the finish line.

I am incredibly grateful for the support of my fellow chemistry graduate students at UIUC. Thank you to everyone I worked with as part of the Women Chemists Committee, Bonding with Chemistry Girls' Day Camp, Encouraging Tomorrow's Chemists, Joint Safety Team, and Student Wellness Coalition. A big shout-out to my friends and colleagues in Analytical Chemistry and the ground floor of Roger Adams Lab.

I would not have made it through graduate school without the many advocacy and mental health resources I sought out during my time here. I am thankful for the UIUC Counseling Center, Molly McLay (formerly of the Women's Resources Center), Jolie Carsten, Dr. Kimberly Glow, and Dr. Claire Hauser. Through my experience here, I have learned that often the difference between a student who leaves with a PhD and one who does not is less about their ability as a scientist and more about their environment and how they are treated. Thank you to Dr. Lloyd

Munjanja and the students fighting tirelessly to make the scientific community welcoming, supportive, and equitable for all.

I dedicate many of my successes to my earliest science teachers, who inspired me to learn chemistry and challenged me to push my limits as a scientist. My greatest thanks go to Dr. Steven Emory and Dr. John Antos, who mentored me and gave me the freedom to learn and make mistakes.

Finally, I want to thank the greatest family and friends on earth, who cheered me on and cared for me from 2,000 miles away: Mom, Dad, Lydia, Archer, Auresa, Caitlin, Eliza, and Noah. I love you all so much.

For Jeff, Nancy, Lydia, and Archer Philip
The absolute best family, no contest

TABLE OF CONTENTS

CHAPTER 1: INTRODUCTION

When exploring the complex chemistry behind the biological systems within and surrounding us, detail in every dimension provides greater understanding of life, from behavior to elements. Chemical investigation of biology reveals the fundamental principles behind behaviors and events and provides us with the tools to address diseases and other problems in our constantly changing world. The chemical questions we ask evolve as we expand our knowledge of biological function and as we improve our ability to measure and analyze complex chemistries. With greater ability to probe individual cells within organs or tissues, great interest has been in investigating the roles that single cells play in biological function. A major avenue of inquiry has been in cellular heterogeneity, or the differences between single cells within a system.[1] Heterogeneity defines function in many biological systems, from organs like the brain[2] to organism development[3] to disease.[4] Studying organisms and tissues on the single cell level has become increasingly crucial to understanding the function of complex biological systems. The work presented here details new strategies for chemical analysis of single cells and for expanding the chemical information we can obtain from a single cell.

Single cell biology presents an exciting challenge for analytical chemists, and the challenges of single cell analysis encapsulates many of the ongoing innovations in measurement science. The most obvious of these challenges is a matter of scale: the concentrations of analytes within a single cell can be vanishingly small, and within a volume of mere picoliters the prospect of detecting the rarest molecules in a single cell is daunting. The field of analytical chemistry has approached this challenge with rigor – there is an increasing number of techniques that can detect as few as single molecules,[5] and low limits of detection using commercial instruments is well within reach for non-experts.[6]

That said, the limit of detection for a given technique is an insufficient metric for analytical performance when it comes to single cells due to their small volume. As our ability to detect fewer molecules improves, the question arises: what conditions are required to make the measurement? In the case of single cell analysis, an analytical method loses its utility if the volume required for analysis is relatively high compared to the volume of a cell. Dilution is a major factor concerning single cell analysis, and an ideal technique would not significantly dilute a single cell, especially beyond the detection limitations of the method. As an example, the average concentration of the amino acid serine in an R2 neuron of *Aplysia californica* is 2.1 mM,[7] which, based on the 14 pL volume of the cell, amounts to approximately 30 pmol of serine. While concentrations on the order of millimolar seems relatively high, diluting the volume to only 10 µL would decrease the concentration of the serine to 670 nM. With such small amounts of material many techniques would only be capable of measuring the most abundant metabolites on the order of mM, leaving out important analytes well below the limit of detection.

So, for single cell chemical measurements, we seek techniques that have low limits of detection and require little sample dilution. Limiting sample dilution includes not only limiting the minimum amount of sample volume or material required, but also reducing the amount of sample preprocessing, where multiple rinsing steps, for example, will inherently result in sample loss. Any sample loss when working with such small amounts of material can have a significant effect on what is detected, identified, and measured in an experiment.

For decades, single cell analysis was mostly limited to spectral and optical analytical techniques, including microscopy and immunocytochemistry. The development of laser technology in particular was ideal for single cell analysis as laser footprints are well below the size of typical cells, thus making fluorescence microscopy an obvious choice for exploring cell

morphology and chemistry. For the most part, however, such optical techniques are limited to the chemical study of proteins and other large molecular structures for which antibodies and other labels can be obtained.

The study of one chemical class with one method is insufficient considering the vast chemical and function complexity contained within a single cell. Besides the varied molecular classes (proteins, lipids, nucleic acids, and metabolites), their concentrations vary widely and can fluctuate rapidly over time in functionally significant ways. Fortunately, in the recent past our ability to chemically probe a single cell has expanded enormously – major advancements of single cell chemical measurements range from mass spectrometry (MS),[8,9] to chromatography and electrophoresis,[10] to nuclear magnetic resonance,[11,12] and more.

The Sweedler Lab has pioneered many mass spectrometry- and separation-based techniques suited for single cell chemical measurements. The technology and methodologies developed in our lab have enabled single cell analysis of many cell types and molecular classes,[13–15] while also improving figures of merit (such as throughput[16] and mass resolution[15]) for a greater understanding of individual aspects of single cell chemistries. There remains, however, a gap in our ability to probe single cell biology: gaining multiple dimensions of chemical information from one single cell. For most analytical techniques, the processing of samples, the conditions of the experiment, and the instruments themselves are often optimized for *one* chemical class, such as peptides, lipids, or metabolites. Should we wish to understand the interplay between, for instance, metabolites and proteins, we would require double the number of cells for analysis, which becomes problematic when the cell in question is rare or difficult to identify. This thesis details versatile methods for analyzing the same cell with multiple analytical techniques, which greatly increases our ability to understand the specific chemistry of single cells.

Chapter 2 provides a fundamental overview of the analytical measurement techniques and instrumentation used in the presented work. A basic knowledge of the varying approaches to separations, mass spectrometry, and chemical analysis of biological samples is required to understand the rationale behind hyphenating these different measurements and to justify the selection of these techniques. Specifically, we discuss two mass spectrometry approaches for chemical analysis of biological samples: electrospray ionization (ESI) MS and matrix-assisted laser desorption/ionization (MALDI) MS. These two complementary techniques are well-suited for biological studies and have both been established as indispensable for single cell analysis. We also discuss our approach to targeting single cells on a surface for analysis, using a lab-build software that uses optical microscopy and point-based registration to determine cell locations on a microscope slide for analysis. Finally, we give an overview of capillary electrophoresis and capillary electrophoresis (CE)–ESI-MS, which further expands the utility of ESI by incorporating a chemical separation. CE is advantageous for single cell analysis specifically for its low volume requirements, thus limiting sample dilution. Each technique discussed provides a large amount of chemical information; and combining them will aid deeper exploration into single cell chemistry and function.

Chapter 3 details the importance and scientific progress of analyzing single cells in neurobiology. The brain and neurological systems are perhaps the most obvious target for single cell analyses as neurological function is closely tied to the synaptic connections between single cells, where the morphology and function of individual, and sometimes irreplaceable, cells are intimately tied to nervous system function in organisms. The chapter focuses on metabolites, the measurement of which poses an interesting and complex analytical challenge due to their small masses, chemical diversity, and temporal variability. The work presented in this thesis is weighed

heavily toward metabolomics and studying the metabolic profiles of single cells. Most presented studies in this thesis use CE–ESI-MS for metabolic profiling, which is particularly suited for analysis of small molecules from small-volume samples. Metabolites most closely reflect the phenotypic state of a cell at any given timepoint, which makes it crucial for a complete understanding of cellular function. In neuroscience and the study of cellular communication, small molecule analysis enables detailed study of the presence and release of many neurotransmitters. Because CE–ESI-MS is a solution-based technique (which inevitably involves some sample dilution and usually requires a large volume for analysis compared to the cell volume), hyphenating this type of metabolic analysis with other chemical measurements is particularly difficult, but would be useful if paired with an orthogonal technique. The context of the state of single cell analysis and of small molecule metabolites is crucial for understanding the full potential of hyphenating such measurements.

The central hyphenation approach of this work is a liquid microjunction (LMJ) extraction probe described in Chapter 4. The LMJ probe is designed to hyphenate orthogonal measurements for increased chemical coverage in single cell analyses. Importantly, the probe also enables cell type identification prior to chemical profiling, which expands the pool of available models for single cell investigations. Briefly, the probe comprises two concentric capillaries assembled within a PEEK mount. An extraction solution is pumped via syringe through the outer capillary and is then aspirated via vacuum through the inset inner capillary. A meniscus of extraction liquid forms at the probe tip, which extracts relevant analytes when placed in contact with a sample. The solution is then collected in a custom sample collection chamber. The probe enables extraction of chemical content directly from a microscope slide. The first demonstration of this device's capabilities, as described in Chapter 4, is to perform optically-guided MALDI-MS on single cells

from dissociated rat islets of Langerhans prior to extraction of small molecule metabolites and follow-up CE–ESI-MS.

The LMJ extraction probe is suited for a variety of analytical hyphenations. We demonstrate two methods for applications in two additional model systems in Chapters 5 and 6. In Chapter 5, we demonstrate hyphenation of CE–ESI-MS and immunocytochemistry (ICC) for metabolite profiling and cell type classification of astrocytes and neurons in rat cerebral tissue. Immunostaining is a gold-standard technique for classifying and identifying cell types. Antibody targets are capable of distinguishing cells in functionally significant dimensions and exploring the chemical profiles of these differing cells is of great interest. Unfortunately, conventional ICC procedures require cell fixation, which crosslinks proteins, peptides, and other molecules, precluding follow-up MS analysis. Former members of our group have successfully performed MALDI-MS and ICC on the same single cells; here we describe a procedure to incorporate CE–ESI-MS and ICC in the same experiment. We use the LMJ probe to extract metabolite content from dispersed single cells, which leaves behind the lipid membrane and other structural features. By selecting cell markers that are either transmembrane or structural proteins, we can perform ICC after extraction. We then correlate cell types, specifically rat cerebral astrocytes and neurons, to their metabolite profiles.

We also demonstrate the LMJ probe for extraction of RNA from *A. californica* buccal ganglia. RNA extraction with the LMJ probe expands the potential applications to transcriptomics and MS analysis of nucleic acids, but it requires different extraction conditions than for small molecule metabolites. To replicate the conventional liquid-liquid RNA extraction procedure for LMJ extraction, we developed an addition to the probe which enables biphasic extraction with an aqueous and organic phase. We applied this extraction procedure to liquid chromatography-MS

analysis of endogenous RNA modifications in buccal ganglia of *A. californica*, and demonstrated not only successful extraction of RNA, but an increased number of identified modified nucleosides using the LMJ extraction procedure compared to conventional extraction.

Chapter 7 describes an addition to our CE–ESI-MS toolkit for sensitive analysis of small molecules in single cells. CE–ESI-MS is well suited to single-cell assays because of its low sample-volume requirements and low detection limits. After sample preparation the typical volume of the lysed cell sample is on the order of a microliter; however, only nanoliters are injected into the CE system, with the volume mismatch limiting analytical performance. We developed an approach for the detection of intracellular metabolites from a single neuron using field amplified sample injection (FASI) CE–ESI-MS. Through the application of FASI, we achieved 100- to 300-fold detection limit enhancement compared to hydrodynamic injections. We also applied FASI CE–ESI-MS to the untargeted profiling of metabolites of *A. californica* pleural sensory neurons with <50 μm diameter cell somata. Our method will enable more sensitive profiling using CE–ESI-MS for certain applications.

The approaches described in this thesis will be of great value as the field of single cell chemical analysis moves toward multi-modal analysis of single cell samples. This work presents one strategy for incorporating solution-based measurements into these multi-modal approaches. Exploration of chemical heterogeneity will benefit from an increased amount of chemical information, especially when correlating profiles of different chemical classes. Hyphenated approaches like the ones presented here are a window into the future of single cell chemical analysis.

1.1 REFERENCES

(1) Altschuler, S. J.; Wu, L. F. Cellular Heterogeneity: Do Differences Make a Difference? *Cell* **2010**, *141* (4), 559–563. https://doi.org/10.1016/j.cell.2010.04.033.

(2) Nemes, P.; Rubakhin, S. S.; Aerts, J. T.; Sweedler, J. V. Qualitative and Quantitative Metabolomic Investigation of Single Neurons by Capillary Electrophoresis Electrospray Ionization Mass Spectrometry. *Nat. Protocols* **2013**, *8* (4), 783–799. https://doi.org/10.1038/nprot.2013.035.

(3) Onjiko, R. M.; Moody, S. A.; Nemes, P. Single-Cell Mass Spectrometry Reveals Small Molecules That Affect Cell Fates in the 16-Cell Embryo. *PNAS* **2015**, *112* (21), 6545–6550. https://doi.org/10.1073/pnas.1423682112.

(4) Patel, A. P.; Tirosh, I.; Trombetta, J. J.; Shalek, A. K.; Gillespie, S. M.; Wakimoto, H.; Cahill, D. P.; Nahed, B. V.; Curry, W. T.; Martuza, R. L.; Louis, D. N.; Rozenblatt-Rosen, O.; Suvà, M. L.; Regev, A.; Bernstein, B. E. Single-Cell RNA-Seq Highlights Intratumoral Heterogeneity in Primary Glioblastoma. *Science* **2014**, *344* (6190), 1396–1401. https://doi.org/10.1126/science.1254257.

(5) Kaneta, T. Laser-Induced Fluorometry for Capillary Electrophoresis. *The Chemical Record* **2019**, *19* (2–3), 452–461. https://doi.org/10.1002/tcr.201800051.

(6) Grebe, S. K.; Singh, R. J. LC-MS/MS in the Clinical Laboratory – Where to From Here? *Clin Biochem Rev* **2011**, *32* (1), 5–31.

(7) Nemes, P.; Knolhoff, A. M.; Rubakhin, S. S.; Sweedler, J. V. Metabolic Differentiation of Neuronal Phenotypes by Single-Cell Capillary Electrophoresis–Electrospray Ionization-Mass Spectrometry. *Anal. Chem.* **2011**, *83* (17), 6810–6817. https://doi.org/10.1021/ac2015855.

(8) Comi, T. J.; Do, T. D.; Rubakhin, S. S.; Sweedler, J. V. Categorizing Cells on the Basis of Their Chemical Profiles: Progress in Single-Cell Mass Spectrometry. *J. Am. Chem. Soc.* **2017**, *139* (11), 3920–3929. https://doi.org/10.1021/jacs.6b12822.

(9) Qi, M.; Philip, M. C.; Yang, N.; Sweedler, J. V. Single Cell Neurometabolomics. *ACS Chem. Neurosci.* **2017**. https://doi.org/10.1021/acschemneuro.7b00304.

(10) Lin, Y.; Trouillon, R.; Safina, G.; Ewing, A. G. Chemical Analysis of Single Cells. *Anal. Chem.* **2011**, *83* (12), 4369–4392. https://doi.org/10.1021/ac2009838.

(11) Rubakhin, S. S.; Lanni, E. J.; Sweedler, J. V. Progress toward Single Cell Metabolomics. *Current Opinion in Biotechnology* **2013**, *24* (1), 95–104. https://doi.org/10.1016/j.copbio.2012.10.021.

(12) Webb, A. Increasing the Sensitivity of Magnetic Resonance Spectroscopy and Imaging. *Anal. Chem.* **2012**, *84* (1), 9–16. https://doi.org/10.1021/ac201500v.

(13) Romanova, E. V.; Sweedler, J. V. Peptidomics for the Discovery and Characterization of Neuropeptides and Hormones. *Trends in Pharmacological Sciences* **2015**, *36* (9), 579–586. https://doi.org/10.1016/j.tips.2015.05.009.

(14) Rubakhin, S. S.; Romanova, E. V.; Nemes, P.; Sweedler, J. V. Profiling Metabolites and Peptides in Single Cells. *Nat Meth* **2011**, *8* (4s), S20–S29. https://doi.org/10.1038/nmeth.1549.

(15) Neumann, E. K.; Ellis, J. F.; Triplett, A. E.; Rubakhin, S. S.; Sweedler, J. V. Lipid Analysis of 30 000 Individual Rodent Cerebellar Cells Using High-Resolution Mass Spectrometry. *Anal. Chem.* **2019**, *91* (12), 7871–7878. https://doi.org/10.1021/acs.analchem.9b01689.

(16) Comi, T. J.; Neumann, E. K.; Do, T. D.; Sweedler, J. V. MicroMS: A Python Platform for Image-Guided Mass Spectrometry Profiling. *J. Am. Soc. Mass Spectrom.* **2017**, *28* (9), 1919–1928. https://doi.org/10.1007/s13361-017-1704-1.

CHAPTER 2: MASS SPECTROMETRY TECHNIQUES FOR SINGLE CELL ANALYSIS

2.1 MASS SPECTROMETRY (MS)

Mass spectrometry measures the mass-to-charge ratio (*m/z*) of gas-phase ions. The variety of instrumentation, hyphenation, and sample preparation compatible with MS makes it a versatile strategy for chemical analysis. MS is often referred to as a "molecular scale" because it measures the mass of ions, either molecules or elements. Mass measurements are immensely useful for molecular identification and structure elucidation.[1–3] Importantly, MS distinguishes sample components based on their *m/z* and thus can analyze the chemical content of complex samples in a single experiment. This makes it an ideal tool for profiling the chemical content of biological samples, where many molecules can be measured simultaneously. The exception to this is in the case of isomeric compounds, which will not be separated or distinguished because they have an identical *m/z*. Though MS is useful for many applications, its inability to distinguish isomers is one significant limitation of the technique. Much research in the field is devoted to overcoming this limitation, including tandem MS and hyphenated separations.[4,5]

The basic anatomy of a mass spectrometer comprises three main components, where many variations of each component exist for varying applications: an ion source, a mass analyzer, and a detector (Figure 2.1).[6] The ion source (often referred to only as the source) ionizes molecules in the sample; molecular species must be charged to be guided through the instrument via electronic optics and for effective operation of both the mass analyzer and detector. The source often simultaneously transfers a solid or liquid sample into the gas phase. Mass spectrometers can analyze either positively or negatively charged ions; switching modes is mostly a matter of changing the applied voltages within the instrument, though there are other considerations that are

described elsewhere.[7,8] Most of the presented work concerns positively charged ions, and thus the instruments are operated in positive mode. Detailed description of two ionization methods relevant to this work are described later in this chapter.

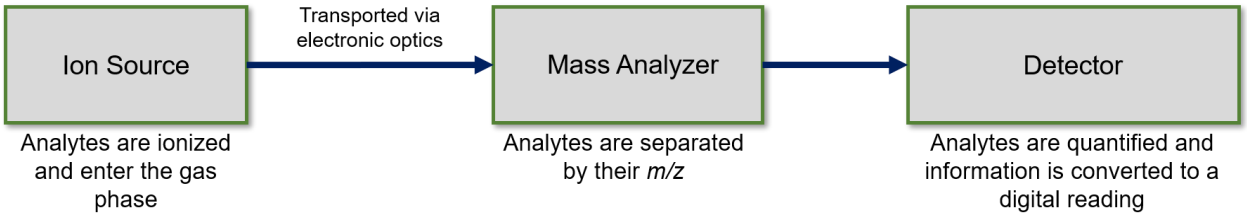

Figure 2.1. Basic anatomy of a mass spectrometer. The ion source ionizes analytes and converts them into the gas phase if needed. The mass analyzer separates analytes by their *m/z*. The analytes then strike the detector, which produces a current proportional to the amount of analyte. Information is then converted to a digital readout.

The mass analyzer performs the fundamental action of separating the sample components based on their *m/z* ratios. There are many different types of mass analyzers most of which operate on entirely different physical principles than one another. Most of the work presented in this thesis uses a time-of-flight (TOF) mass analyzer for MS analysis. Complete descriptions of other mass analyzers can be found elsewhere.[6] TOF-MS separates the ions by applying an equal force to a packet of ions and measure the time it takes for the ions to travel from one end of a drift tube to a detector at the other end. Based on the principle of kinetic energy, when an equal force is applied to objects of differing masses, their velocities will differ as well. Practically speaking, ions of a smaller mass will have a greater velocity and will reach the detector first, whereas ions of a larger mass will reach the detector later. The time at which each ion reaches the detector through a drift tube of known length is converted to the *m/z* of each ion.

A key component of this process, however, is the additional factor of charge. The gas-phase ions are guided through the mass spectrometer using voltages, including the force applied at the beginning of the TOF drift tube. Thus, the resulting velocity will also depend on the charge of the ion – an ion with a greater charge will reach the detector faster than an ion with equal mass

but less charge. The velocity resulting from the combination of an ion's mass and charge ultimately creates the measured quantity of *m/z* ratio instead of mass alone. This interdependence between mass and charge for MS operation applies to all mass analyzers.

The final component of a mass spectrometer is the detector. The detector is often confused for the mass analyzer; however, this component only detects the ions after being separated by *m/z*. Here, the ion signal is converted to an electrical signal, which facilitates conversion to a digital readout. Importantly, the detector is where the *amount* of ions of a certain *m/z* is measured, resulting in the intensity axis of a mass spectrum. Most modern MS detectors are electron multipliers, including those used in this work. An electron multiplier comprises a series of metal plates which, when struck with an incoming ion, emits a number of electrons greater than the original number of ions. The electrons are then accelerated via voltage to the next plate, where another increased number of electrons is released. The electrons are multiplied in this way through a series of plates which ultimately results in a current that is directly proportional to the original number of ions which initially hit the detector. This current can then be converted to a digital readout of ion intensity.

Selecting a mass spectrometer for an experiment will require considering primarily the source and mass analyzer. The type of sample and its chemical complexity is also a significant factor in selecting an instrument. Source selection will depend on the sample type (for instance, whether it is in solution or a solid) and the class of molecules to be analyzed. Mass analyzer selection is typically based on desired mass resolution and analysis time – prioritizing either factor tends to result in a trade-off of the other. For instance, ion trap mass analyzers have a fast analysis time but suffer in resolution; whereas Fourier transform-ion cyclotron resonance (FT-ICR) MS can achieve the highest known mass resolution, but each analysis takes seconds or longer. It should

be noted that higher-resolution instruments tend to be costlier as well. TOF-MS instruments are a popular choice as a reasonable-cost option with a good balance between analysis time and resolution.

2.1.1 Electrospray ionization (ESI) MS

Of the ionization methods suited for analysis of biological samples, perhaps none is more popular than electrospray ionization (ESI).[8] ESI transfers molecules in solution to the gas phase while simultaneously transferring charge to the molecules. Crucially, ESI is what is known as a "soft" ionization method; i.e., little to no fragmentation of the molecules occurs during ionization. Soft ionization is particularly important when analyzing large molecules such as peptides and nucleic acid chains, for instance – preserving the structure of the ions greatly simplifies analysis of complex mixtures. That said, controlled fragmentation is often used in MS experiments to elucidate the structures of molecules; this process is called tandem MS or MS/MS, where ions are mass analyzed, fragmented, and analyzed again.

In positive-mode ESI, which is the primary focus of this work, an acidic solution containing the sample flows through a hollow conductive needle with an applied positive voltage. The acidic solution exits the needle due to the repulsive charge and forms a cone at the tip, where a stream of charged droplets emerges. As the droplets traverse along the charge gradient between the needle and the inlet of the MS, the solution evaporates creating charged droplets of decreasing size but increasing charge density. At the point at which the charge density is so great it can no longer persist as a single droplet (known as the Raleigh limit), the droplet will experience a "coulombic explosion," where concurrently the remaining liquid dissipates, charge is transferred to the

molecules, and the molecules enter the gas phase. It is then that the sample enters the inlet is the mass spectrometer and is guided via voltage optics to the mass analyzer(s) (Figure 2.2).

ESI is a useful technique for vaporizing and ionizating many biological samples. Samples which are prepared in solution do not need to be dried or further processed specifically for MS analysis. In some cases, the solution-phase structures or states can be conserved into the gas phase, including, for instance, non-covalent bonds and quaternary protein structures.[9] ESI is also suitable for a large mass range, from small molecules to kilodalton-size proteins. Finally, ESI can be easily hyphenated to separation techniques such as liquid chromatography and capillary electrophoresis. Hyphenated separation addresses many of the limitations of the mass analyzer, including sample complexity and dynamic range. A detailed description of one such hyphenation, capillary electrophoresis mass spectrometry, is described in a later section.

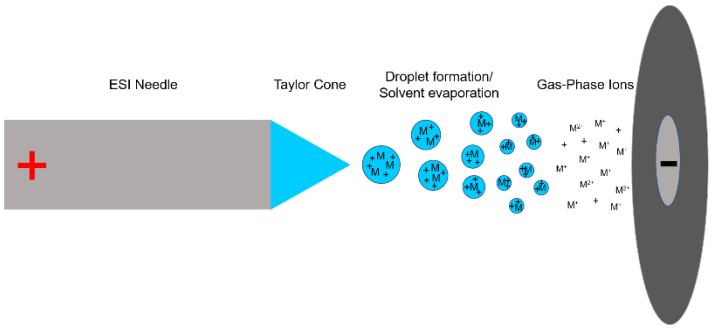

Figure 2.2. Electrospray ionization mechanism. Voltage is applied at the MS inlet and can also be applied to the ESI needle. A cone of liquid forms at the needle tip, extruding droplets. The liquid evaporates eventually leaving behind charge, analytes in the gas phase, which can be guided into the mass spectrometer.

Solution-phase ionization, however, has its drawbacks. Specifically, dilution of the sample may occur, which can be particularly problematic for single cell analysis. In some applications the charge of the resulting ions can be difficult to control, and this unpredictability can confound results.[10] When hyphenated with separation methods or other sample preparation techniques, analysis time per sample can be long – up to an hour in some cases. Despite these limitations, ESI

serves as a versatile ionization method to probe the chemical complexity of biological samples, including single cells. Some of the strategies to adapt ESI to single cell analysis are described in Section 2.3.

2.1.2 Matrix-assisted laser desorption/ionization (MALDI) MS

Matrix-assisted laser desorption/ionization (MALDI) MS is a useful complement to ESI as an ionization technique for biological samples. As a fast, solid-phase ionization, MALDI overcomes many of the disadvantages from which ESI suffers.

The basis of MALDI is the laser ablation of a sample within a crystallized matrix.[6] The key ingredient for this process is the matrix, which is selected to absorb the incoming laser wavelength. When the laser (typically in the ultraviolet range) strikes the plate, the matrix mixture ablates into a plume containing gas-phase matrix molecules and sample molecules, matrix clusters, and nanodroplets. The gas-phase ions can then be directed for mass analysis (Figure 2.3). At some point during this process, sample molecules are charged in a transfer of either protons or electrons with the matrix molecules. In the case of positive-mode MS, the most common transfer is that of a proton addition to the sample molecule. The exact mechanism of ionization is not exactly understood,[11] but its application has been immensely useful for expanding use of laser desorption to biomolecules.

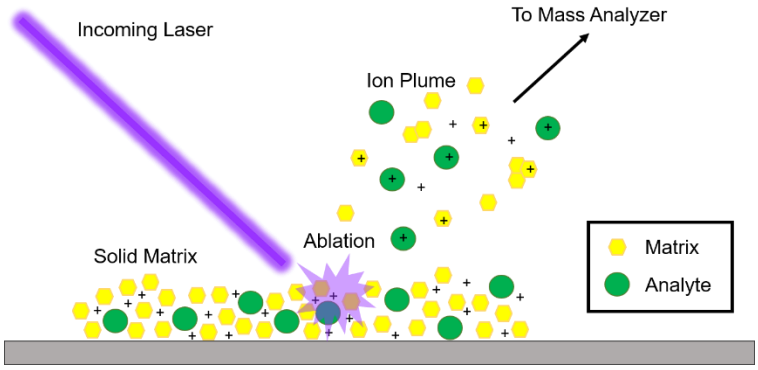

Figure 2.3. Matrix-assisted laser desorption/ionization mechanism. An incoming laser strikes a solid matrix containing the analytes, which ablates into a plume of gas phase ions. These ions are then guided to the mass analyzer.

The MALDI matrix serves as a mediator during the ionization

process – it strongly absorbs the UV light and transfers that energy in the form of ablation and ionization to the analyte.[12] The matrix is selected based on its ability to absorb the laser wavelength and ionize the analytes, and they typically feature extensive conjugation. The most common matrices for biomolecule analysis are 2,5-dihydroxybenzoic acid (DHB) and α-cyano-4-hydroxycinnamic acid (CHCA) for positive mode and 9-aminoacridine (9AA) for negative mode.

Most samples for MALDI analysis are prepared in one of two ways: the sample can be mixed with the matrix in solution before spotting onto a conductive MALDI plate or slide to dry before analysis, or the sample can be placed on the plate and the matrix coated thereon via airbrushing or sublimation. The latter method is particularly useful for biological preparations because it preserves the structural and spatial distribution of the sample, enabling mass spectrometry imaging and single cell profiling. Coating also minimally dilutes the sample, especially compared with solution-based ionizations.

Like ESI, MALDI is a soft ionization technique, but it less frequently imparts more than a couple of charges to a sample. This can be advantageous when seeking less complex spectra containing only singly or doubly charged ions, but requires involved optimization if the analytes are large. The mass range can also be limited at the lower end; matrices tend to be hundreds of Daltons and can cause interference in that mass range. MALDI is extremely fast compared to ESI – a handful of laser shots takes fractions of a second, thus profiling single cells rapidly become feasible. Because the incorporation of analytes into the crystalline matrix depends on many competing factors, no-linear effects such as ion suppression can occur, which complicates quantitative measurements. Finally, MALDI is inconvenient to hyphenate to separation techniques, creating a challenge in data analysis. Combining the advantages of both MALDI and ESI for single cell analysis would be ideal for in-depth single cell characterization.

2.1.3 Single cell targeting with microMS

The application of MS for single cell analysis is constantly evolving and improving. Though great strides have been made in the field, challenges remain, mostly regarding sample preparation. Because of their microscopic size, single cells are difficult to collect and target individually. For an overview of single cell sampling techniques, see Chapter 3. The conventional strategy for single cell MALDI-MS measurements in the Sweedler lab was to manually isolate cells and place them on specific locations on the target.[13] The work presented here tackles single cell analysis by randomly distributing many cells onto a target, then using a software package developed in the Sweedler lab which uses optical microscopy to guide single cell targeting.[14] The software (called microMS) is suitable for diverse applications, from laser targeting with MALDI and Raman spectroscopy to extraction with capillary-based probes.

microMS approaches the problem of small sample size by using optical and fluorescence microscopy to determine cell locations on a microscope slide, then loads those locations into the program used for controlling the probe (either laser, ion beam, or extraction probe). The probe can then target the cells individually without precise sample placement or whole-slide mass spectrometry imaging.

The software uses fiducial-based registration to determine cell locations. Briefly, the perimeter of a microscope slide is etched with X's using a diamond-tipped pen. These marks serve as the fiducial markers to transfer image information between sampling regimes. The sample is then added to the slide within the fiducials – for single cell analysis, this is usually done by dispersing the sample in solution and pipetting it onto the slide. The cells must be stained with a nuclear dye for the microscopy; most protocols call for Hoechst 33342. Fluorescence and bright-field images are then taken of the slide.

At this point, the cells to be analyzed must be selected for analysis. Importantly, fluorescent debris and extracellular material must be removed from the pool of analyzable cells. microMS includes functionalities that automatically perform cell finding based on user-selected parameters such as circularity and size. After cell finding, the image and cell locations can be loaded into the instrument of choice. To correlate the microscopy image and cell locations to the image, the fiducials must be registered into the instrument software. Now the instrument has a "map" of the cell locations to target and can analyze or collect the cells systematically.

The first application of this software was for rapid single cell profiling with MALDI-MS. Using this method, hundreds to thousands of cells can be profiled in an hour. The Sweedler group has demonstrated multiple uses of this technology,[15–17] and this work presents one further application of the software for single cell extraction in Chapter 4.

2.2 CAPILLARY ELECTROPHORESIS

Capillary electrophoresis (CE) is a useful tool for separation of samples and additionally benefits from a diverse selection of detection techniques, including MS. The operating principle of CE is the application of a voltage across a narrow capillary to induce a separation of a sample based on the size to charge ratio of its constituents.[18] The small volume of the capillary and fast separations makes CE particularly useful for single cell analysis.[19]

In CE, a high voltage (on the order of kilovolts) is applied across a capillary to facilitate the migration of a buffered solution and its constituents.[18] Each molecule will have a distinct electrophoretic mobility which depends upon the molecule's charge, size, and shape. In addition to electrophoretic transport through the capillary, the voltage induces movement of the buffer itself through the capillary (called electroosmotic flow, or EOF), which transports neutral molecules and some constituents of opposing charge.

Multiple detection strategies can be used for analysis after CE separation, including fluorescence spectroscopy, electrochemistry, and MS, among others. The outlet end of the capillary in each case is modified to facilitate the detection regime of choice. In hyphenating CE to MS (the focus in this thesis), the outlet of the separation capillary serves as an ESI source in most cases. The ESI source-end can be constructed with a coaxial sheath flow to form a larger and more stable Taylor cone or with a sheathless source that uses only the end of the capillary itself as the ESI needle.[20] A shealthless ESI source offers the highest sensitivity and lowest limits of detection because it does not further dilute the sample and limits stochastic gas-phase loss, but it tends to suffer in stability and is more difficult to operate.

Capillary electrophoresis is an excellent option for single cell-scale analysis because the small scale of the experiments more closely matches the volume requirements of individual cell samples. Capillaries used for CE are typically 100 μm or less in inner diameter, and depending on the length, range from nL to μL in volume. The small volumes inherent to CE analysis impart minimal sample dilution, which is ideal for single cell analysis. CE is also suitable for separating a wide range of analytes, such as metabolites, proteins, lipids, and others. The fused-silica capillary walls can be easily functionalized to facilitate separation of the analytes of interest and prevent issues such as clogging (an important consideration especially when analyzing proteins, which tend to aggregate).

2.2.1 Capillary Electrophoresis–Electrospray Ionization-Mass Spectrometry

The CE–ESI-MS system used for the work in this thesis was developed in the Sweedler lab for small volume MS analysis.[21] A 65-75 cm capillary with an inner diameter/outer diameter of 40/150 μm with an ESI emitter is assembled and mounted to the mass spectrometer. We use a sheath flow interface to balance sensitivity with electrospray stability. The emitter comprises an

IDEX MicroTee Mounting Assembly with Mounting Hole (IDEX Health & Science, Oak Harbor, WA, Part # P-875) through which the capillary is thread, a 90/10 platinum/iridium hollow needle on the emitter end to serve as the sheath for ESI (Johnson Matthey Inc., Wayne, PA, Part # 29910E) and a perpendicular capillary for delivery of sheath liquid through the platinum needle (Figure 2.4A). The electrospray is monitored with a microscope camera (Figure 2.4B).

A plexiglass box, designed to protect the user from electrical hazards, houses the apparatus for sample injection into the capillary. The box contains a vertically mobile platform which contains the sample and buffer (or background electrolyte, BGE) vials (Figure 2.4C). The custom injection vials (nanovials) are stainless steel cylinders with a 2mm diameter containing an indentation at one end. The nanovials can contain between 0.3-2 µL of solution. Because only 300 nL of sample is required for injection, sample dilution is greatly limited. State-of-the-art commercial instruments require about 5 µL minimum for sample injection – our system improves sensitivity in this parameter alone by 10-fold.

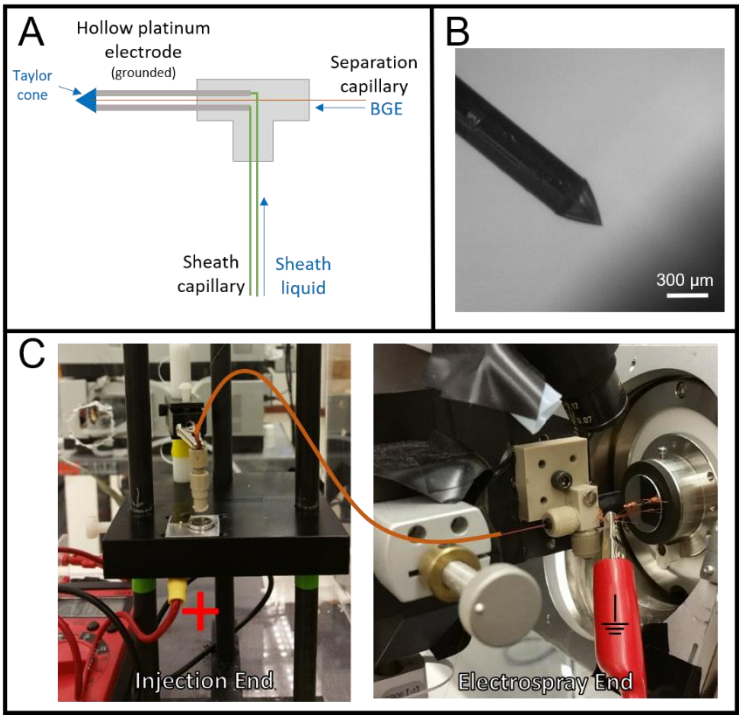

Figure 2.4. The Sweedler Lab CE–ESI-MS system. (A) Diagram of ESI emitter. (B) Microscope image of emitter in operation. (C) Diagram of separation setup. At the injection end, a platform contains buffer and sample vials to which high voltage is applied to induce migration of buffer and analytes through the capillary. The platform can be raised and lowered for injection. At the electrospray end, the emitter is mounted to an XYZ stage for accurate positioning in front of the MS inlet. The emitter is grounded to complete the circuit, and the electrospray is initiated by a negative voltage applied at the MS inlet.

Separation is induced via application of a high voltage (±10-20 kV, though most experiments concern cations and thus we apply a positive voltage) to the injection end of the capillary. The voltage is delivered through a 10 kΩ resistor, across which a multimeter is connected in parallel to monitor current, then to a stainless steel inset in the injection platform. Current travels from the stainless steel platform to the inset stainless steel vials and through the buffers therein to the injection end of the capillary. The ESI emitter is grounded at the other end of the capillary.

The injection platform is capable of two types of sample injection – the selection of which will vary based on the experiment. The first, and most common for the following experiments, is hydrodynamic injection, where a pressure differential prompts buffer migration into the capillary. We can inject a sample plug by raising the injection platform to create a siphoning effect to the emitter end of the capillary. The platform is then lowered to the same height as the source. Using this method, we can inject 5-20 nL of solution into the capillary for separation.

The second type of injection is electrokinetic, where high voltage is applied when the capillary is placed in the sample vial and analytes enter the capillary via electrophoresis. On our system, this method is more user-friendly and typically results in a greater number of analytes entering the capillary in a comparable amount of time. However, electrokinetic injection is heavily biased toward more charged analytes. This can create several problems such as injecting salts that can cause interference and reducing the amount of less-charged and neutral analytes – a real disadvantage when performing untargeted profiling. Additionally, it is impractical to calculate the number of moles of any given molecule injected, which limits some applications. Electrokinetic injection can also cause electrolysis of certain analytes (the neurotransmitter serotonin, for example), which confounds results. Overall, hydrodynamic injection tends to be the optimal choice for our metabolomic profiling applications, though electrokinetic can be considered when higher

sensitivity is needed, for instance. We address some of the challenges of electrokinetic injection in Chapter 6, where we incorporated field-amplified sample stacking into our protocol.

CE–ESI-MS is used in most of the applications described here because of its utility in single cell profiling. Particularly, we are interested in studying metabolite profiles as a snapshot of a cell's phenotype. Chapter 3 goes into further detail on the importance of metabolomic studies for neurobiology and compares techniques, including CE–ESI-MS and other mass spectrometry approaches.

2.3 CONCLUSIONS

Mass spectrometry can provide an incomparable level of chemical detail when profiling biological samples. Applying MS to single cell analyses is an ongoing challenge, though great strides have been made in the past few decades. MS is now the go-to method for omics investigations; scaling down such experiments is the new frontier. Chapter 3 will go into detail on how MS has been applied to single cells for metabolomic analysis – since the inception of such approaches, the field has flourished and expanded in creative ways. The purpose of the work presented in later chapters is to push the bounds of single cell analyses by combining multiple strategies into the same experiment. Importantly, the hyphenation approach described here is not instrument or method-specific; that is, its utility expands beyond MS alone. Such combinations can address instrument limitations and expand knowledge of the chemical complexity of single cells.

2.4 REFERENCES

(1) De Vijlder, T.; Valkenborg, D.; Lemière, F.; Romijn, E. P.; Laukens, K.; Cuyckens, F. A Tutorial in Small Molecule Identification via Electrospray Ionization-mass Spectrometry: The

Practical Art of Structural Elucidation. *Mass Spectrom Rev* **2018**, *37* (5), 607–629. https://doi.org/10.1002/mas.21551.

(2) Benninghoven, Alfred.; Sichtermann, W. K. Detection, Identification, and Structural Investigation of Biologically Important Compounds by Secondary Ion Mass Spectrometry. *Anal. Chem.* **1978**, *50* (8), 1180–1184. https://doi.org/10.1021/ac50030a043.

(3) Schymanski, E. L.; Jeon, J.; Gulde, R.; Fenner, K.; Ruff, M.; Singer, H. P.; Hollender, J. Identifying Small Molecules via High Resolution Mass Spectrometry: Communicating Confidence. *Environ. Sci. Technol.* **2014**, *48* (4), 2097–2098. https://doi.org/10.1021/es5002105.

(4) Jansson, E. T. Strategies for Analysis of Isomeric Peptides. *Journal of Separation Science* **2018**, *41* (1), 385–397. https://doi.org/10.1002/jssc.201700852.

(5) Bai, L.; Romanova, E. V.; Sweedler, J. V. Distinguishing Endogenous D-Amino Acid-Containing Neuropeptides in Individual Neurons Using Tandem Mass Spectrometry. *Anal. Chem.* **2011**, *83* (7), 2794–2800. https://doi.org/10.1021/ac200142m.

(6) Gross, J. H. *Mass Spectrometry: A Textbook*, 2. ed.; Springer: Berlin, 2011.

(7) Liigand, P.; Kaupmees, K.; Haav, K.; Liigand, J.; Leito, I.; Girod, M.; Antoine, R.; Kruve, A. Think Negative: Finding the Best Electrospray Ionization/MS Mode for Your Analyte. *Anal. Chem.* **2017**, *89* (11), 5665–5668. https://doi.org/10.1021/acs.analchem.7b00096.

(8) Cole, R. B. *Electrospray and MALDI Mass Spectrometry: Fundamentals, Instrumentation, Practicalities, and Biological Applications*; John Wiley & Sons, 2011.

(9) Farmer, T. B.; Caprioli, R. M. Electrospray Ionization Mass Spectrometry: Protein Structure. In *Mass Spectrometry in Biomolecular Sciences*; Caprioli, R. M., Malorni, A., Sindona, G., Eds.; NATO ASI Series; Springer Netherlands: Dordrecht, 1996; pp 61–88. https://doi.org/10.1007/978-94-009-0217-6_4.

(10) Zhang, Z.; Marshall, A. G. A Universal Algorithm for Fast and Automated Charge State Deconvolution of Electrospray Mass-to-Charge Ratio Spectra. *Journal of the American Society for Mass Spectrometry* **1998**, *9* (3), 225–233. https://doi.org/10.1016/S1044-0305(97)00284-5.

(11) Siuzdak, G. An Introduction to Mass Spectrometry Ionization: An Excerpt from The Expanding Role of Mass Spectrometry in Biotechnology, 2nd Ed.; MCC Press: San Diego, 2005: *JALA: Journal of the Association for Laboratory Automation* **2016**. https://doi.org/10.1016/j.jala.2004.01.004.

(12) Zenobi, R.; Knochenmuss, R. Ion Formation in MALDI Mass Spectrometry. *Mass Spectrometry Reviews* **1998**, *17* (5), 337–366. https://doi.org/10.1002/(SICI)1098-2787(1998)17:5<337::AID-MAS2>3.0.CO;2-S.

(13) Li, L.; Garden, R. W.; Sweedler, J. V. Single-Cell MALDI: A New Tool for Direct Peptide Profiling. *Trends in Biotechnology* **2000**, *18* (4), 151–160. https://doi.org/10.1016/S0167-7799(00)01427-X.

(14) Comi, T. J.; Neumann, E. K.; Do, T. D.; Sweedler, J. V. MicroMS: A Python Platform for Image-Guided Mass Spectrometry Profiling. *J. Am. Soc. Mass Spectrom.* **2017**, *28* (9), 1919–1928. https://doi.org/10.1007/s13361-017-1704-1.

(15) Neumann, E. K.; Ellis, J. F.; Triplett, A. E.; Rubakhin, S. S.; Sweedler, J. V. Lipid Analysis of 30 000 Individual Rodent Cerebellar Cells Using High-Resolution Mass Spectrometry. *Anal. Chem.* **2019**, *91* (12), 7871–7878. https://doi.org/10.1021/acs.analchem.9b01689.

(16) Neumann, E. K.; Comi, T. J.; Rubakhin, S. S.; Sweedler, J. V. Lipid Heterogeneity between Astrocytes and Neurons Revealed by Single-Cell MALDI-MS Combined with Immunocytochemical Classification. *Angewandte Chemie International Edition* **2019**, *58* (18), 5910–5914. https://doi.org/10.1002/anie.201812892.

(17) Do, T. D.; Ellis, J. F.; Neumann, E. K.; Comi, T. J.; Tillmaand, E. G.; Lenhart, A. E.; Rubakhin, S. S.; Sweedler, J. V. Optically Guided Single Cell Mass Spectrometry of Rat Dorsal Root Ganglia to Profile Lipids, Peptides and Proteins. *ChemPhysChem* **2018**, *19* (10), 1180–1191. https://doi.org/10.1002/cphc.201701364.

(18) Colyer, C. L. High-Performance Capillary Electrophoresis: Theory, Techniques, and Applications Edited by Morteza G. Khaledi (North Carolina State University). Wiley Press: New York. 1998. 1014 Pp. $150.00. ISBN 0-471-14851-2. *J. Am. Chem. Soc.* **1999**, *121* (20), 4930–4931. https://doi.org/10.1021/ja985694e.

(19) DeLaney, K.; Sauer, C. S.; Vu, N. Q.; Li, L. Recent Advances and New Perspectives in Capillary Electrophoresis-Mass Spectrometry for Single Cell "Omics." *Molecules* **2019**, *24* (1), 42. https://doi.org/10.3390/molecules24010042.

(20) Risley, J. M.; Jong, C. A. G. D.; Chen, D. D. Y. Electrospray Ionization Interface Development for Capillary Electrophoresis–Mass Spectrometry. In *Capillary Electrophoresis–Mass Spectrometry (CE-MS)*; John Wiley & Sons, Ltd, 2016; pp 7–39. https://doi.org/10.1002/9783527693801.ch2.

(21) Nemes, P.; Rubakhin, S. S.; Aerts, J. T.; Sweedler, J. V. Qualitative and Quantitative Metabolomic Investigation of Single Neurons by Capillary Electrophoresis Electrospray Ionization Mass Spectrometry. *Nat. Protocols* **2013**, *8* (4), 783–799. https://doi.org/10.1038/nprot.2013.035.

CHAPTER 3: SINGLE CELL NEUROMETABOLOMICS

This chapter is an update of an invited review for a special issue in *ACS Chemical Neuroscience*, **2018**, (DOI: 10.1021/acschemneuro.7b00304) on precision medicine in brain cancer with coauthors M. Qi, N. Yang, and J.V. Sweedler.

3.1 INTRODUCTION

Cellular heterogeneity is integral to most central nervous system physiological processes, including memory, neuronal network formation, function, and cellular homeostasis. Distinct cell types, such as neurons, astrocytes, and oligodendrocytes, are intertwined at the cellular scale. As a result, tissue measurements that provide information on an average set of metabolites in a region may not reflect the actual levels found in the cells of interest. Within the brain, even closely located cells can have distinct cellular and synaptic connections, and protein and metabolite profiles; these differences can be important for function. Investigation of chemical cellular heterogeneity is an expanding field of inquiry, with relevance to understanding the mechanisms of both health and disease.[1–4]

Explorations of heterogeneity at the level of the transcriptome, proteome, peptidome, lipidome, and metabolome provide key insights into brain function and dysfunction on the cellular level.[5,6] Single cell metabolomics is of particular interest to neuroscience due to the diverse functions of neuronal cells that are correlated to the small-molecule metabolite profiles of cell types and disease states.[7–9] The metabolites of interest range from amino acids, classical neurotransmitters, fatty acids and lipids, and small peptides to a variety of precursor and intermediate molecules. The ability to detect and quantify this diverse set of molecules enables an enhanced understanding of neurochemical pathways and dysfunction related to disease. Each of the available measurement approaches has unique advantages and disadvantages that must be

considered when adapted to the level of an individual cell. The challenges of single cell measurements involve cell isolation, sample processing, the metabolomics measurement process, and the integration of the data with other disparate data sets.

We begin with a discussion of single cell sampling techniques, followed by the mass spectrometry (MS)-based approaches that are suitable for single cell neurometabolomics, including a brief overview of some other single cell methods. Next, we turn our attention to highlighting specific applications of metabolomics to single cell investigations, concluding with some thoughts about the future of the field.

3.2 SAMPLING FOR SINGLE CELL ANALYSIS

Proper sampling is the prerequisite for a successful chemical analysis, especially when collecting volume-limited samples like single cells. First, careful attention needs to be paid to sampling accuracy so that only the selected individual cells or cellular components of interest are isolated. Second, although it is difficult to perform sampling without coisolation of any extracellular content, effort should be made to minimize the effects of these interfering materials. Additionally, cell metabolism quenching or stabilization should be performed whenever applicable so that the samples to be measured reflect the real metabolic status of normally functioning cells.[10,11] A recent review by Gallion, *et al.*, [12] explores specific strategies to preserve the chemical profile of a single cell at the time and location of sampling.

Sampling techniques can vary from manual manipulations to automated methods. Manual sampling can be a simple and convenient means to isolate cells and collect samples. Experience and good practice directly affect sample quality and are integral to ensuring experimental success. Manual isolation of large neurons from invertebrates, like *Aplysia californica*, has been reported using surgical scissors, sharp tungsten needles, and fine-tip glass capillaries.[13–15] Manual sampling

of smaller neurons and even subcellular organelles is also possible.[16–18] Micromanipulators and glass pipettes have been utilized collectively to isolate fluorescently labeled mammalian neurons from brain slices. For example, the use of a patch clamp/MS-based platform enabled the direct correlation of electrophysiological recordings to the metabolite content of single cells from rodent brain slices.[19] Recently, in situ microsampling from live single cells in developing *Xenopus laevis* embryos eliminated the need for dissection and cell isolation, addressing the technical gap between live single cell analysis and comprehensive untargeted metabolomics.[20] Another recent study demonstrated the use of fluid force microscopy, a modification of atomic force microscopy, to collect live-cell extracts for MS-based metabolomic analysis.[21]

Two sampling methods that require less manual handling, laser capture microdissection (LCM) and optical trapping (OT), use microscopy-guided approaches to sample cells. In LCM, cell- or region-specific physical features of a target sample area are visually identified using a microscope, and then the cell(s) are removed via laser surgery. LCM has been used to isolate neurons from various brain structures, including the cortex, cerebellum, suprachiasmatic nucleus, and pituitary.[22–25] In OT, the cell is moved by a laser under the gradient force present between the high-intensity region of a focused light beam and the cell itself. Our group developed an approach that combines OT with capillary electrophoresis (CE), sampling single neurons for downstream indolamine and catecholamine measurement through fluorescence.[26] Hosokawa *et al.*[27] demonstrated successful trapping of synaptic vesicles in a hippocampal neuron using an infrared laser, supporting the feasibility of using OT to manipulate subcellular features.

Microfluidic devices enable cells to be isolated and sampled using a variety of approaches, as reviewed recently.[28,29] Due to the ability to reduce fluidic volumes to the size of cells and control the laminar flow in microfluidic devices, in most cases, cells can be transported one-by-one

through the device. Oil droplet-based single cell isolation has been accomplished with microfluidic devices, in which individual cells are contained in a stream of droplets and segregated by the immiscible solvent from other cell-containing droplets.[30–32] Some microfluidic devices use a pneumatic membrane valve to control the passage of individual cells and isolate them from others.[33] Selected neurons have been cultured in a capillary, allowing efficient collection of cell release for follow-up MS characterization.[34]

While less commonly used for single cell metabolomic studies, fluorescence-activated cell sorting (FACS) and magnetic-activated cell sorting (MACS) also serve as efficient methods to select single cells of interest. FACS often is based on the interaction between a fluorescently labeled antibody and marker expressed on the surface of target cells. The fluorescently labeled antibodies are added into a cell suspension, and the cells in the suspension are sorted based on their fluorescence signal and other properties, for example, size. Multiple research groups have used FACS to sort different types of cells in various brain regions for mRNA and protein analysis.[35,36] MACS relies on magnetic beads coated with an antibody, streptavidin, or other molecules that can specifically interact with proteins on target cells. After cell binding to coated magnetic beads, a magnetic field is applied so that only targeted or unwanted cells are retained and separated from other cells. In one example, MACS was used to sort cells and generate cultures of mammalian neuronal restricted progenitors, which later differentiated into neurons.[37] Proper sample collection is important for most measurements and becomes even more crucial as sample sizes are reduced to the single cell level.

With single cell metabolomics, preserving the endogenous state of metabolites contained within the cells and minimizing their distortion becomes critical. A common strategy is to keep cells in their original microenvironment as long as possible and shorten the time spent on

operations that can interrupt and change ongoing cellular activities.[2] For some techniques, such as microfluidics and electrophysiological recording, isolated cells can be placed and cultured under conditions closer to their physiological state. When cell culturing is not feasible, other approaches can be used, for example, shock freezing and rapid cellular activity quenching using cold organic solvents.[38,39]

3.3 CHARACTERIZATION METHODS IN SMALL-VOLUME NEUROMETABOLOMICS

Large-scale metabolomic measurements oftentimes use a number of preprocessing and sample conditioning steps, such as salt removal or extraction, to isolate specific analyte classes. These processes increase the robustness of the measurements; however, they often result in sample loss. Thus, to enhance metabolite detection, most single cell metabolomic methods usually use less sample cleanup.

After the cells are isolated and prepared, the chemical measurements are performed. The two most common metabolomic approaches are CE or liquid chromatography (LC) coupled with MS and nuclear magnetic resonance (NMR). However, because NMR requires larger sample volumes and masses than single cells, NMR-based metabolomic studies are more commonly performed with tissue samples or bodily fluids and so are not covered here.

MS is the most commonly used technique in small-volume metabolomics, due to its low detection limits and high chemical information capacity.[40] For single cell measurements via MS,[41] we have organized the discussion according to the ionization method used, as it often dictates other aspects of the measurement.

3.3.1 Electrospray-ionization (ESI) mass spectrometry

Samples are typically introduced to an ESI source by direct infusion or following a separation. Much of the single cell work done via ESI-MS has involved CE-MS. CE, which

separates molecules based on their electrophoretic mobility, offers the advantages of high separation efficiency and low sample volumes and is well suited to characterizing many of the charged molecules in a single cell. For thorough perspectives on CE-MS-based metabolomics, the reader is directed to several recent reviews.[42–44]

Neurometabolomic analyses using CE-MS have been used to characterize a broad range of metabolites, such as nucleotides and nucleotide derivatives[45] and neurotransmitters.[46] Nemes *et al.*[7] profiled and quantified metabolites contained in single freshly isolated and overnight cultured *A. californica* neurons and found a significant change in the metabolome between the two sample preparation methods for B1 neurons. They noted the presence of over 300 cell-related ion signals and identified a fraction as relevant metabolites. Employing a whole-cell patch clamp technique following electrophysiology measurements, Aerts and colleagues[46] analyzed approximately 1–3 pL of sample extracted from individual rat thalamic cells, correlating the metabolic profiles of single cells to electrical activity. An advantage of CE-MS is that the separation can be tailored to allow characterization of a broad range of analytes over a wide dynamic range.

CE-MS- and LC–MS-based measurements offer a number of advantages, including the ability to characterize complex, large dynamic-range samples. While they tend to be lower throughput compared to direct MS measurements, usually only a few cells per hour, there have been reports of higher-throughput methods for CE-MS. One of the more recent examples is multisegment injection, which can increase throughput by several fold.[47] The capillaries can also be embedded in devices to allow higher-speed separations. Mellors and colleagues[48] fabricated a microchip for automated analysis of single human erythrocytes, which combined on-chip cell lysis, cellular constituent separation, and ESI-MS detection. Their method enables automated, real-time

CE-MS analysis and has the additional benefit of being relatively high-throughput at 12 cells per minute, as compared to traditional CE-MS methods.

Additionally, direct infusion into an ESI-MS platform has been accomplished for metabolomic analysis, including modification of the ESI interface for improved single cell analysis. Wei *et al.*[49] recently introduced one such modification to extend the analysis time of small-volume samples. Instead of a continuous electrospray, the electrospray was pulsed and synchronized to the frequency of the mass analyzer. They were able to extend the analysis time of a picoliter sample to several minutes, allowing the collection of tandem MS (MS/MS) spectra of multiple compounds from a single sample. Moreover, this method requires no or minimal sample dilution. As a result, low-abundant molecules at zeptomole levels in single HeLa cells were detected. The benefits of such a development are twofold: the reduction of detection limits due to low sample dilution and the ability to identify unknown molecules using MS/MS.

In another example using ESI, Gong et al.[50] inserted a tungsten probe into target single cells for metabolite enrichment, then immediately positioned it at the MS inlet with voltage applied. With the help of a solvent spray, metabolites enriched on the probe could be detected with about 30-fold increased sensitivity when compared with a traditional method in which enriched analytes are first eluted and then subjected to nanoESI-MS. The same group has more recently expanded this technology to be compatible with droplet-based microextraction.[51]

Probe-based ESI was also designed to enable in situ single cell metabolite analysis. The Yang group[52,53] fabricated a three-component integrated probe, composed of a dual-bore quartz needle for sampling, a silica capillary for solvent delivery, and a nanoESI emitter (Figure 3.1).[52] Once positioned into single cells of interest, cellular content was directly guided into the emitter

for in situ real-time analysis. This method introduced minimal disruption to the original cell conditions. The average analysis speed of 3 min per cell allowed a large number of cells to be analyzed within a short time period.

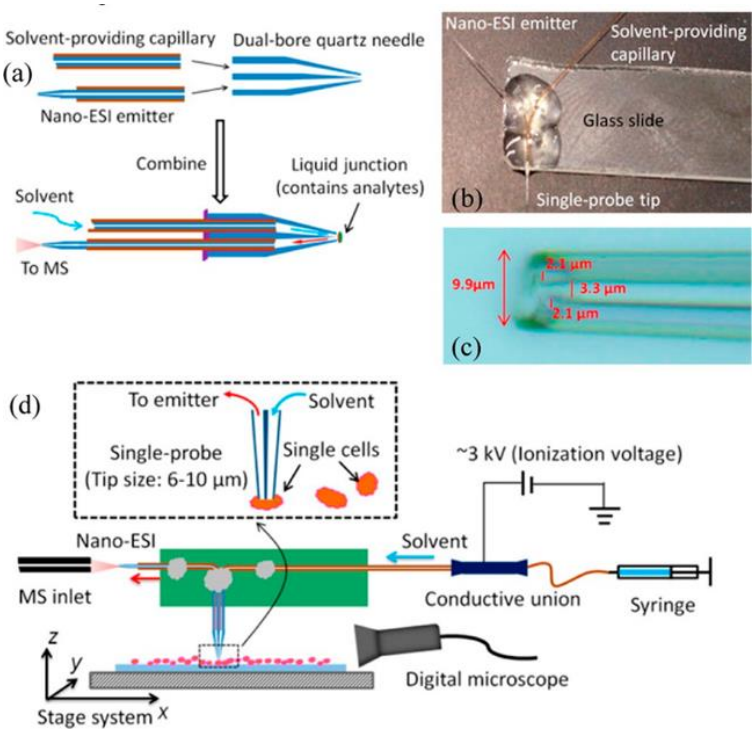

Figure 3.1. (a) Fabrication steps and structure of a single-probe for ESI-MS; (b) photograph of a working single-probe; (c) 40× magnification of the single-probe tip with measurements obtained from the calibrated digital microscope; (d) setup schematic of an *in situ* real-time single cell MS analysis.[52]

These probe-based ESI approaches are capable of in situ analysis and extracting the contents of living cells within their native biological environment, including cells within live tissue and cells circulating in biofluids.[54] Use of the single probe has expanded in recent years to numerous applications. In an early example, single mitochondria were identified in live cells with fluorescent probes and selectively isolated with a single probe for ESI-MS analysis.[55] The single probe has also expanded to ambient imaging applications in recent years.[56]

3.3.2 Matrix-assisted laser desorption/ionization mass spectrometry

Direct single cell measurement via MALDI-MS analysis has a long history, especially for peptides within individual cells.[57] MALDI-MS offers many advantages for single cell metabolomics, including good tolerance for salts, simple sample preparation, and attomole detection limits with little sample consumption.[58,59] One caveat is that MALDI matrix interference

can limit the observation of many metabolites. A few early MALDI-MS-based studies revealed neuropeptide profiles in single neurons of invertebrates such as *A. californica*, *Lymnaea stagnalis*, *Periplaneta americana*, and *Cherax destructor*.[57,60–64] Many novel neurohormones in single invertebrate neurons have been discovered by MALDI-MS.[65,66]

These earlier studies isolated the cells manually. With the advent of improved automated sampling and instrumentation, the application of MALDI-MS has been extended to larger numbers of smaller cells. Ong and co-workers[67] dispersed rat pituitary cells on a microscope slide and recorded the coordinates of individual cells, with the locations used to perform automated MALDI-MS measurements of thousands of targeted cells. They successfully determined major subpopulations of pituitary cells and even found rare cells containing unique features in the neuropeptide mass range. In a follow-up study, cell heterogeneity within islets of Langerhans and between different regions of the pancreas were investigated using a similar method.[68]

In addition to peptides, lipids are also well suited for single cell MALDI-MS because this mass range is not affected by matrix interference. Comi, *et al.*[69] improved the throughput of single cell MALDI-MS analysis by developing an open-access software package that enables image-guided single cell MALDI-MS. After acquiring whole-slide microscopy images, the software uses point-based registration to direct laser shots only to slide locations containing a single cell. Following MALDI-MS screening of a large cell population, rare or representative cells with signals of interest, lipids in this case, were further analyzed by Fourier transform-ion cyclotron resonance (FT-ICR) MS for high-resolution detection (Figure 3.2A).[69] This work also points to an

important trend: improvements in time-of-flight (TOF) mass analyzers and development of interfaces that couple MALDI with FT-ICR and Orbitrap MS have greatly improved the data obtained from tissues and cells by providing accurate mass measurements (resolution <5 ppm).[70–72] A recent publication from Neumann, *et al.*,[73] illustrations the benefits of combining rapid single

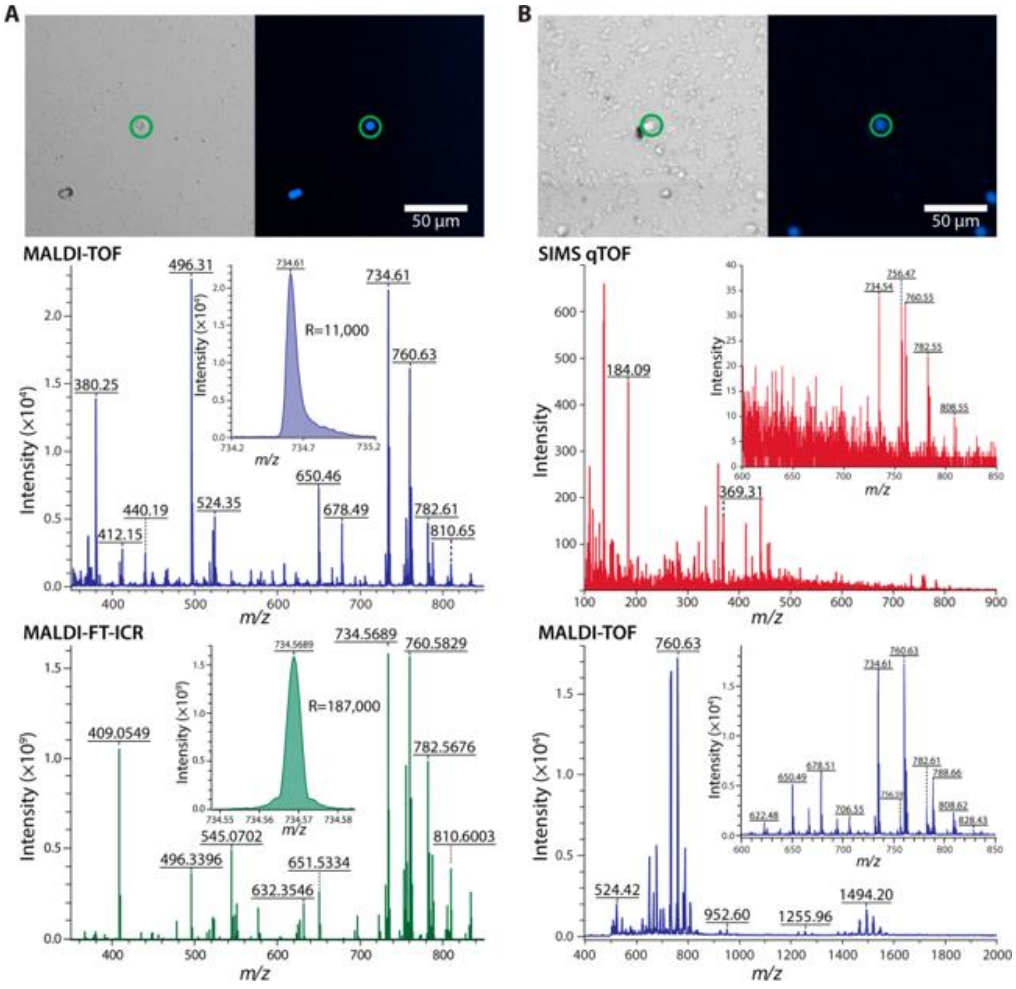

Figure 3.2. Sequential analysis of the same individual cell with two separate MS systems. Once a cell has been located in the optical image (top), its location remains fixed through multiple analyses, allowing two instruments to probe the same set of selected cells. (A) MALDI-TOF MS (middle) of a rat cerebellum-derived cell followed by MALDI-FT-ICR MS (bottom). MALDI-TOF MS provides high throughput screening of thousands of cells to highlight rare or representative individuals. Here, FT-ICR MS provides high mass resolution and high mass accuracy for unequivocal elemental composition of selected cellular contents. (B) SIMS profiling (middle) followed by MALDI-TOF MS (bottom) with a DHB-coated, SCN-derived cell. SIMS provides information on small molecule compounds while MALDI-TOF MS effectively detects larger species, such as lipid dimers and peptides. The insets demonstrate overlap of intact lipid coverage from each modality.[69]

cell profiling and high resolution MS using microMS: they profiled 30,000 single cells with MALDI-FT-ICR-MS and categorized biologically relevant subtypes by their lipid profiles.

3.3.3 Secondary ionization mass spectrometry (SIMS)

The throughput of MALDI-MS is exciting, but as noted earlier, matrix interferences tend to limit its application for metabolomics measurements. An alternative and widely used matrix-free ionization technique is SIMS, in which a focused beam of primary ions bombards the sample surface, producing secondary ions from the analyte. Though fragmentation of large biological molecules is common, SIMS works well for smaller analytes, including many metabolites and lipids. SIMS also has a higher spatial resolution, oftentimes smaller than a micrometer, which can enable subcellular profiling.[74,75] While most SIMS instruments do not obtain MS/MS information, newer instrumentation has become available[76–78] that greatly facilitates metabolite identification. Though SIMS is often used in lipidomic[79] and targeted analyses, as described further below, it is less common for comprehensive metabolomic analyses. A 2013 study by the Vickerman group[80] evaluated TOF-SIMS specifically for metabolomics and demonstrated its ability to complement more traditional methods of metabolomic analysis. The authors found that LC–MS/MS and SIMS spectra for the same metabolite standards tended to correspond well, suggesting it is possible to use LC–MS databases to aid in metabolite identification with TOF-SIMS. In the aforementioned study by Comi and colleagues,[69] SIMS was used in combination with MALDI-MS. Image-guided SIMS and MALDI-MS analysis uncovered small molecules, lipids, and peptides from the same individual cell, highlighting the benefits of obtaining both high-throughput and high-molecular information content from selected cells, as illustrated in Figure 3.2B.[69]

SIMS has been successfully employed to investigate lipid and fatty acid distribution and abundance changes in tissue sections and single cells.[81,82] As one example, distribution of vitamin

E on the cell membrane of individual *A. californica* neurons was uncovered using TOF-SIMS.[83] Metabolite visualization through SIMS has also been extended into the 3D spatial world. Lipids and lipid fatty acid side chain distributions were revealed as a function of depth in isolated *X. laevis* oocytes, perhaps the first demonstration of 3D biomolecular imaging in a real biological system.[84] Our group has also implemented both MALDI and SIMS together with optical microscopy to perform high-throughput profiling of neurons.[67,85]

3.3.4 Other matrix-free ionization approaches

Several other ionization methods have been applied to individual cell measurements, including direct desorption electrospray ionization (DESI), laser ablation electrospray ionization (LAESI), and nanophotonic ionization, all with different measurement capabilities and advantages. At present, DESI is rarely applied to individual cell measurements,[86,87] partly because of spatial resolution and detection sensitivity issues, but we expect its application to increase.

LAESI is a variant of MS that is useful for metabolomics; a mid-IR laser ablates a sample in situ, the plume from which is then intercepted by an electrospray for MS analysis.[88] LAESI allows in situ metabolite sampling directly from tissue and single cells. In addition, LAESI has a clear chemical background that is analogous to ESI. The technique has been shown to distinguish subcellular features in lipid profiles between the vegetal and animal poles of *X. laevis* eggs, while detecting 52 small metabolites and 92 various lipids.[89] Despite being a relatively new ionization method, LAESI has the potential to make great contributions to small-scale metabolomics as the technology improves. The *in situ* capabilities in particular make LAESI an ideal technique for experiments on cultured brain tissue, though without single cell resolution.

Nanophotonic ionization using nanoscale silicon materials to perform surface-assisted laser desorption/ionization MS enables matrix-free analysis of small molecules with low detection

limits. The architecture of the silicon structures has been shown to have a significant effect on ionization efficiency[90] and sensitivity.[91] The technique's applicability to single cell analysis was demonstrated by the Vertes lab;[92] using nanophotonic ionization to analyze individual yeast cells deposited on a nanopost array chip, they achieved detection of analytes in the zeptomole range. The same group demonstrated the technique's metabolomic capabilities by screening more than 600 metabolite standards.[93]

3.3.5 Mass spectrometry imaging (MSI)

The approaches discussed thus far are used to assay a user-selected sample, such as a single cell, for its metabolomic content. Methods that sample a location on a surface can be adapted to an imaging mode where the sampling location is rastered across the surface, building an image of a sample one location at a time (there are other modes of acquiring an image, but this is the most common). This approach has been used since the 1960s with SIMS and was adapted to MALDI and other ionization methods to form the collection of measurement techniques known as MSI. MSI has been used to study tissues down to the individual cell level, although when the cells are not separated, the information obtained will be from a blend of cells; in the brain, for example, astrocytic processes, oligodendrocyte extensions, and nerve terminals can be within the same micrometer field of view of a focused laser. Thus, even when several micrometer resolution is achieved, below the size of many cells, multiple cells may be sampled. However, MSI has the advantage of measuring many metabolites while simultaneously preserving spatial information.

Differences between MSI and conventional MS measurements of a cell involve data collection and processing. For example, during MALDI-MSI, the spectrum at each location across the sample is recorded along with the (X, Y) coordinates, defining the location being analyzed. Signals from different mass-to-charge ratios (m/z) at each analyzed position are extracted and

processed to construct the distribution map of each m/z, with intensity shown in a false color scale. An area of rapid growth is the development of approaches to improve the spatial resolution. Common spatial resolutions achieved with MALDI-MSI are between 10 and 200 μm, which hinders accurate measurement of single cells from tissues. However, higher spatial resolutions at 2–10 μm have been reported,[70,94,95] with recent work from the Spengler group[96] achieving 1.4 μm resolution while detecting lipids, peptides, and other metabolites within individual cells. Recent work by Neumann, *et al.*,[97] improved MSI resolution through chemical pan sharpening after multimodal imaging with MALDI-MS and infrared spectroscopic imaging. Data fusion of the two images resolved anatomical structures within hippocampal tissue that could not be discriminated by either technique alone.

An alternative way to improve the spatial resolution of MSI is to use SIMS instead of MALDI. SIMS has a reported spatial resolution of 50 nm to 1 μm,[41] with different molecular information obtained across this range. In all cases, there is a trade-off between detection limits and resolution; as the sample probe diameter is decreased, the number of molecules within the probe decreases. For example, decreasing a probe beam from 50 to 5 μm should reduce the number of molecules 100-fold; at some point, the measurement becomes limited by instrumental detection limits and not the probe beam geometry, a situation common in SIMS with its smaller probe diameters.

3.4 SINGLE CELL METABOLOMIC ANALYSES

3.4.1 Enhancing metabolite coverage in single cells

Metabolites within an individual cell account for a vast array of functionalities, but the analytes are present over many orders of magnitude, at levels ranging from millimolar to less than nanomolar. One issue is that nanomolar levels of a molecule in a picoliter volume sample are

present at zeptomole amounts, which are not usually characterizable. Because of the analyte amounts, an individual cell's metabolomic measurement uncovers fewer metabolites than larger-volume measurements. As highlighted previously, the specific fraction of the metabolome characterized depends on sample properties as well as the figures of merit for the measurement approach used. Our group has demonstrated metabolic heterogeneity in neuronal cell types from both *A. californica* and rat, with more than one hundred chemical features putatively identified with CE−MS.[8,46] We have also been able to detect metabolic differences between subcellular regions of single cells.[98] Onjiko *et al.*[99] used CE-MS to distinguish more than 80 molecular features in *X. laevis* embryonic cells and were able to metabolically distinguish cell fates of the differentiated cells.

Efforts to improve metabolite coverage require enhanced sampling approaches; for example, the mismatch between collected sample volumes and the injected volumes used in CE needs to be addressed. One approach is to inject more analyte onto the capillary via analyte stacking. This involves concentrating metabolites into a narrow zone at the entrance to the separation capillary. Liu *et al.*[45] used a large-volume sample stacking method to improve the detection of endogenous nucleotides in an individual *A. californica* neuron. They detected 51 fg of material, which is 200 times less than in previous studies. CE-MS stacking has also been used for detection of drugs and metabolites in urine samples, with limits of detection as low as 2 ng/mL.[100] We in the Sweedler group have also applied field-amplified sample injection to CE-MS analysis and developed an approach to avoid inorganic salt interference. This method will be discussed further in Chapter 7 of this thesis.

Additional improvements to metabolome coverage can also be made by developing metabolite-specific CE-MS conditions. Although in cases where methods that successfully

increase metabolome coverage are not initially demonstrated on individual cells, these approaches could be adapted to small-volume sample measurements. For instance, in one study, a fused silica capillary was coated with poly(N,N,N′,N′-tetraethyldiethylenetriamine, N-(2-hydroxypropyl) methacrylamide) to shorten separation time and enhance signal intensity for metabolites suffering from poor negative-mode MS response.[101] The authors reported detection of 87 metabolites in orange juice and 142 metabolites in red wine, demonstrating the method's ability to expand the detectable metabolite pool.

Sheathless CE-MS interfaces have also been reported to enhance metabolite coverage. Ramautar et al.[102] used a porous tip sprayer as a CE-MS interface to eliminate the need for a sheath liquid. Due to the improved ionization efficiency, they were able to detect three times more molecular features, improve sensitivity by 2 orders of magnitude, and expand metabolome coverage for polar ionogenic metabolites in human urine samples. Other recent works have also demonstrated the use of sheathless CE-MS in enhancing anionic metabolite profiling, although still in bulk samples as opposed to single cells.[103,104] While metabolome coverage is inherently limited in single cell analysis due to the low concentration of many small molecules in single cells, such advancements will prove useful when paired with improvements in CE-MS sensitivity.

3.4.2 Mapping the single cell metabolome

As highlighted above, one goal of MSI is to characterize the metabolites that are present and their localization and abundance. In a rat cerebral ischemia reperfusion model, MALDI-MSI was used to obtain diverse metabolite profiles in both single mammalian cells and brain sections. The density, intensity, and distribution of over 30 metabolites covering nucleotides, cofactors, sugars, amino acids, lipids, and carboxylic acids were revealed.[105] Another study used quantitative MALDI-MSI together with CE-MS and visualized a spatiotemporal behavior of adenylates and

NADH regulated by ischemia reperfusion.[106] Application of SIMS for single cell measurements from tissue slices has been reported. Karlsson *et al.*[107] used high-resolution SIMS to probe the biochemical changes in situ altered by neurotoxin-induced brain pathology. In addition to endogenous metabolites, MSI can be used to study drugs, nutrients, and their related metabolites in cells, toward a fundamental understanding of in vivo distribution and metabolism of drugs.[108,109] Fernandez-Lima and colleagues[109] employed a 3D TOF-SIMS system to investigate the delivery and distribution of a chemotherapeutic drug in single cells with 250 nm spatial resolution. Chemical maps of molecular markers indicated the presence of the drug on the cell surface instead of the nucleus.

In addition to profiling metabolites at cellular or subcellular resolution across tissue slices, MALDI and SIMS imaging have also been used directly on dispersed cells. Lanni *et al.*[78] created a MALDI/SIMS dual source instrument with 5–250 μm resolution. Using the hybrid instrument, they imaged cultured *A. californica* neurons and neuronal networks (Figure 3.3).[78] Recently, an atmospheric pressure MALDI-MSI instrument was reported with 1.4 μm lateral resolution, over 100000 mass resolution, and an average accuracy below 2 ppm.[96] The authors were able to localize 220 peptides, lipids, and metabolites in cilia and oral grooves in a single *Paramecium caudatum*. The highest spatial resolution MSI so far uses nanoSIMS; Lovrić *et al.*[110] employed nanoSIMS and correlated the MS data with transmission electron microscopy. By combining these two techniques, they measured the distribution and dynamics of newly synthesized dopamine across single nanometer neuroendocrine vesicles in neuron-like cells.

3.4.3 Targeted metabolite analysis

The goal of many omics measurements is untargeted analysis; however, there are a number of important targeted metabolic single cell assays. While omics scale measurements lead to insight

into function and disease states, complementary targeted analysis provides critical information for many studies. There are also some metabolites that are difficult to characterize using traditional MS-based metabolomic methods. For instance, d-amino acids have been established as being present at biologically relevant concentrations and, in the case of d-serine, shown to have functional significance in the human brain.[111] Many metabolites, such as both l- and d-amino acids, can be differentiated and detected after derivatization, followed by CE with laser-induced fluorescence (LIF) detection. Thus, CE-LIF is effective for chiral measurements from single neurons and other cells.[112–114]

Metabolite-specific probes have also been employed. Fluorescent probes designed for cysteine, glutathione, and hydrogen peroxide were used in a microfluidic electrophoresis platform for single cell analysis; 12 fmol, 840 amol, and 0.49 amol of cysteine, glutathione, and hydrogen peroxide, respectively, were quantified through a multichannel fluorescence detector.[115] Heath *et al.*[116] successfully utilized immunoreactivity-based probes, implemented them in a barcode chip, and achieved simultaneous quantitation of metabolites such as cyclic adenosine monophosphate, cyclic guanosine monophosphate, glutathione, and proteins in single cells.

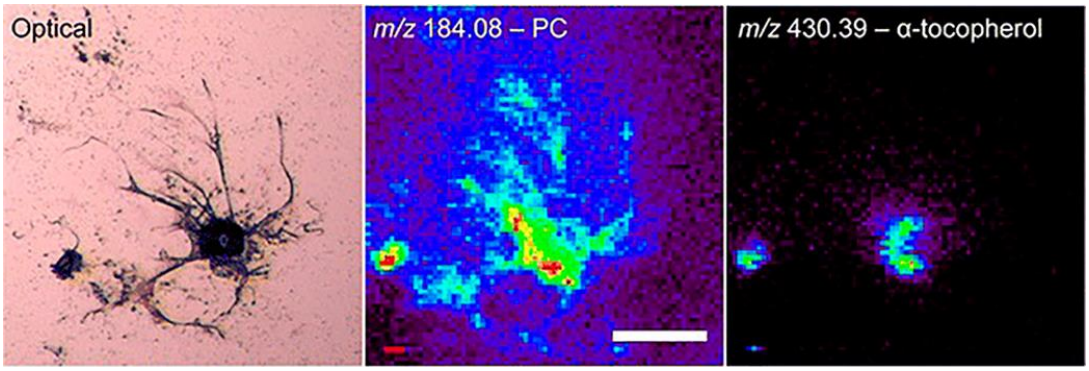

Figure 3.3. Distribution of metabolites in cultured *A. californica* buccal neurons was performed by C_{60}-SIMS imaging. Cells were cultured on silicon tiles and stabilized with glycerol. C_{60}-SIMS ion images revealed that phosphocholine (PC) and α-tocopherol showed different locations in neurons. Cell bodies and processes are apparent in the PC image (*m*/*z* 184.08, 0–200 counts), while α-tocopherol accumulated almost exclusively within the cell bodies (*m*/*z* 430.39, 0–50 counts).[78]

An important targeted approach for studying selected metabolites within single cells is electrochemical detection. Easily oxidizable neurotransmitters, such as dopamine and norepinephrine, are well suited for electrochemical-based approaches as they offer nano- to micromolar detection limits and can be used to assay selected cells, cellular release, and individual exocytosis events, as reported in several recent studies. Mao and colleagues[117] fabricated a carbon fiber microelectrode and achieved the first measurement of exocytosis of endogenous ascorbate from cultured adrenal chromaffin cells via single cell amperometry. A gold-ring pipet electrode was used to successfully detect catecholamines released from individual single chromaffin cells.[118] In addition, to measure release from living cells, electrochemistry has been used to uncover single cell spatial behavior. Ewing and co-workers[119] packed over 60 thin film microelectrodes into an array and measured chemicals released from different locations over a single cell surface during exocytosis. Further details on many of the recent advancements in the use of single cell electrochemistry for neuroscience research can be found in a variety of recent reviews.[120–123]

3.4.4 Integrating metabolomics with other omics-scale measurements

Investigations in the different omics disciplines have greatly enhanced scientists' understanding of specific biological systems, such as DNA, RNA, proteins, peptides, metabolites, and lipids. A trend but also a challenge is to integrate the omics fields of study, gain access to complementary information from different classes of molecules, and obtain a more comprehensive insight on processes occurring in biological systems as a whole. Early work in this field was not on the single cell scale but did include small volume analyses. Knolhoff, *et al.*[124] combined CE-MS metabolomics and gene array transcriptomics to study small caudal hippocampal samples in mice with a mas cell mutation. Combined analysis of the transcriptomic and metabolomic data led to the notation of pathways altered due to the loss of mast cells, which were evident from both

analyses. In another example, zebrafish embryos subjected to metabolomic analysis using NMR, LC–MS, and transcriptomic revealed metabolism dynamics and underlying gene expression during development.[125] More recently, Do, *et al.*,[126] profiled single cells from rat dorsal root ganglia (DRG) with high-mass and low-mass MALDI-TOF-MS for proteins, peptides, and lipids. They then performed LC-MS and ESI-FT-ICR-MS on DRG extracts to confidently identify the present molecules and classify cell types.

3.5 FUTURE PERSPECTIVES

As one of the important omics used in systems biology, metabolomics applies analytical tools coupled with bioinformatic approaches to determine the identity, abundance, flux, pathways, and even distribution of small molecular metabolites in biological systems. Metabolites are changed by a pathogenic status; accordingly, their comprehensive study helps to uncover mechanisms of action and facilitate the diagnosis of devastating diseases such as cancer. In brain cancer, for example, several investigations of serum and tumor tissue metabolomics using NMR or MS have been performed for tumor diagnosis, grade determination, type differentiation, etc.[127–129] With further improvements to single cell measurement approaches, which promise to lead to new insights in the diagnosis and treatment of brain tumors, it becomes feasible to understand the cell-by-cell transition from a normal to cancerous state.

The potential of single cell metabolomics has been recognized at the national level, as both metabolomics and single cell analysis were early foci of the National Institutes of Health's Common Fund Initiatives.[130] While a number of approaches have been outlined here that provide details on the chemical content of individual cells, this is a rapidly evolving measurement field, and further enhancements to performance are needed. Future technologies will boost the ability to probe the single cell brain metabolome. Obvious advances that are still needed include more

complete metabolome coverage, the addition of details on metabolite localization through MSI,[131] and improvements in small-scale sampling.[98] Perhaps the most important goal involves integration of the cellular omics, including transcriptomics, peptidomics, and proteomics. As our understanding of how gene transcription, translation, protein modifications, and metabolites interact to determine cell phenotype and fate, the integration of the data obtained will allow the most complete and accurate understanding of individual cells and their role in health and disease. The resulting single cell information will require improved approaches for processing the unique and large individual cell data sets. Collaborative efforts have resulted in shared data and common data formats for MSI, but these standards have yet to be applied to single cell data.

The metabolic content of cells, tissues, organs, and beyond reflect the phenotypic state of an individual at that time, in good or poor health. The evolving field of metabolomics will be crucial to precision medicine,[132] especially as we scale down to understanding disease on the single cell level.

3.6 REFERENCES

(1) Fessenden, M. Metabolomics: Small Molecules, Single Cells. *Nature* **2016**, *540* (7631), 153–155. https://doi.org/10.1038/540153a.

(2) Zenobi, R. Single-Cell Metabolomics: Analytical and Biological Perspectives. *Science* **2013**, *342* (6163), 1243259. https://doi.org/10.1126/science.1243259.

(3) Rubakhin, S. S.; Romanova, E. V.; Nemes, P.; Sweedler, J. V. Profiling Metabolites and Peptides in Single Cells. *Nat Meth* **2011**, *8* (4s), S20–S29. https://doi.org/10.1038/nmeth.1549.

(4) Rubakhin, S. S.; Lanni, E. J.; Sweedler, J. V. Progress toward Single Cell Metabolomics. *Current Opinion in Biotechnology* **2013**, *24* (1), 95–104. https://doi.org/10.1016/j.copbio.2012.10.021.

(5) Altschuler, S. J.; Wu, L. F. Cellular Heterogeneity: Do Differences Make a Difference? *Cell* **2010**, *141* (4), 559–563. https://doi.org/10.1016/j.cell.2010.04.033.

(6) Yang, L.; George, J.; Wang, J. Deep Profiling of Cellular Heterogeneity by Emerging Single-Cell Proteomic Technologies. *PROTEOMICS n/a* (n/a), 1900226. https://doi.org/10.1002/pmic.201900226.

(7) Nemes, P.; Knolhoff, A. M.; Rubakhin, S. S.; Sweedler, J. V. Single-Cell Metabolomics: Changes in the Metabolome of Freshly Isolated and Cultured Neurons. *ACS Chem. Neurosci.* **2012**, *3* (10), 782–792. https://doi.org/10.1021/cn300100u.

(8) Nemes, P.; Knolhoff, A. M.; Rubakhin, S. S.; Sweedler, J. V. Metabolic Differentiation of Neuronal Phenotypes by Single-Cell Capillary Electrophoresis–Electrospray Ionization-Mass Spectrometry. *Anal. Chem.* **2011**, *83* (17), 6810–6817. https://doi.org/10.1021/ac2015855.

(9) Jové, M.; Portero-Otín, M.; Naudí, A.; Ferrer, I.; Pamplona, R. Metabolomics of Human Brain Aging and Age-Related Neurodegenerative Diseases. *J Neuropathol Exp Neurol* **2014**, *73* (7), 640–657. https://doi.org/10.1097/NEN.0000000000000091.

(10) Hu, P.; Zhang, W.; Xin, H.; Deng, G. Single Cell Isolation and Analysis. *Front. Cell Dev. Biol.* **2016**, *4*. https://doi.org/10.3389/fcell.2016.00116.

(11) Cecala, C.; Sweedler, J. V. Sampling Techniques for Single-Cell Electrophoresis. *Analyst* **2012**, *137* (13), 2922–2929. https://doi.org/10.1039/C2AN16211C.

(12) Gallion, L. A.; Anttila, M. M.; Abraham, D. H.; Proctor, A.; Allbritton, N. L. Preserving Single Cells in Space and Time for Analytical Assays. *TrAC Trends in Analytical Chemistry* **2020**, *122*, 115723. https://doi.org/10.1016/j.trac.2019.115723.

(13) Miao, H.; Rubakhin, S. S.; Scanlan, C. R.; Wang, L.; Sweedler, J. V. D-Aspartate as a Putative Cell–Cell Signaling Molecule in the Aplysia Californica Central Nervous System.

Journal of Neurochemistry **2006**, *97* (2), 595–606. https://doi.org/10.1111/j.1471-4159.2006.03791.x.

(14) Kim, W.-S.; Dahlgren, R. L.; Moroz, L. L.; Sweedler, J. V. Ascorbic Acid Assays of Individual Neurons and Neuronal Tissues Using Capillary Electrophoresis with Laser-Induced Fluorescence Detection. *Anal. Chem.* **2002**, *74* (21), 5614–5620. https://doi.org/10.1021/ac025917q.

(15) Neupert, S.; Rubakhin, S. S.; Sweedler, J. V. Targeted Single-Cell Microchemical Analysis: MS-Based Peptidomics of Individual Paraformaldehyde-Fixed and Immunolabeled Neurons. *Chemistry & Biology* **2012**, *19* (8), 1010–1019. https://doi.org/10.1016/j.chembiol.2012.05.023.

(16) Rubakhin, S. S.; Churchill, J. D.; Greenough, W. T.; Sweedler, J. V. Profiling Signaling Peptides in Single Mammalian Cells Using Mass Spectrometry. *Anal. Chem.* **2006**, *78* (20), 7267–7272. https://doi.org/10.1021/ac0607010.

(17) Rubakhin, S. S.; Garden, R. W.; Fuller, R. R.; Sweedler, J. V. Measuring the Peptides in Individual Organelles with Mass Spectrometry. *Nature Biotechnology* **2000**, *18* (2), 172–175. https://doi.org/10.1038/72622.

(18) Rubakhin, S. S.; Greenough, W. T.; Sweedler, J. V. Spatial Profiling with MALDI-MS: Distribution of Neuropeptides within Single Neurons. *Anal. Chem.* **2003**, *75* (20), 5374–5380. https://doi.org/10.1021/ac034498+.

(19) Zhu, H.; Zou, G.; Wang, N.; Zhuang, M.; Xiong, W.; Huang, G. Single-Neuron Identification of Chemical Constituents, Physiological Changes, and Metabolism Using Mass Spectrometry. *PNAS* **2017**, *114* (10), 2586–2591. https://doi.org/10.1073/pnas.1615557114.

(20) Onjiko, R. M.; Portero, E. P.; Moody, S. A.; Nemes, P. In Situ Microprobe Single-Cell Capillary Electrophoresis Mass Spectrometry: Metabolic Reorganization in Single Differentiating Cells in the Live Vertebrate (Xenopus Laevis) Embryo. *Anal. Chem.* **2017**, *89* (13), 7069–7076. https://doi.org/10.1021/acs.analchem.7b00880.

(21) Guillaume-Gentil, O.; Rey, T.; Kiefer, P.; Ibáñez, A. J.; Steinhoff, R.; Brönnimann, R.; Dorwling-Carter, L.; Zambelli, T.; Zenobi, R.; Vorholt, J. A. Single-Cell Mass Spectrometry of Metabolites Extracted from Live Cells by Fluidic Force Microscopy. *Anal. Chem.* **2017**. https://doi.org/10.1021/acs.analchem.7b00367.

(22) Park, J.; Zhu, H.; O'Sullivan, S.; Ogunnaike, B. A.; Weaver, D. R.; Schwaber, J. S.; Vadigepalli, R. Single-Cell Transcriptional Analysis Reveals Novel Neuronal Phenotypes and Interaction Networks Involved in the Central Circadian Clock. *Front. Neurosci.* **2016**, *10*. https://doi.org/10.3389/fnins.2016.00481.

(23) Lloyd, R. V.; Qian, X.; Jin, L.; Ruebel, K.; Bayliss, J.; Zhang, S.; Kobayashi, I. Analysis of Pituitary Cells by Laser Capture Microdissection. In *Laser Capture Microdissection: Methods and Protocols*; Murray, G. I., Curran, S., Eds.; Methods in Molecular Biology™; Humana Press: Totowa, NJ, 2005; pp 233–241. https://doi.org/10.1385/1-59259-853-6:233.

(24) Watanabe, H.; Tanaka, F.; Doyu, M.; Riku, S.; Yoshida, M.; Hashizume, Y.; Sobue, G. Differential Somatic CAG Repeat Instability in Variable Brain Cell Lineage in Dentatorubral Pallidoluysian Atrophy (DRPLA): A Laser-Captured Microdissection (LCM)-Based Analysis. *Hum Genet* **2000**, *107* (5), 452–457. https://doi.org/10.1007/s004390000400.

(25) Grunewald, A.; Rygiel, K. A.; Hepplewhite, P. D.; Morris, C. M.; Picard, M.; Turnbull, D. M. Mitochondrial DNA Depletion in Respiratory Chain-Deficient Parkinson Disease Neurons. *Ann Neurol* **2016**, *79* (3), 366–378. https://doi.org/10.1002/ana.24571.

(26) Cecala, C.; S. Rubakhin, S.; W. Mitchell, J.; U. Gillette, M.; V. Sweedler, J. A Hyphenated Optical Trap Capillary Electrophoresis Laser Induced Native Fluorescence System for Single-Cell Chemical Analysis. *Analyst* **2012**, *137* (13), 2965–2972. https://doi.org/10.1039/C2AN35198F.

(27) Hosokawa, C.; Kudoh, S. N.; Kiyohara, A.; Taguchi, T. Optical Trapping of Synaptic Vesicles in Neurons. *Appl. Phys. Lett.* **2011**, *98* (16), 163705. https://doi.org/10.1063/1.3579191.

(28) Iv, C. W. S.; Reyes, C. D.; López, G. P. Microfluidic Cell Sorting: A Review of the Advances in the Separation of Cells from Debulking to Rare Cell Isolation. *Lab Chip* **2015**, *15* (5), 1230–1249. https://doi.org/10.1039/C4LC01246A.

(29) Prakadan, S. M.; Shalek, A. K.; Weitz, D. A. Scaling by Shrinking: Empowering Single-Cell "omics" with Microfluidic Devices. *Nat Rev Genet* **2017**, *18* (6), 345–361. https://doi.org/10.1038/nrg.2017.15.

(30) Zhang, Q.; Wang, T.; Zhou, Q.; Zhang, P.; Gong, Y.; Gou, H.; Xu, J.; Ma, B. Development of a Facile Droplet-Based Single-Cell Isolation Platform for Cultivation and Genomic Analysis in Microorganisms. *Sci Rep* **2017**, *7* (1), 1–11. https://doi.org/10.1038/srep41192.

(31) Wen, N.; Zhao, Z.; Fan, B.; Chen, D.; Men, D.; Wang, J.; Chen, J. Development of Droplet Microfluidics Enabling High-Throughput Single-Cell Analysis. *Molecules* **2016**, *21* (7), 881. https://doi.org/10.3390/molecules21070881.

(32) Zhang, W.; Li, N.; Lin, L.; Huang, Q.; Uchiyama, K.; Lin, J.-M. Concentrating Single Cells in Picoliter Droplets for Phospholipid Profiling on a Microfluidic System. *Small n/a* (n/a), 1903402. https://doi.org/10.1002/smll.201903402.

(33) Zhao, L.; Ma, C.; Shen, S.; Tian, C.; Xu, J.; Tu, Q.; Li, T.; Wang, Y.; Wang, J. Pneumatic Microfluidics-Based Multiplex Single-Cell Array. *Biosensors and Bioelectronics* **2016**, *78*, 423–430. https://doi.org/10.1016/j.bios.2015.09.055.

(34) Lee, C. Y.; Fan, Y.; Rubakhin, S. S.; Yoon, S.; Sweedler, J. V. A Neuron-in-Capillary Platform for Facile Collection and Mass Spectrometric Characterization of a Secreted Neuropeptide. *Sci Rep* **2016**, *6*. https://doi.org/10.1038/srep26940.

(35) Guez-Barber, D.; Fanous, S.; Harvey, B. K.; Zhang, Y.; Lehrmann, E.; Becker, K. G.; Picciotto, M. R.; Hope, B. T. FACS Purification of Immunolabeled Cell Types from Adult Rat Brain. *Journal of Neuroscience Methods* **2012**, *203* (1), 10–18. https://doi.org/10.1016/j.jneumeth.2011.08.045.

(36) Schwarz, J. M. Using Fluorescence Activated Cell Sorting to Examine Cell-Type-Specific Gene Expression in Rat Brain Tissue. *JoVE (Journal of Visualized Experiments)* **2015**, No. 99, e52537–e52537. https://doi.org/10.3791/52537.

(37) Welzel, G.; Seitz, D.; Schuster, S. Magnetic-Activated Cell Sorting (MACS) Can Be Used as a Large-Scale Method for Establishing Zebrafish Neuronal Cell Cultures. *Scientific Reports* **2015**, *5*, 7959. https://doi.org/10.1038/srep07959.

(38) Fujii, T.; Matsuda, S.; Tejedor, M. L.; Esaki, T.; Sakane, I.; Mizuno, H.; Tsuyama, N.; Masujima, T. Direct Metabolomics for Plant Cells by Live Single-Cell Mass Spectrometry. *Nat. Protocols* **2015**, *10* (9), 1445–1456. https://doi.org/10.1038/nprot.2015.084.

(39) Ibáñez, A. J.; Fagerer, S. R.; Schmidt, A. M.; Urban, P. L.; Jefimovs, K.; Geiger, P.; Dechant, R.; Heinemann, M.; Zenobi, R. Mass Spectrometry-Based Metabolomics of Single Yeast Cells. *PNAS* **2013**, *110* (22), 8790–8794. https://doi.org/10.1073/pnas.1209302110.

(40) Dettmer, K.; Aronov, P. A.; Hammock, B. D. Mass Spectrometry-Based Metabolomics. *Mass Spectrom. Rev.* **2007**, *26* (1), 51–78. https://doi.org/10.1002/mas.20108.

(41) Comi, T. J.; Do, T. D.; Rubakhin, S. S.; Sweedler, J. V. Categorizing Cells on the Basis of Their Chemical Profiles: Progress in Single-Cell Mass Spectrometry. *J. Am. Chem. Soc.* **2017**, *139* (11), 3920–3929. https://doi.org/10.1021/jacs.6b12822.

(42) Ramautar, R.; Somsen, G. W.; de Jong, G. J. CE-MS for Metabolomics: Developments and Applications in the Period 2010–2012. *ELECTROPHORESIS* **2013**, *34* (1), 86–98. https://doi.org/10.1002/elps.201200390.

(43) García, A.; Godzien, J.; López-Gonzálvez, Á.; Barbas, C. Capillary Electrophoresis Mass Spectrometry as a Tool for Untargeted Metabolomics. *Bioanalysis* **2016**, *9* (1), 99–130. https://doi.org/10.4155/bio-2016-0216.

(44) Ramautar, R.; Somsen, G. W.; Jong, G. J. de. CE-MS for Metabolomics: Developments and Applications in the Period 2016–2018. *ELECTROPHORESIS* **2019**, *40* (1), 165–179. https://doi.org/10.1002/elps.201800323.

(45) Liu, J.-X.; Aerts, J. T.; Rubakhin, S. S.; Zhang, X.-X.; Sweedler, J. V. Analysis of Endogenous Nucleotides by Single Cell Capillary Electrophoresis-Mass Spectrometry. *The Analyst* **2014**, *139* (22), 5835. https://doi.org/10.1039/c4an01133c.

(46) Aerts, J. T.; Louis, K. R.; Crandall, S. R.; Govindaiah, G.; Cox, C. L.; Sweedler, J. V. Patch Clamp Electrophysiology and Capillary Electrophoresis–Mass Spectrometry Metabolomics for Single Cell Characterization. *Anal. Chem.* **2014**, *86* (6), 3203–3208. https://doi.org/10.1021/ac500168d.

(47) Yamamoto, M.; Ly, R.; Gill, B.; Zhu, Y.; Moran-Mirabal, J.; Britz-McKibbin, P. Robust and High-Throughput Method for Anionic Metabolite Profiling: Preventing Polyimide Aminolysis and Capillary Breakages under Alkaline Conditions in Capillary Electrophoresis-Mass

Spectrometry. *Anal. Chem.* **2016**, *88* (21), 10710–10719. https://doi.org/10.1021/acs.analchem.6b03269.

(48) Mellors, J. S.; Jorabchi, K.; Smith, L. M.; Ramsey, J. M. Integrated Microfluidic Device for Automated Single Cell Analysis Using Electrophoretic Separation and Electrospray Ionization Mass Spectrometry. *Anal. Chem.* **2010**, *82* (3), 967–973. https://doi.org/10.1021/ac902218y.

(49) Wei, Z.; Xiong, X.; Guo, C.; Si, X.; Zhao, Y.; He, M.; Yang, C.; Xu, W.; Tang, F.; Fang, X.; et al. Pulsed Direct Current Electrospray: Enabling Systematic Analysis of Small Volume Sample by Boosting Sample Economy. *Anal. Chem.* **2015**, *87* (22), 11242–11248. https://doi.org/10.1021/acs.analchem.5b02115.

(50) Gong, X.; Zhao, Y.; Cai, S.; Fu, S.; Yang, C.; Zhang, S.; Zhang, X. Single Cell Analysis with Probe ESI-Mass Spectrometry: Detection of Metabolites at Cellular and Subcellular Levels. *Anal. Chem.* **2014**, *86* (8), 3809–3816. https://doi.org/10.1021/ac500882e.

(51) Zhang, X.-C.; Wei, Z.-W.; Gong, X.-Y.; Si, X.-Y.; Zhao, Y.-Y.; Yang, C.-D.; Zhang, S.-C.; Zhang, X.-R. Integrated Droplet-Based Microextraction with ESI-MS for Removal of Matrix Interference in Single-Cell Analysis. *Sci Rep* **2016**, *6* (1), 1–9. https://doi.org/10.1038/srep24730.

(52) Pan, N.; Rao, W.; Kothapalli, N. R.; Liu, R.; Burgett, A. W. G.; Yang, Z. The Single-Probe: A Miniaturized Multifunctional Device for Single Cell Mass Spectrometry Analysis. *Anal. Chem.* **2014**, *86* (19), 9376–9380. https://doi.org/10.1021/ac5029038.

(53) Pan, N.; Rao, W.; Standke, S. J.; Yang, Z. Using Dicationic Ion-Pairing Compounds To Enhance the Single Cell Mass Spectrometry Analysis Using the Single-Probe: A Microscale Sampling and Ionization Device. *Anal. Chem.* **2016**, *88* (13), 6812–6819. https://doi.org/10.1021/acs.analchem.6b01284.

(54) Hiyama, E.; Ali, A.; Amer, S.; Harada, T.; Shimamoto, K.; Furushima, R.; Abouleila, Y.; Emara, S.; Masujima, T. Direct Lipido-Metabolomics of Single Floating Cells for Analysis of Circulating Tumor Cells by Live Single-Cell Mass Spectrometry. *Analytical Sciences* **2015**, *31* (12), 1215–1217. https://doi.org/10.2116/analsci.31.1215.

(55) Esaki, T.; Masujima, T. Fluorescence Probing Live Single-Cell Mass Spectrometry for Direct Analysis of Organelle Metabolism. *Analytical Sciences* **2015**, *31* (12), 1211–1213. https://doi.org/10.2116/analsci.31.1211.

(56) Rao, W.; Pan, N.; Yang, Z. High Resolution Tissue Imaging Using the Single-Probe Mass Spectrometry under Ambient Conditions. *J. Am. Soc. Mass Spectrom.* **2015**, *26* (6), 986–993. https://doi.org/10.1007/s13361-015-1091-4.

(57) Li, L.; Garden, R. W.; Sweedler, J. V. Single-Cell MALDI: A New Tool for Direct Peptide Profiling. *Trends in Biotechnology* **2000**, *18* (4), 151–160. https://doi.org/10.1016/S0167-7799(00)01427-X.

(58) Clark, A. E.; Kaleta, E. J.; Arora, A.; Wolk, D. M. Matrix-Assisted Laser Desorption Ionization–Time of Flight Mass Spectrometry: A Fundamental Shift in the Routine Practice of Clinical Microbiology. *Clinical Microbiology Reviews* **2013**, *26* (3), 547–603. https://doi.org/10.1128/CMR.00072-12.

(59) Yang, N.; Irving, S. J.; Romanova, E. V.; Mitchell, J. W.; Gillette, M. U.; Sweedler, J. V. Neuropeptidomics. In *Molecular Neuroendocrinology*; John Wiley & Sons, Ltd, 2016; pp 155–169. https://doi.org/10.1002/9781118760369.ch8.

(60) Garden, R. W.; Moroz, L. L.; Moroz, T. P.; Shippy, S. A.; Sweedler, J. V. Excess Salt Removal with Matrix Rinsing: Direct Peptide Profiling of Neurons from Marine Invertebrates Using Matrix-Assisted Laser Desorption/Ionization Time-of-Flight Mass Spectrometry. *Journal*

of Mass Spectrometry **1996**, *31* (10), 1126–1130. https://doi.org/10.1002/(SICI)1096-9888(199610)31:10<1126::AID-JMS403>3.0.CO;2-7.

(61) Jimenez, C. R.; Veelen, P. A. van; Li, K. W.; Wildering, W. C.; Geraerts, W. P. M.; Tjaden, U. R.; Greef, J. van der. Rapid Communication: Neuropeptide Expression and Processing as Revealed by Direct Matrix-Assisted Laser Desorption Ionization Mass Spectrometry of Single Neurons. *Journal of Neurochemistry* **1994**, *62* (1), 404–407. https://doi.org/10.1046/j.1471-4159.1994.62010404.x.

(62) Jiménez, C. R.; Li, K. W.; Dreisewerd, K.; Spijker, S.; Kingston, R.; Bateman, R. H.; Burlingame, A. L.; Smit, A. B.; van Minnen, J.; Geraerts, W. P. M. Direct Mass Spectrometric Peptide Profiling and Sequencing of Single Neurons Reveals Differential Peptide Patterns in a Small Neuronal Network. *Biochemistry* **1998**, *37* (7), 2070–2076. https://doi.org/10.1021/bi971848b.

(63) Neupert, S.; Predel, R. Mass Spectrometric Analysis of Single Identified Neurons of an Insect. *Biochemical and Biophysical Research Communications* **2005**, *327* (3), 640–645. https://doi.org/10.1016/j.bbrc.2004.12.086.

(64) Skiebe, P.; Dreger, M.; Meseke, M.; Evers, J. F.; Hucho, F. Identification of orcokinins in single neurons in the stomatogastric nervous system of the crayfish, Cherax destructor. *Journal of Comparative Neurology* **2002**, *444* (3), 245–259. https://doi.org/10.1002/cne.10145.

(65) Neupert, S.; Predel, R.; Russell, W. K.; Davies, R.; Pietrantonio, P. V.; Nachman, R. J. Identification of Tick Periviscerokinin, the First Neurohormone of Ixodidae: Single Cell Analysis by Means of MALDI-TOF/TOF Mass Spectrometry. *Biochemical and Biophysical Research Communications* **2005**, *338* (4), 1860–1864. https://doi.org/10.1016/j.bbrc.2005.10.165.

(66) Fujisawa, Y.; Furukawa, Y.; Ohta, S.; Ellis, T. A.; Dembrow, N. C.; Li, L.; Floyd, P. D.; Sweedler, J. V.; Minakata, H.; Nakamaru, K.; et al. The Aplysia Mytilus Inhibitory Peptide-Related Peptides: Identification, Cloning, Processing, Distribution, and Action. *J. Neurosci.* **1999**, *19* (21), 9618–9634. https://doi.org/10.1523/JNEUROSCI.19-21-09618.1999.

(67) Ong, T.-H.; Kissick, D. J.; Jansson, E. T.; Comi, T. J.; Romanova, E. V.; Rubakhin, S. S.; Sweedler, J. V. Classification of Large Cellular Populations and Discovery of Rare Cells Using Single Cell Matrix-Assisted Laser Desorption/Ionization Time-of-Flight Mass Spectrometry. *Anal. Chem.* **2015**, *87* (14), 7036–7042. https://doi.org/10.1021/acs.analchem.5b01557.

(68) Jansson, E. T.; Comi, T. J.; Rubakhin, S. S.; Sweedler, J. V. Single Cell Peptide Heterogeneity of Rat Islets of Langerhans. *ACS Chem. Biol.* **2016**, *11* (9), 2588–2595. https://doi.org/10.1021/acschembio.6b00602.

(69) Comi, T. J.; Neumann, E. K.; Do, T. D.; Sweedler, J. V. MicroMS: A Python Platform for Image-Guided Mass Spectrometry Profiling. *J. Am. Soc. Mass Spectrom.* **2017**, *28* (9), 1919–1928. https://doi.org/10.1007/s13361-017-1704-1.

(70) Römpp, A.; Spengler, B. Mass Spectrometry Imaging with High Resolution in Mass and Space. *Histochem Cell Biol* **2013**, *139* (6), 759–783. https://doi.org/10.1007/s00418-013-1097-6.

(71) Moreno-Gordaliza, E.; Esteban-Fernández, D.; Lázaro, A.; Humanes, B.; Aboulmagd, S.; Tejedor, A.; Linscheid, M. W.; Gómez-Gómez, M. M. MALDI-LTQ-Orbitrap Mass Spectrometry Imaging for Lipidomic Analysis in Kidney under Cisplatin Chemotherapy. *Talanta* **2017**, *164*, 16–26. https://doi.org/10.1016/j.talanta.2016.11.026.

(72) Buck, A.; Ly, A.; Balluff, B.; Sun, N.; Gorzolka, K.; Feuchtinger, A.; Janssen, K.-P.; Kuppen, P. J.; van de Velde, C. J.; Weirich, G.; et al. High-Resolution MALDI-FT-ICR MS

Imaging for the Analysis of Metabolites from Formalin-Fixed, Paraffin-Embedded Clinical Tissue Samples. *J. Pathol.* **2015**, *237* (1), 123–132. https://doi.org/10.1002/path.4560.

(73) Neumann, E. K.; Ellis, J. F.; Triplett, A. E.; Rubakhin, S. S.; Sweedler, J. V. Lipid Analysis of 30 000 Individual Rodent Cerebellar Cells Using High-Resolution Mass Spectrometry. *Anal. Chem.* **2019**, *91* (12), 7871–7878. https://doi.org/10.1021/acs.analchem.9b01689.

(74) Tucker, K. R.; Li, Z.; Rubakhin, S. S.; Sweedler, J. V. Secondary Ion Mass Spectrometry Imaging of Molecular Distributions in Cultured Neurons and Their Processes: Comparative Analysis of Sample Preparation. *J. Am. Soc. Mass Spectrom.* **2012**, *23* (11), 1931–1938. https://doi.org/10.1007/s13361-012-0472-1.

(75) Ostrowski, S. G.; Bell, C. T. V.; Winograd, N.; Ewing, A. G. Mass Spectrometric Imaging of Highly Curved Membranes During Tetrahymena Mating. *Science* **2004**, *305* (5680), 71–73. https://doi.org/10.1126/science.1099791.

(76) Durairaj, A.; Winograd, N. Tandem MS and C60 SIMS for the Identification and Characterization of Lipids. *Surface and Interface Analysis* **2014**, *46* (S1), 118–122. https://doi.org/10.1002/sia.5664.

(77) Fisher, G. L.; Bruinen, A. L.; Ogrinc Potočnik, N.; Hammond, J. S.; Bryan, S. R.; Larson, P. E.; Heeren, R. M. A. A New Method and Mass Spectrometer Design for TOF-SIMS Parallel Imaging MS/MS. *Anal. Chem.* **2016**, *88* (12), 6433–6440. https://doi.org/10.1021/acs.analchem.6b01022.

(78) Lanni, E. J.; Dunham, S. J. B.; Nemes, P.; Rubakhin, S. S.; Sweedler, J. V. Biomolecular Imaging with a C60-SIMS/MALDI Dual Ion Source Hybrid Mass Spectrometer: Instrumentation, Matrix Enhancement, and Single Cell Analysis. *J. Am. Soc. Mass Spectrom.* **2014**, *25* (11), 1897–1907. https://doi.org/10.1007/s13361-014-0978-9.

(79) Denbigh, J. L.; Lockyer, N. P. ToF-SIMS as a Tool for Profiling Lipids in Cancer and Other Diseases. *Materials Science and Technology* **2015**, *31* (2), 137–147. https://doi.org/10.1179/1743284714Y.0000000648.

(80) Fletcher, J. S.; Kotze, H. L.; Armitage, E. G.; Lockyer, N. P.; Vickerman, J. C. Evaluating the Challenges Associated with Time-of-Fight Secondary Ion Mass Spectrometry for Metabolomics Using Pure and Mixed Metabolites. *Metabolomics* **2013**, *9* (3), 535–544. https://doi.org/10.1007/s11306-012-0487-4.

(81) Passarelli, M. K.; Ewing, A. G.; Winograd, N. Single-Cell Lipidomics: Characterizing and Imaging Lipids on the Surface of Individual Aplysia Californica Neurons with Cluster Secondary Ion Mass Spectrometry. *Anal. Chem.* **2013**, *85* (4), 2231–2238. https://doi.org/10.1021/ac303038j.

(82) Passarelli, M. K.; Winograd, N. Lipid Imaging with Time-of-Flight Secondary Ion Mass Spectrometry (ToF-SIMS). *Biochimica et Biophysica Acta (BBA) - Molecular and Cell Biology of Lipids* **2011**, *1811* (11), 976–990. https://doi.org/10.1016/j.bbalip.2011.05.007.

(83) Monroe, E. B.; Jurchen, J. C.; Lee, J.; Rubakhin, S. S.; Sweedler, J. V. Vitamin E Imaging and Localization in the Neuronal Membrane. *J. Am. Chem. Soc.* **2005**, *127* (35), 12152–12153. https://doi.org/10.1021/ja051223y.

(84) Fletcher, J. S.; Lockyer, N. P.; Vaidyanathan, S.; Vickerman, J. C. TOF-SIMS 3D Biomolecular Imaging of Xenopus Laevis Oocytes Using Buckminsterfullerene (C60) Primary Ions. *Anal. Chem.* **2007**, *79* (6), 2199–2206. https://doi.org/10.1021/ac061370u.

(85) Do, T. D.; Comi, T. J.; Dunham, S. J. B.; Rubakhin, S. S.; Sweedler, J. V. Single Cell Profiling Using Ionic Liquid Matrix-Enhanced Secondary Ion Mass Spectrometry for Neuronal Cell Type Differentiation. *Anal. Chem.* **2017**, *89* (5), 3078–3086. https://doi.org/10.1021/acs.analchem.6b04819.

(86) Pirro, V.; Oliveri, P.; Ferreira, C. R.; González-Serrano, A. F.; Machaty, Z.; Cooks, R. G. Lipid Characterization of Individual Porcine Oocytes by Dual Mode DESI-MS and Data Fusion. *Analytica Chimica Acta* **2014**, *848*, 51–60. https://doi.org/10.1016/j.aca.2014.08.001.

(87) González-Serrano, A. F.; Pirro, V.; Ferreira, C. R.; Oliveri, P.; Eberlin, L. S.; Heinzmann, J.; Lucas-Hahn, A.; Niemann, H.; Cooks, R. G. Desorption Electrospray Ionization Mass Spectrometry Reveals Lipid Metabolism of Individual Oocytes and Embryos. *PLOS ONE* **2013**, *8* (9), e74981. https://doi.org/10.1371/journal.pone.0074981.

(88) Nemes, P.; Vertes, A. Laser Ablation Electrospray Ionization for Atmospheric Pressure, in Vivo, and Imaging Mass Spectrometry. *Anal. Chem.* **2007**, *79* (21), 8098–8106. https://doi.org/10.1021/ac071181r.

(89) Shrestha, B.; Sripadi, P.; Reschke, B. R.; Henderson, H. D.; Powell, M. J.; Moody, S. A.; Vertes, A. Subcellular Metabolite and Lipid Analysis of Xenopus Laevis Eggs by LAESI Mass Spectrometry. *PLOS ONE* **2014**, *9* (12), e115173. https://doi.org/10.1371/journal.pone.0115173.

(90) Tsao, C.-W.; Lin, Y.-J.; Chen, P.-Y.; Yang, Y.-L.; Tan, S. H. Nanoscale Silicon Surface-Assisted Laser Desorption/Ionization Mass Spectrometry: Environment Stability and Activation by Simple Vacuum Oven Desiccation. *Analyst* **2016**, *141* (16), 4973–4981. https://doi.org/10.1039/C6AN00659K.

(91) Trauger, S. A.; Go, E. P.; Shen, Z.; Apon, J. V.; Compton, B. J.; Bouvier, E. S. P.; Finn, M. G.; Siuzdak, G. High Sensitivity and Analyte Capture with Desorption/Ionization Mass Spectrometry on Silylated Porous Silicon. *Anal. Chem.* **2004**, *76* (15), 4484–4489. https://doi.org/10.1021/ac049657j.

(92) Walker, B. N.; Stolee, J. A.; Vertes, A. Nanophotonic Ionization for Ultratrace and Single-Cell Analysis by Mass Spectrometry. *Anal. Chem.* **2012**, *84* (18), 7756–7762. https://doi.org/10.1021/ac301238k.

(93) Korte, A. R.; Stopka, S. A.; Morris, N.; Razunguzwa, T.; Vertes, A. Large-Scale Metabolite Analysis of Standards and Human Serum by Laser Desorption Ionization Mass Spectrometry from Silicon Nanopost Arrays. *Anal. Chem.* **2016**, *88* (18), 8989–8996. https://doi.org/10.1021/acs.analchem.6b01186.

(94) Römpp, A.; Guenther, S.; Takats, Z.; Spengler, B. Mass Spectrometry Imaging with High Resolution in Mass and Space (HR2 MSI) for Reliable Investigation of Drug Compound Distributions on the Cellular Level. *Anal Bioanal Chem* **2011**, *401* (1), 65–73. https://doi.org/10.1007/s00216-011-4990-7.

(95) Römpp, A.; Guenther, S.; Schober, Y.; Schulz, O.; Takats, Z.; Kummer, W.; Spengler, B. Histology by Mass Spectrometry: Label-Free Tissue Characterization Obtained from High-Accuracy Bioanalytical Imaging. *Angewandte Chemie International Edition* **2010**, *49* (22), 3834–3838. https://doi.org/10.1002/anie.200905559.

(96) Kompauer, M.; Heiles, S.; Spengler, B. Atmospheric Pressure MALDI Mass Spectrometry Imaging of Tissues and Cells at 1.4-Mm Lateral Resolution. *Nat Meth* **2017**, *14* (1), 90–96. https://doi.org/10.1038/nmeth.4071.

(97) Neumann, E. K.; Comi, T. J.; Spegazzini, N.; Mitchell, J. W.; Rubakhin, S. S.; Gillette, M. U.; Bhargava, R.; Sweedler, J. V. Multimodal Chemical Analysis of the Brain by High Mass Resolution Mass Spectrometry and Infrared Spectroscopic Imaging. *Anal. Chem.* **2018**, *90* (19), 11572–11580. https://doi.org/10.1021/acs.analchem.8b02913.

(98) Lapainis, T.; Rubakhin, S. S.; Sweedler, J. V. Capillary Electrophoresis with Electrospray Ionization Mass Spectrometric Detection for Single-Cell Metabolomics. *Anal. Chem.* **2009**, *81* (14), 5858–5864. https://doi.org/10.1021/ac900936g.

(99) Onjiko, R. M.; Moody, S. A.; Nemes, P. Single-Cell Mass Spectrometry Reveals Small Molecules That Affect Cell Fates in the 16-Cell Embryo. *PNAS* **2015**, *112* (21), 6545–6550. https://doi.org/10.1073/pnas.1423682112.

(100) Kohler, I.; Schappler, J.; Rudaz, S. Highly Sensitive Capillary Electrophoresis-Mass Spectrometry for Rapid Screening and Accurate Quantitation of Drugs of Abuse in Urine. *Anal. Chim. Acta* **2013**, *780*, 101–109. https://doi.org/10.1016/j.aca.2013.03.065.

(101) Acunha, T.; Simó, C.; Ibáñez, C.; Gallardo, A.; Cifuentes, A. Anionic Metabolite Profiling by Capillary Electrophoresis–Mass Spectrometry Using a Noncovalent Polymeric Coating. Orange Juice and Wine as Case Studies. *Journal of Chromatography A* **2016**, *1428*, 326–335. https://doi.org/10.1016/j.chroma.2015.08.001.

(102) Ramautar, R.; Busnel, J.-M.; Deelder, A. M.; Mayboroda, O. A. Enhancing the Coverage of the Urinary Metabolome by Sheathless Capillary Electrophoresis-Mass Spectrometry. *Anal. Chem.* **2012**, *84* (2), 885–892. https://doi.org/10.1021/ac202407v.

(103) Gulersonmez, M. C.; Lock, S.; Hankemeier, T.; Ramautar, R. Sheathless Capillary Electrophoresis-Mass Spectrometry for Anionic Metabolic Profiling. *ELECTROPHORESIS* **2016**, *37* (7–8), 1007–1014. https://doi.org/10.1002/elps.201500435.

(104) Yuan, F.; Zhang, X.-H.; Nie, J.; Chen, H.-X.; Zhou, Y.-L.; Zhang, X.-X. Ultrasensitive Determination of 5-Methylcytosine and 5-Hydroxymethylcytosine in Genomic DNA by Sheathless Interfaced Capillary Electrophoresis–Mass Spectrometry. *Chem. Commun.* **2016**, *52* (13), 2698–2700. https://doi.org/10.1039/C5CC10155G.

(105) Miura, D.; Fujimura, Y.; Yamato, M.; Hyodo, F.; Utsumi, H.; Tachibana, H.; Wariishi, H. Ultrahighly Sensitive in Situ Metabolomic Imaging for Visualizing Spatiotemporal Metabolic Behaviors. *Anal. Chem.* **2010**, *82* (23), 9789–9796. https://doi.org/10.1021/ac101998z.

(106) Hattori, K.; Kajimura, M.; Hishiki, T.; Nakanishi, T.; Kubo, A.; Nagahata, Y.; Ohmura, M.; Yachie-Kinoshita, A.; Matsuura, T.; Morikawa, T.; et al. Paradoxical ATP Elevation in Ischemic Penumbra Revealed by Quantitative Imaging Mass Spectrometry. *Antioxidants & Redox Signaling* **2010**, *13* (8), 1157–1167. https://doi.org/10.1089/ars.2010.3290.

(107) Hanrieder, J.; Gerber, L.; Persson Sandelius, Å.; Brittebo, E. B.; Ewing, A. G.; Karlsson, O. High Resolution Metabolite Imaging in the Hippocampus Following Neonatal Exposure to the Environmental Toxin BMAA Using ToF-SIMS. *ACS Chem. Neurosci.* **2014**, *5* (7), 568–575. https://doi.org/10.1021/cn500039b.

(108) Passarelli, M. K.; Newman, C. F.; Marshall, P. S.; West, A.; Gilmore, I. S.; Bunch, J.; Alexander, M. R.; Dollery, C. T. Single-Cell Analysis: Visualizing Pharmaceutical and Metabolite Uptake in Cells with Label-Free 3D Mass Spectrometry Imaging. *Anal. Chem.* **2015**, *87* (13), 6696–6702. https://doi.org/10.1021/acs.analchem.5b00842.

(109) Vanbellingen, Q. P.; Castellanos, A.; Rodriguez-Silva, M.; Paudel, I.; Chambers, J. W.; Fernandez-Lima, F. A. Analysis of Chemotherapeutic Drug Delivery at the Single Cell Level Using 3D-MSI-TOF-SIMS. *J. Am. Soc. Mass Spectrom.* **2016**, *27* (12), 2033–2040. https://doi.org/10.1007/s13361-016-1485-y.

(110) Lovrić, J.; Dunevall, J.; Larsson, A.; Ren, L.; Andersson, S.; Meibom, A.; Malmberg, P.; Kurczy, M. E.; Ewing, A. G. Nano Secondary Ion Mass Spectrometry Imaging of Dopamine Distribution Across Nanometer Vesicles. *ACS Nano* **2017**, *11* (4), 3446–3455. https://doi.org/10.1021/acsnano.6b07233.

(111) Wolosker, H.; Dumin, E.; Balan, L.; Foltyn, V. N. D-Amino Acids in the Brain: D-Serine in Neurotransmission and Neurodegeneration. *FEBS Journal* **2008**, *275* (14), 3514–3526. https://doi.org/10.1111/j.1742-4658.2008.06515.x.

(112) Jakó, T.; Szabó, E.; Tábi, T.; Zachar, G.; Csillag, A.; Szökő, É. Chiral Analysis of Amino Acid Neurotransmitters and Neuromodulators in Mouse Brain by CE-LIF. *ELECTROPHORESIS* **2014**, *35* (19), 2870–2876. https://doi.org/10.1002/elps.201400224.

(113) Ota, N.; Rubakhin, S. S.; Sweedler, J. V. D-Alanine in the Islets of Langerhans of Rat Pancreas. *Biochemical and Biophysical Research Communications* **2014**, *447* (2), 328–333. https://doi.org/10.1016/j.bbrc.2014.03.153.

(114) Scanlan, C.; Shi, T.; Hatcher, N. G.; Rubakhin, S. S.; Sweedler, J. V. Synthesis, Accumulation, and Release of d-Aspartate in the Aplysia Californica CNS. *Journal of Neurochemistry* **2010**, *115* (5), 1234–1244. https://doi.org/10.1111/j.1471-4159.2010.07020.x.

(115) Li, Q.; Chen, P.; Fan, Y.; Wang, X.; Xu, K.; Li, L.; Tang, B. Multicolor Fluorescence Detection-Based Microfluidic Device for Single-Cell Metabolomics: Simultaneous Quantitation of Multiple Small Molecules in Primary Liver Cells. *Anal. Chem.* **2016**, *88* (17), 8610–8616. https://doi.org/10.1021/acs.analchem.6b01775.

(116) Xue, M.; Wei, W.; Su, Y.; Kim, J.; Shin, Y. S.; Mai, W. X.; Nathanson, D. A.; Heath, J. R. Chemical Methods for the Simultaneous Quantitation of Metabolites and Proteins from Single Cells. *J. Am. Chem. Soc.* **2015**, *137* (12), 4066–4069. https://doi.org/10.1021/jacs.5b00944.

(117) Wang, K.; Xiao, T.; Yue, Q.; Wu, F.; Yu, P.; Mao, L. Selective Amperometric Recording of Endogenous Ascorbate Secretion from a Single Rat Adrenal Chromaffin Cell with Pretreated Carbon Fiber Microelectrodes. *Anal. Chem.* **2017**, *89* (17), 9502–9507. https://doi.org/10.1021/acs.analchem.7b02508.

(118) Wang, K.; Zhao, X.; Li, B.; Wang, K.; Zhang, X.; Mao, L.; Ewing, A.; Lin, Y. Ultrasonic-Aided Fabrication of Nanostructured Au-Ring Microelectrodes for Monitoring Transmitters Released from Single Cells. *Anal. Chem.* **2017**, *89* (17), 8683–8688. https://doi.org/10.1021/acs.analchem.7b02814.

(119) Wang, J.; Trouillon, R.; Dunevall, J.; Ewing, A. G. Spatial Resolution of Single-Cell Exocytosis by Microwell-Based Individually Addressable Thin Film Ultramicroelectrode Arrays. *Anal. Chem.* **2014**, *86* (9), 4515–4520. https://doi.org/10.1021/ac500443q.

(120) Amatore, C.; Arbault, S.; Guille, M.; Lemaître, F. Electrochemical Monitoring of Single Cell Secretion: Vesicular Exocytosis and Oxidative Stress. *Chem. Rev.* **2008**, *108* (7), 2585–2621. https://doi.org/10.1021/cr068062g.

(121) Actis, P.; Tokar, S.; Clausmeyer, J.; Babakinejad, B.; Mikhaleva, S.; Cornut, R.; Takahashi, Y.; López Córdoba, A.; Novak, P.; Shevchuck, A. I.; et al. Electrochemical Nanoprobes for Single-Cell Analysis. *ACS Nano* **2014**, *8* (1), 875–884. https://doi.org/10.1021/nn405612q.

(122) Bucher, E. S.; Wightman, R. M. Electrochemical Analysis of Neurotransmitters http://www.annualreviews.org/doi/10.1146/annurev-anchem-071114-040426 (accessed Apr 12, 2017).

(123) Clausmeyer, J.; Schuhmann, W. Nanoelectrodes: Applications in Electrocatalysis, Single-Cell Analysis and High-Resolution Electrochemical Imaging. *TrAC Trends in Analytical Chemistry* **2016**, *79*, 46–59. https://doi.org/10.1016/j.trac.2016.01.018.

(124) Knolhoff, A. M.; Nautiyal, K. M.; Nemes, P.; Kalachikov, S.; Morozova, I.; Silver, R.; Sweedler, J. V. Combining Small-Volume Metabolomic and Transcriptomic Approaches for Assessing Brain Chemistry. *Anal. Chem.* **2013**, *85* (6), 3136–3143. https://doi.org/10.1021/ac3032959.

(125) Soanes, K. H.; Achenbach, J. C.; Burton, I. W.; Hui, J. P. M.; Penny, S. L.; Karakach, T. K. Molecular Characterization of Zebrafish Embryogenesis via DNA Microarrays and Multiplatform Time Course Metabolomics Studies. *J. Proteome Res.* **2011**, *10* (11), 5102–5117. https://doi.org/10.1021/pr2005549.

(126) Do, T. D.; Ellis, J. F.; Neumann, E. K.; Comi, T. J.; Tillmaand, E. G.; Lenhart, A. E.; Rubakhin, S. S.; Sweedler, J. V. Optically Guided Single Cell Mass Spectrometry of Rat Dorsal Root Ganglia to Profile Lipids, Peptides and Proteins. *ChemPhysChem* **2018**, *19* (10), 1180–1191. https://doi.org/10.1002/cphc.201701364.

(127) Pandey, R.; Caflisch, L.; Lodi, A.; Brenner, A. J.; Tiziani, S. Metabolomic Signature of Brain Cancer. *Molecular Carcinogenesis* **2017**, *56* (11), 2355–2371. https://doi.org/10.1002/mc.22694.

(128) Mörén, L.; Bergenheim, A. T.; Ghasimi, S.; Brännström, T.; Johansson, M.; Antti, H. Metabolomic Screening of Tumor Tissue and Serum in Glioma Patients Reveals Diagnostic and Prognostic Information. *Metabolites* **2015**, *5* (3), 502–520. https://doi.org/10.3390/metabo5030502.

(129) Griffin, J. L.; Kauppinen, R. A. A Metabolomics Perspective of Human Brain Tumours. *The FEBS Journal* **2007**, *274* (5), 1132–1139. https://doi.org/10.1111/j.1742-4658.2007.05676.x.

(130) Research Funding | NIH Common Fund https://commonfund.nih.gov/grants/fundedresearch#tab3 (accessed Jan 14, 2020).

(131) Petras, D.; Jarmusch, A. K.; Dorrestein, P. C. From Single Cells to Our Planet—Recent Advances in Using Mass Spectrometry for Spatially Resolved Metabolomics. *Current Opinion in Chemical Biology* **2017**, *36*, 24–31. https://doi.org/10.1016/j.cbpa.2016.12.018.

(132) Kohler, I.; Hankemeier, T.; van der Graaf, P. H.; Knibbe, C. A. J.; van Hasselt, J. G. C. Integrating Clinical Metabolomics-Based Biomarker Discovery and Clinical Pharmacology to Enable Precision Medicine. *European Journal of Pharmaceutical Sciences* **2017**, *109*, S15–S21. https://doi.org/10.1016/j.ejps.2017.05.018.

CHAPTER 4: MALDI-MS GUIDED LIQUID MICROJUNCTION EXTRACTION FOR CAPILLARY ELECTROPHORESIS-ELECTROSPRAY IONIZATION MS ANALYSIS OF SINGLE PANCREATIC ISLET CELLS

This chapter is adapted with permission from an original research article published in *Analytical Chemistry* **2017**, DOI: 10.1021/acs.analchem.7b01782 coauthored by T.J. Comi, M.A. Makurath, S.S. Rubakhin, and J.V. Sweedler. M.C. Philip performed single cell extraction, LMJ validation, single cell capillary electrophoresis-mass spectrometry, and data analysis. T.J. Comi performed MALDI-MS, data analysis, wrote control software, isolated islets, and assisted with extractions. M.A. Makurath designed the initial extraction system and performed radiography experiments. Dr. Ta-Hsuan Ong is acknowledged for help with initial testing and Dr. Meng Qi for assistance with data analysis. We thank the UIUC School of Chemical Sciences machine shop for their expertise in designing and machining components of the vacuum chamber and stage. This work was financially supported by the National Institutes of Health, Award Number P30 DA018310 from the National Institute on Drug Abuse, and the National Institutes of Mental Health Award Number 1U01 MH109062.

4.1 INTRODUCTION

Assessing the cellular chemical heterogeneity of biological tissues is an ongoing challenge in many research fields.[1–4] Frequently, the analysis of bulk homogenates masks unique features of individual cells by averaging the molecular content of cell populations.[5] While a biological organ or tissue requires many distinct cells to function properly, a malfunction can manifest from small cellular subpopulations or even a single cell.[6,7] Furthermore, cells that are morphologically indistinguishable may possess unique intracellular chemistries and, therefore, physiologies.

Mass spectrometry (MS) is among the most commonly used analytical methods for

nontargeted single-cell analysis.[4] Matrix-assisted laser desorption/ionization (MALDI) MS,[8,9] electrospray ionization (ESI)-MS,[1,10–13] and secondary ion MS (SIMS)[14–17] are well-suited for multiplexed analysis of a wide range of biological molecules.[18] Measurements are typically label-free and often consume only a fraction of surface-available analytes. Page and Sweedler utilized radiography to demonstrate that, even after the MALDI-MS signal is fully depleted, about 30% of a protein standard is removed.[19] The recent progress in single-cell MS can be attributed to advances in sensitivity, mass resolution, and sample throughput of modern mass spectrometers, as well as hyphenation of MS to other approaches. For example, optical microscopy combined with single-cell MALDI-MS allows rapid characterization of dispersed cell populations.[20] By locating cells with optical microscopy, the analysis can proceed at an acquisition rate of approximately 1 Hz.[21] Using this approach, differential peptide processing was detected in γ cells derived from islets of Langerhans located in the dorsal and ventral regions of the rat pancreas.[22] This finding supports the view that the chemical cellular heterogeneity of different organs is neither well-understood nor well-characterized. As another example, flow cytometry and transcriptomic analyses of insulin-secreting β cells identified up to four β-cell subtypes in humans with significantly different glucose-stimulated insulin secretion.[23] Motivated by these examples, islet cells were chosen as a single-cell sample system in an attempt to discover previously unknown heterogeneity or chemical messengers.

MALDI-MS is well-suited to detecting peptides and lipids as their high molecular masses minimize interference from the MALDI matrix; however, many smaller metabolites are not detectable. A complementary method for single-cell analysis is capillary electrophoresis (CE)–ESI-MS, which is well suited for metabolomics measurements as it can quantitatively identify metabolites from individual cells.[11,24,25] Sample preparation for CE–ESI-MS typically involves

manual cell isolation, microfluidic cell sorting, or collection of cell cytoplasm using a patch-clamp pipette.[26,27] Metabolite detection using CE–ESI-MS generally requires injection of the sample content from an entire cell.[28] In contrast to MALDI-MS, CE–ESI-MS has relatively low throughput and is limited to a few cells per hour, a time constraint that precludes the cell-by-cell analysis of even modestly sized populations.

Preliminary classification of the most informative individual cells in a population via MALDI-MS facilitates targeted CE–ESI-MS analysis of rare and representative cells from among hundreds to thousands of cells. Previous attempts to combine MALDI-MS and CE–ESI-MS utilized microfluidic[29,30] and hydrodynamic[31,32] interfaces. Although the same sample was analyzed with both instruments, the methods had relatively low throughput due to the lack of automated target collection, which therefore required excessive manual sample handling. To reveal chemical heterogeneity in large populations of cells, it is important that the interface method is capable of collecting small sample volumes with high efficiency.

With that goal in mind, we developed a semiautomated, microscopy-guided liquid microjunction probe system for collection of analytes from single cells that have been classified by their MALDI-MS profiles. The first coupling of CE and MALDI worked in the reverse of the system described here in that the CE effluent was deposited onto a membrane or MALDI target for analyte detection after the CE separation.[30,33,34] In our approach, the MALDI measurement is performed first, and then samples are collected from the target for CE separation and analysis. The collection probe utilizes two coaxial capillaries, similar to previous designs from our lab,[32] and liquid microjunction surface sampling probes.[35,36]

Single-cell targeting is achieved with precise motion in three axes of linear freedom controlled by a lab-built graphical user interface that allows microscopy-guided cell targeting. The

software, microMS,[37] is an extension of software we originally developed for microscopy-guided MALDI-MS[22] and SIMS,[38] which directly controls the extraction probe. While MALDI-MS is not required for performing liquid extraction, it can complement the microscopy information by providing label-free classification of large populations. By interfacing two powerful analytical tools for small-volume samples, the combined data obtained from CE–ESI-MS and MALDI-MS were used to successfully classify and analyze six α and five β cells. Each cell was identified by MALDI-MS as a standard histological class by the detection of glucagon and insulin, respectively. Small molecules detected with CE–ESI-MS include 18 proteinogenic amino acids as well as dopamine. While the enzymes for dopamine synthesis suggest the presence of dopamine in β cells,[39,40] it appears that dopamine has not been directly characterized at the single-cell level in either α or β cells.

4.2 EXPERIMENTAL

4.2.1 Chemicals

All chemicals were purchased from Sigma-Aldrich (St. Louis, MO) and used without further purification.

4.2.2 Isolation of islets of Langerhans and single-cell preparation

A 1.5-month-old, male Sprague–Dawley outbred rat (*Rattus norvegicus*) was housed on a 12 h light cycle and fed ad libitum. Animal euthanasia was performed in accordance with the appropriate institutional animal care protocols (the Illinois Institutional Animal Care and Use Committee), and in full compliance with federal guidelines for the humane care and treatment of animals. Islets of Langerhans were manually isolated from an enzymatically digested and mechanically treated pancreas, as previously reported.[22] Briefly, the pancreas is injected through the bile duct with 2 mL of 1.4 mg/mL collagenase P in modified Gey's balanced salt solution (mGBSS) supplemented with 5 mM glucose and 1% (w/v) bovine serum albumin (BSA). The mGBSS contained 1.5 mM $CaCl_2$, 4.9 mM KCl, 0.2 mM KH_2PO_4, 11 mM $MgCl_2$, 0.3 mM $MgSO_4$, 138 mM NaCl, 27.7 mM $NaHCO_3$, 0.8 mM NaH_2PO_4, and 25 mM HEPES dissolved in Milli-Q water (Millipore, Billerica, MA), with the pH adjusted to 7.2. The pancreas was then surgically dissected and placed into 8 mL of the collagenase P solution. Solutions were incubated in a recirculating water bath for 20–30 min at 37 °C with agitation to dissociate bulk tissue. Excess collagenase P was washed from the resulting tissue with mGBSS containing glucose and BSA and centrifuged for 3 min at 300*g*. The resulting tissue pellet was dispersed into mGBSS, and islets were manually isolated with a micropipette. Single islets were incubated in 20 μL of 40% (v/v) glycerol and 60% mGBSS with glucose, BSA, and 0.1 mg/mL Hoechst 33342. This step resulted in staining of cell nuclei while mechanically stabilizing cellular morphology.[41] After 30 min, single cells were dissociated onto clean indium–tin oxide (ITO)-coated glass slides by gentle trituration in the staining solution and allowed to adhere to the slides overnight. Prior to imaging, excess glycerol was aspirated and the surface rinsed with 150 mM ammonium acetate (pH 10).

4.2.3 Optically guided single cell profiling

The next step in the experimental workflow, as outlined in Scheme 4.1, is to locate cells by optical microscopy. ITO-coated glass slides were prepared for optically guided single-cell profiling by marking the perimeter of dissociated cells with ~20 fiducial marks. Each mark consisted of an etched "x" (see Figure 4.6A), which remained visible during MALDI-MS acquisition and liquid microjunction extraction. The locations of fiducials and cells were determined by whole-slide bright-field and fluorescence microscopy using an Axio Imager M2 (Carl Zeiss, Jena, Germany). Images were acquired with a 10× objective and tiled to cover the entire region of interest. Florescence imaging of Hoechst 33342 utilized an X-CITE 120 mercury lamp (Lumen Dynamics, Mississauga, Canada) and a 31000v2 DAPI filter set (Chroma Technology, Irvine, CA).

Whole-slide images were utilized for optically guided single-cell profiling with microMS.[37] Before MALDI-MS acquisition, the pixel locations of each fiducial were correlated to their physical positions in the mass spectrometer. A point-based similarity registration was then used to map cell locations on the image to their corresponding physical locations.

After optical imaging, samples were coated with MALDI matrix, using an artist's airbrush, containing 50 mg/mL 2,5-dihydroxy-benzoic acid (DHB) in 1:1 (v/v) ethanol/water with 0.1% trifluoroacetic acid (TFA), nebulized with 40 psi nitrogen. Coating thickness was assessed

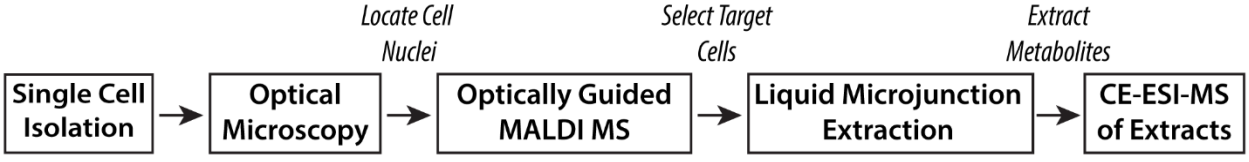

Scheme 4.1. Overview of the MALDI-MS Guided Liquid Microjunction Extraction Approach. Islets of Langerhans are isolated from a rat pancreas and dissociated onto an ITO-coated glass slide. MALDI-MS is used to assay the hormone profile of individual cells from a large population to identify extraction targets. The liquid microjunction probe collects cell contents from specified locations on the ITO-coated glass slide for follow-up CE–ESI-MS analysis.

optically during matrix application, with typical thicknesses of 0.2–0.4 mg/cm2. Samples were stored at room temperature (~22 °C) in a nitrogen drybox until analyzed.

4.2.4 MALDI-MS

Pancreatic cell populations were rapidly profiled with MALDI-MS to stratify the population into traditional histological classes. Specifically, the α and β cells were identified based on the detection of glucagon (monoisotopic m/z 3481.6) or insulin-1 C peptide (m/z 3259.8). To prevent detection of the cellular content of several cells simultaneously, as well as collection of multicellular content during follow-up analyte extraction, cell coordinates were first passed through a 300 μm distance filter. From a single islet dispersed on an ITO-coated glass slide, approximately 200–400 pancreatic cells satisfied the sample analysis criteria.

Mass spectra were acquired on a ultrafleXtreme MALDI TOF/TOF mass spectrometer with a frequency tripled Nd:YAG solid-state laser (Bruker Daltonics, Billerica, MA). Each cell was profiled with 1000 shots using a 1 kHz laser repetition rate with the "Ultra" laser setting (spot

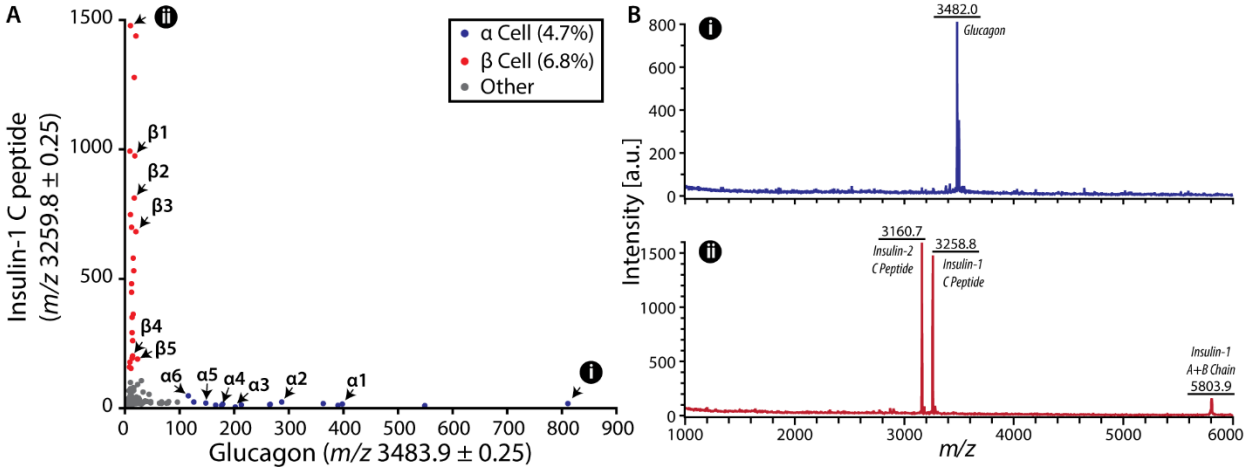

Figure 4.1. MALDI-MS classification of pancreatic islet cells. (A) A single dorsal pancreas islet is composed primarily of glucagon-containing α cells (blue) and insulin-containing β cells (red). Classifications are based on a threshold signal abundance to identify cell types for follow-up CE–ESI-MS analysis. Cell identities correspond to labeling of cell number for the α and β cells. (B) Spectra of single pancreatic cells identified in panel A, parts i and ii.

diameter ~100 μm). The resulting spectra were read into MATLAB 8.6.0 with the readbrukermaldi function (https://github.com/AlexHenderson/readbrukermaldi). Data from molecular mass windows containing signals from the peptide hormones of interest were extracted and signal intensities were plotted, as shown in Figure 4.1. Cells were classified based on their spectral profiles as α or β using signal intensities at m/z 3483.9 and m/z 3259.8, respectively. For each mass channel, a threshold value for signal intensity was manually determined to identify cell types with high confidence. Because of the stringent filter values, fewer than 100 cells were successfully classified by this approach for each islet. Images of classified cells were then examined to ensure the analyte extraction area contained no adjacent cells.

4.2.5 Liquid microjunction extraction probe system

The liquid microjunction extraction probe utilizes two coaxial capillaries. The inner and outer fused-silica capillaries are 100 μm/170 μm and 250 μm/350 μm in diameter, respectively (Polymicro Technologies, Phoenix, AZ). Fluid flow is directed via an IDEX MicroTee Assembly with Mounting Hole (IDEX Health and Science Part # P-875). The inner diameter of the MicroTee is approximately 150 μm; to accommodate the inner extraction capillary (O.D. 170 μm), a 0.008 in diameter circuit board drill (Hertel via MSC, Part # 74458720) was used to expand the through-hole. MicroTight sleeves to accommodate the capillaries are IDEX Health and Science Part # F-183 and Part # F-185. Extra MicroTight ferrules are IDEX Health and Science Part # F-172. The probe position was monitored in real time with a digital video camera (Sony, Park Ridge, NJ; P/N DFW-X700). Extraction liquid was delivered with a PHD 2000 syringe pump (Harvard Apparatus, Holliston, MA) and aspirated with 7–10 in Hg of vacuum, supplied with a diaphragm vacuum/pressure pump (Cole-Parmer, Vernon Hills, IL). The liquid microjunction was positioned with three linear stages (Zaber Technologies, Vancouver, BC, Canada) controlled with the in-

house written software, microMS.[37] Samples collected by the probe were dried using a Mi-Vac sample concentrator (SP Scientific, Warminster, PA) and stored at −20 °C prior to CE–ESI-MS analysis.

4.2.6 Radioactive material and radiation detection

Tritiated (^{3}H) angiotensin II, with the specific activity of 50 Ci/mmol at 1 mCi/mL, was purchased from American Radiolabeled Chemicals (St. Louis, MO). Radioactivity experiments were performed in accordance with the Illinois Radiation Protection Act under the University of Illinois at Urbana–Champaign Type A Broad Scope Radioactive Materials License issued by the Illinois Emergency Management Agency.

Radioactive material deposition and extraction was visually monitored using a Wild M3Z stereomicroscope (Leica, Buffalo Grove, IL). The pre- and postextraction radioactivity of the deposited sample was determined with a storage phosphor screen (BAS-IP TR 2025 E Tritium Screen, Sigma-Aldrich) exposed to the sample for 6 h. Developing the screen with a phosphorimager (Phosphorimager SI, Molecular Dynamics, Sunnyvale, CA) allowed for relative quantitation of the sample/analyte removal. Image processing was performed with custom MATLAB scripts. The fraction of material removed was determined by the background-corrected, normalized intensity at each pixel, before and after extraction.

4.2.7 CE–ESI-MS analysis

Each cell extract was dried and resuspended in 1 μL of 1% formic acid in liquid chromatography–MS grade water. CE–ESI-MS was performed as reported previously using a micrOTOF mass spectrometer (Bruker Daltonics).[27] Analyses were conducted in positive ion mode using a 70.7 cm long CE fused-silica capillary (Polymicro Technologies), a separation potential of 17 kV, and a sample injection volume of ∼15 nL. Extracted ion electropherograms

were exported using custom scripts in Bruker DataAnalysis version 4.4. Compounds were identified from the electropherograms by matching the migration order and mass-to-charge (m/z) values with standards. In MATLAB, each extracted ion electropherogram was baseline-subtracted and smoothed with a seven point moving average filter. Analyte migration times were aligned to corresponding analyte migration times in a reference mass electropherogram (α1), as shown in Figure 4.2. The alignment used a linear regression between migration times of a set of amino acids found in each sample (i.e., glycine, alanine, threonine, leucine/isoleucine, histidine, phenylalanine). To confirm the presence of dopamine, a standard mix of 10 μM glycine, alanine, threonine, leucine, histidine, and phenylalanine in 1% formic acid in water was analyzed with a 68 cm long CE capillary at 10 kV with and without the addition of 10 μM dopamine.

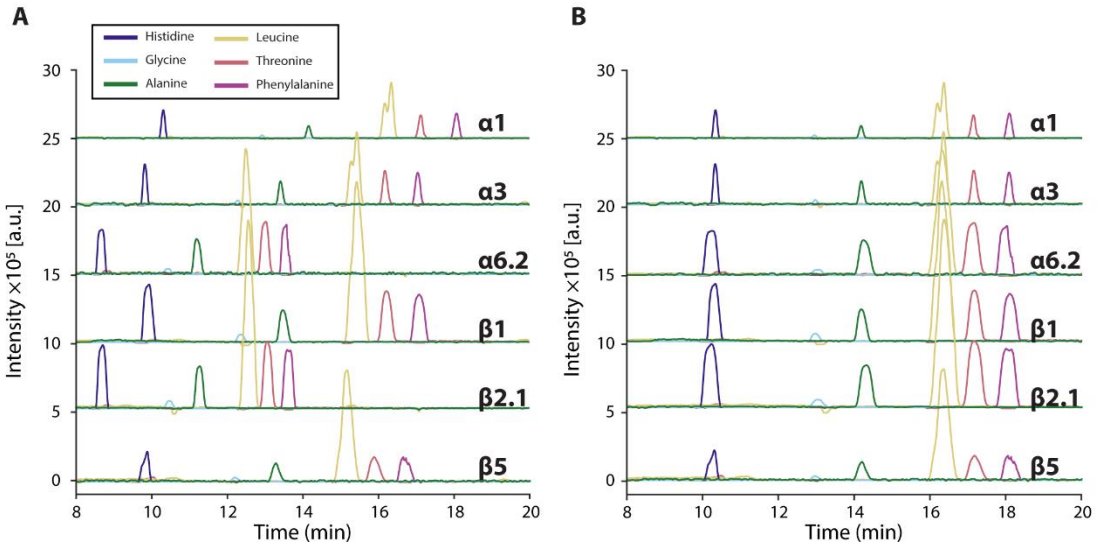

Figure 4.2. Extracted ion electropherograms (EIEs) of compounds utilized for migration time alignment. (A) The migration time of each signal with a particular *m/z* value is determined from the raw EIEs. The migration times are mapped to one sample (α1) to determine a linear regression between the time scales of reference and additional EIEs. The resulting equation is used to calculate (B) a new set of aligned migration times.

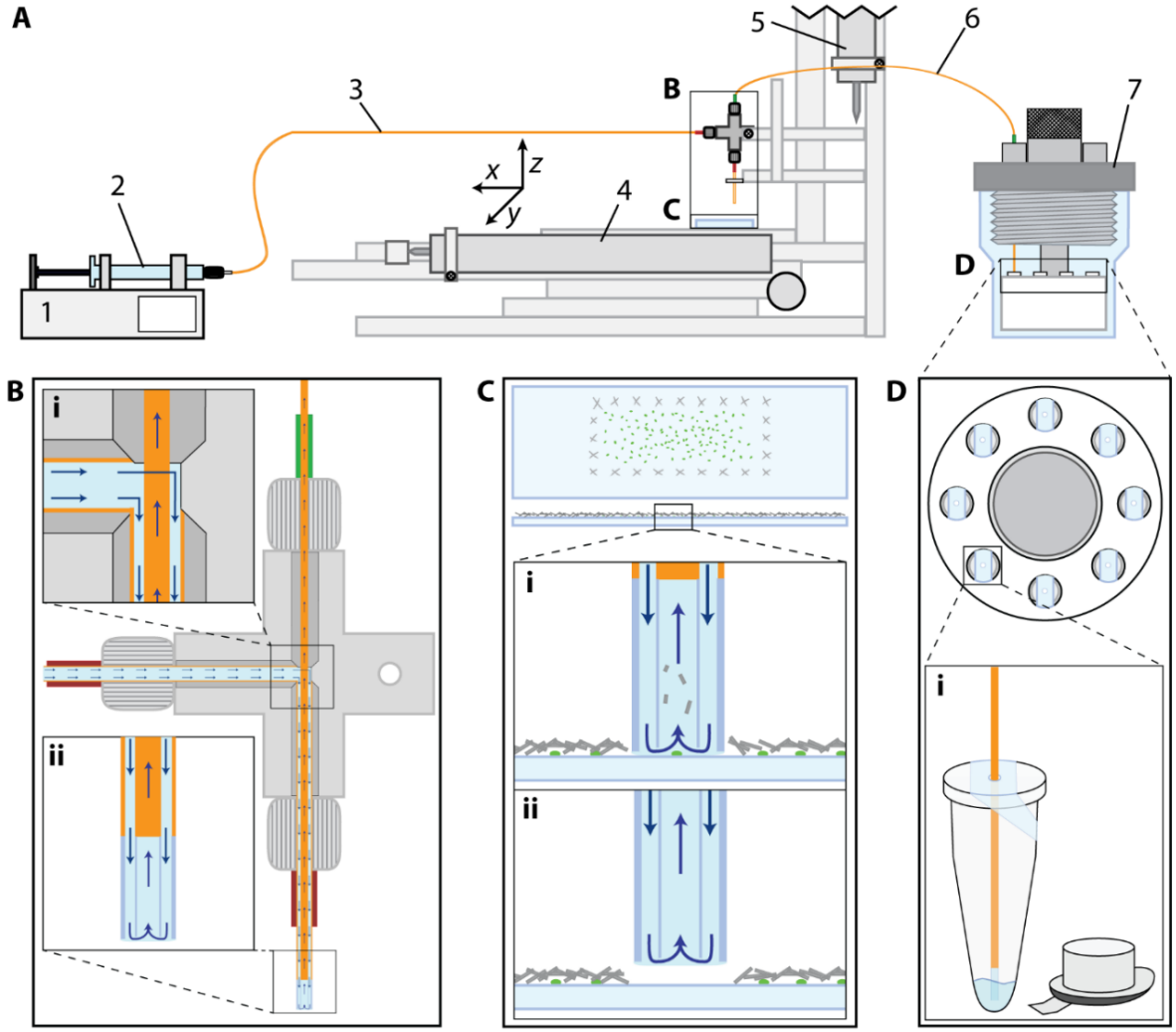

Figure 4.3. The liquid microjunction extraction system. (A) The system consists of a syringe pump (1) to deliver analyte extraction solution (2) through the liquid supply side (3) of the liquid microjunction probe (B). The position of the sample and manifold are controlled through an *xyz* system of linear actuators (4 and 5, *y* axis not shown). Solution is delivered to the target surface (C) to extract from target locations before being aspirated through the capillary (6) attached to the collection chamber (7 and D) held at vacuum. (B) Expanded view of the liquid microjunction extraction probe. i) The extraction solution is delivered through the inlet capillary to the outer capillary. Solution aspirated from the surface is drawn through the t-joint to the collection chamber. ii) The inner capillary is slightly withdrawn from the outer capillary. (C) Overview of the interaction with the target surface. Several x marks (fiducials) are positioned around the perimeter of a field of cells to correlate stage positions with optical images. i) The probe is moved over the top of a cell of interest and lowered to begin extraction. ii) After 60 s, the probe is retracted and solution continues to flush the capillaries and transfer extracts to the collection tube. (D) A custom vacuum chamber aspirates extract solution from the surface into microcentrifuge tubes covered with Parafilm M. The collection carousel accommodates eight tubes with indexed positions to simplify alignment. i) Parafilm M prevents droplets on the capillary from transferring between samples but must be open to aspirate the extraction solution.

4.3.1 Liquid microjunction extraction probe system

As shown in Figure 4.3, the liquid microjunction extraction system consists of a lab-built, concentric capillary probe coupled to a three-axis linear actuator positioning system. The single-cell collection setup was designed to transfer cell metabolites from an ITO-coated glass slide into a 200 µL microcentrifuge tube. The basic operating principle is similar to a liquid microjunction surface sampling probe except the solution is aspirated by vacuum pressure instead of an electrospray. The diameters of the probe capillaries were selected to be larger than the diameter of individual pancreatic cells to ensure complete extraction, prevent clogging, and accommodate the stage accuracy. The sizes of the inner and outer capillaries were 100 µm/170 µm and 250 µm/350 µm in diameter, respectively; the diameter of pancreatic cells is ~10–15 µm.[42] Sample carryover may result in cross-contamination of samples; therefore, ~5 mm of the polyimide coating was thermally removed at the ends of both capillaries.[43] Following each sample collection, the probe was immersed in extraction solution to thoroughly wash out its interior.

The extraction solution consisted of 1:1 methanol/water with 0.5% acetic acid (v/v), which was previously shown to facilitate metabolite extraction and detection with CE–ESI-MS.[27] As shown in Figure 4.4, a small meniscus forms at the probe tip during operation. Collections can be performed sequentially without having to open the vacuum chamber. The number of collections corresponds to the number

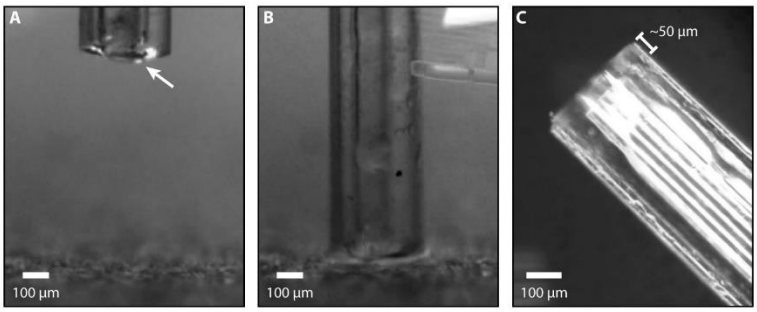

Figure 4.4. Micrographs of the liquid microjunction probe. (A) While operating, the extraction solution forms a meniscus at the probe tip, indicated with a white arrow. (B) When the probe touches the surface, solution flow remains constant, without air entering the capillary. (C) The inner capillary is withdrawn from the edge of the outer capillary by ~50 µm for stable flow.

of sample tubes the system can accommodate (our system holds eight tubes). Extraction liquid is delivered at 1.5 μL/min and aspirated with vacuum.

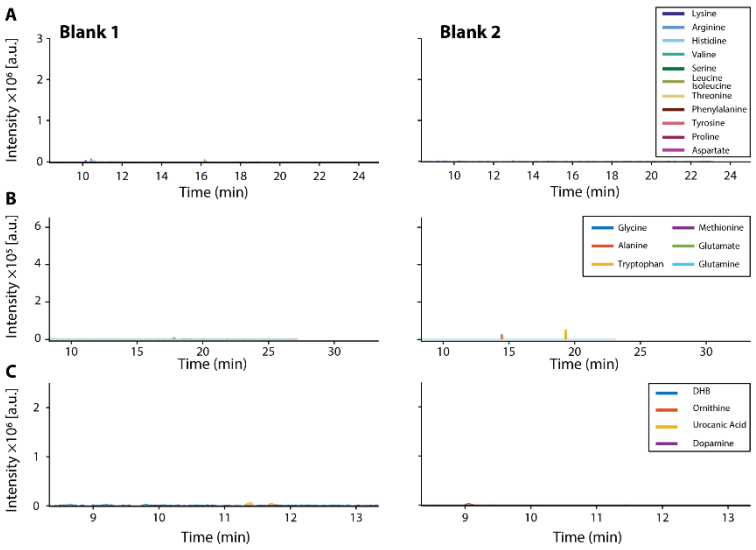

Figure 4.5. Results of CE–ESI-MS analysis on method blank samples. EIEs are presented with mass channels used for sample analysis and varying intensity scales.

During system operation, the user moves the x,y-translation stage away from the sample area and lowers the probe to the surface. The software records the z-axis position at the slide surface to enable automatic analyte extraction. The probe position is monitored in real time with a digital video camera. Next, coordinates from the whole-slide image and linear actuator positions are correlated with a point-based similarity registration utilizing more than 18 etched fiducial marks. Choosing a targeted cell on the image activates the motion of the x,y-translation stage, moving it into position for analyte extraction. The user initiates semiautomatic extractions by signaling the microMS software with a key press. During extraction, the probe is lowered to the slide for 60 s and then retracted. Alternatively, analytes from a population of cells may be sequentially extracted and pooled into a single collection vial. Following either collection scheme, the probe is returned to the home position and submerged into a reservoir of extraction solution for 90 s to rinse the probe exterior, flush the inner capillary, and prevent carryover between samples. As seen in Figure 4.5, blanks acquired from locations adjacent to cells between extractions contained negligible background signal.

The cell content collected at each coordinate travels from the MALDI sample plate (e.g., ITO glass slide), through the inner capillary of the coaxial system, and into one of the microcentrifuge tubes contained in the vacuum chamber. Inside the vacuum chamber, the microcentrifuge tubes are covered with a thin strip of Parafilm M to prevent extraction solution from clinging on the capillary when moving between collection vials. The inner capillary is retracted from the current collection tube, the tube carousel is indexed to the next position, and the inner capillary is placed into the next collection tube without breaking vacuum in the chamber. Individual samples were dried and stored at −20 °C prior to CE–ESI-MS analysis.

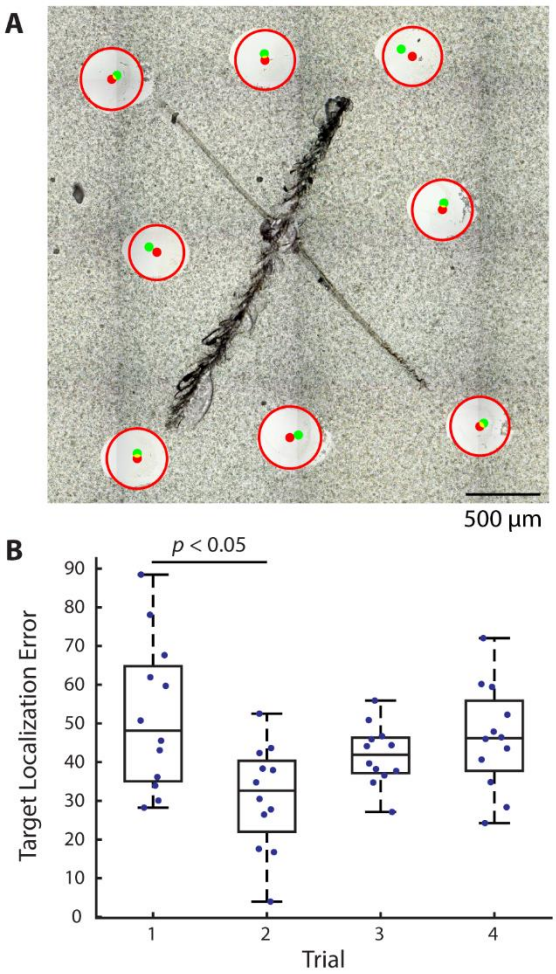

Figure 4.6. Representative extractions for determining target localization error. Target points were positioned around fiducial marks placed in the center of a glass slide. (A) Overlay of microscope image with the position of target locations (green) and extraction areas (red). (B) Box plot of the accuracies over four trials of fiducial registration. The registration trial was the only confounding variable found to significantly affect target localization error.

4.3.2 Determination of target localization error

To ensure that each analyte extraction is from the expected cell, it is imperative to determine the target localization error. Analyte extraction locations were visualized and characterized by the removal of MALDI matrix from the sample plate. Image registration of fiducial markers allowed the spatial correlation of requested target points and realized analyte extraction positions (Figure 4.6).

A glass slide was etched with 18 fiducial marks for point-based registration, similar to typical cell extractions. An additional six etched marks were placed within these fiducials to assist with image registration, as they remain visible after MALDI matrix application and extraction. Eight target locations were manually placed around each of the six, interior etched marks in pairs to assess the effect of repeated registrations. The slide was then coated with DHB and placed into the liquid extraction stage as before. Two users each performed two sets of extractions with 12 targets spread over the six etched marks. This experimental design allowed evaluation of the influence of the user, registration, and location on the target localization error. Each target was extracted for 5 s, and the probe was washed for 60 s after each set of 12 extractions.

Following extraction, the sample was imaged again to locate target etched marks and extraction locations. Extraction centers and diameters were manually annotated. A custom MATLAB script was utilized to assess the target localization error of each extraction. Regions surrounding each etched mark were cropped from the whole-slide image. Several locations on each mark were utilized to overlay the pre- and postextraction images. Target locations on the pre-extraction image were then mapped to the postextraction image with the same coordinate transformation. The pixel distances between the target and actual positions were scaled to micrometers. A three-way linear analysis of variance (ANOVA) was utilized to assess the effect of each confounding variable. While the operator and target spot location did not significantly influence the target localization

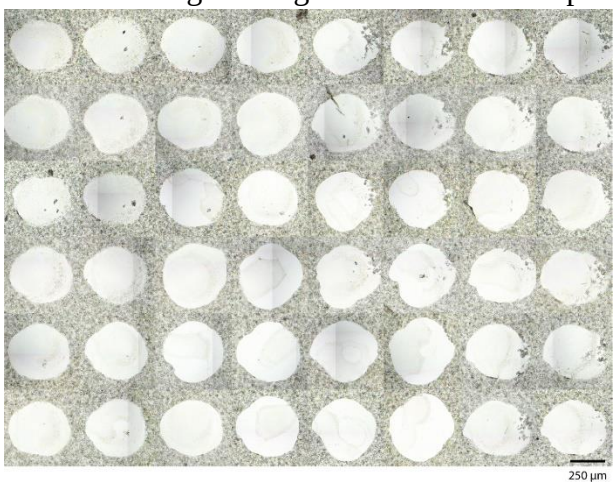

Figure 4.7. Montage of extraction areas. Each spot is the result of a 5 s extraction time from a DHB-coated microscope slide. The extraction profile is roughly circular, with an average radius of 206.3 ± 1.7 µm.

error ($p = 0.15$ and 0.06, respectively), there was a significant effect from performing replicates with the same sample and images ($p = 0.004$). This highlights that the accurate determination of fiducial locations has the largest influence on target localization error. The overall target localization error was determined as 42.8 ± 2.3 μm (±SEM, n = 48; range 3.9–88.5 μm), which is well within the average extraction radius of 206.3 ± 1.7 μm, as determined by measurement of the size of the spot of removed DHB from the surface (Figure 4.7). Therefore, it is assumed that each extraction would contain only the target cell when a cell-to-cell distance filter is set to be larger than 250 μm. This approach ensures that the collection of single-cell samples is free from cross-contamination by neighboring cells.

4.3.3 Characterization of analyte removal efficiency

^{3}H-angiotensin II was spotted onto an ITO-coated glass slide to determine the extraction profile and analyte removal efficiency. Five spots of ∼1 μL of 1000 pCi of ^{3}H-angiotensin II in mGBSS supplemented with 5 mg/mL Fast green were deposited onto the surface of an ITO-coated glass slide and allowed to dry for 24 h at room temperature (∼22 °C). Liquid microjunction extraction of the radioactive material was performed as described above, with minor adjustments to minimize the possibility of radioactive contamination of the equipment. To replicate single-cell extraction conditions, each ^{3}H-angiotensin II spot was extracted for 60 s. The removal efficiency was estimated by fitting the two-dimensional distribution to a general Gaussian function, as described in Table 4.1.

Table 4.1. Summary of fitting values for determining the fraction of 3H-angiotensin II removed. The fraction removed was modeled as a general, two-dimensional Gaussian distribution centered on each sub-image. The model equation is:

$$f(x,y) = A\exp\left(-\left(a(x-\mu_x)^2 - 2b(x-\mu_x)(y-\mu_y) + c(y-\mu_y)\right)\right)$$

Where A is the fraction removed at the center, e.g., (x,y) = (μ_x, μ_y) and (μ_x, μ_y) is the center of the distribution. The variables a,b,c are further defined as:

$$a = \frac{\cos^2\theta}{2\sigma_x^2} + \frac{\sin^2\theta}{2\sigma_y^2}$$

$$b = -\frac{\sin 2\theta}{4\sigma_x^2} + \frac{\sin 2\theta}{4\sigma_y^2}$$

$$c = \frac{\sin^2\theta}{2\sigma_x^2} + \frac{\cos^2\theta}{2\sigma_y^2}$$

Where σ_x, σ_y are the standard deviation of the distribution and θ is the rotation in radians. With the constraints that $A \in [0,2]$, $\mu_x, \mu_y \in [-s, s]$, $\sigma_x, \sigma_y \in [0, s], \theta \in [0,2\pi]$ where s is half the subregion size, 500 μm. Reported values represent the 95% confidence intervals for each parameter.

Spot	A	μ_x (μm)	μ_y (μm)	θ (radians)	σ_x (μm)	σ_y (μm)
1	0.889 ± 0.079	15 ± 10	18.9 ± 7.9	1.51 ± 0.25	88.4 ± 7.9	114 ± 10
2	0.91 ± 0.14	24 ± 15	9 ± 13	5.08 ± 0.72	77 ± 13	91 ± 15
3	0.908 ± 0.094	4 ± 12	35 ± 11	5.68 ± 0.90	115 ± 12	106 ± 11
4	0.904 ± 0.099	0 ± 12	16.5 ± 9.0	3.04 ± 0.24	112 ± 12	82.2 ± 9.0
5	0.92 ± 0.13	20 ± 13	24.1 ± 8.9	0.09 ± 0.24	96 ± 13	64.9 ± 8.9

Fitting results (Figure 4.8) provide an estimated removal efficiency of 90.6 ± 0.6% (Table 4.1). While the extraction efficiency may be dependent on the target analyte, the high removal efficiency found with angiotensin suggests that the solvent composition and extraction time are suitable for collecting small and intermediate-sized polar compounds, such as the amino acids. The extraction footprint was found to be elliptical, with a major diameter of 422 ± 21 μm and minor diameter of 335 ± 27 μm. The estimated diameter from optical measurements of DHB removal falls within the range of the minor and major diameters. The eccentricity of the extraction footprint

is likely due to imperfect fabrication of the probe tip or stochastic wetting of the rough, matrix-covered surface.

4.3.4 Profiles of small molecules

CE–ESI-MS complements MALDI-MS analyses by identifying small molecules from a single cell. We present example extracted ion electropherograms with corresponding MALDI mass spectra in Figure 4.9. All collected electropherograms and corresponding MALDI mass spectra are provided in Figure 4.11.

Detected compounds include the majority of the proteinogenic amino acids, precursor molecules, and endocrine signaling molecules. In contrast to characteristic peptide signatures, no obvious differences were found between α and β cells in their metabolite profiles. However,

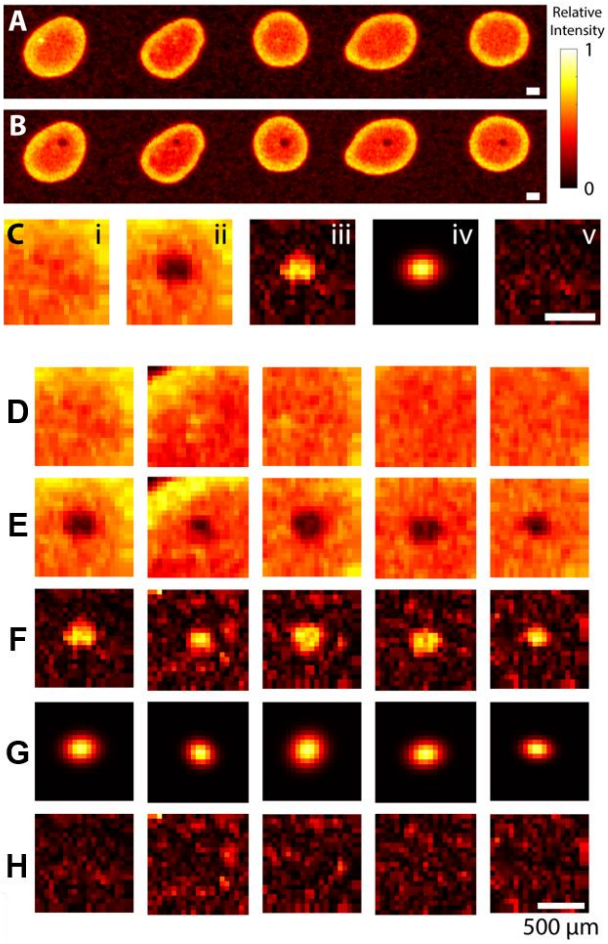

Figure 4.8. Measurement of removal efficiency of ^{3}H-angiotensin. A phosphorimager was utilized to measure angiotensin distributions pre- and post-extraction, shown in panels A and B, respectively. (C) Sample analysis of the left-most spot. Subregions surrounding each extraction (i and ii) are utilized to determine the distribution of the fraction of radioactivity removed (iii). The distribution is fit to a general two-dimensional Gaussian (iv) to determine the fraction removed. Residuals of the fit (v) are nonstructured, indicating the model is appropriate. (D-H) Complete set of subregions and Gaussian fits for determination of analyte removal efficiency using Phosphorimager scans of ^{3}H-angiotensin II samples. Each column of images corresponds to a single extraction from spot #1 (left) to #5 (right), with the columns representing the data from the various spot images. (A) Normalized intensity distribution prior to extraction. (B) Same region after extraction. (C) Background-corrected, fraction-removed signal intensity. (D) Two-dimensional Gaussian fit of image in (C). (E) Absolute, residual signal intensity scaled the same as (C). All scale bars are 500 µm.

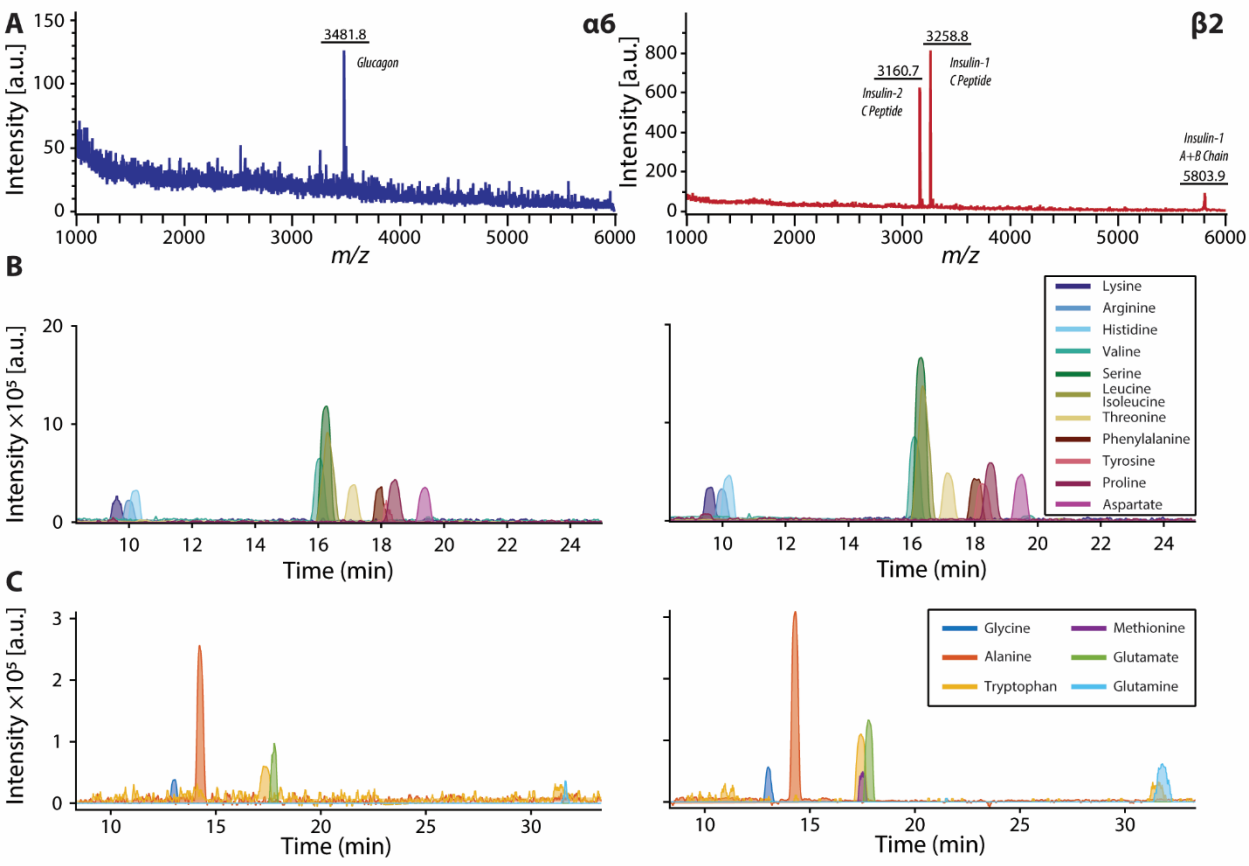

Figure 4.9. Single pancreatic islet cell analysis using MALDI-MS and CE–ESI-MS interfaced with the off-line liquid microjunction extraction system. (A) Representative single-cell MALDI-MS profiles of single α and β cells. (B) Corresponding CE–ESI-MS extracted ion electropherograms of the same cells showing signals of amino acids with high intensities and (C) signals of amino acids with lower signal intensities.

increasing the number of replicates and performing quantitative measurements (e.g., including a labeled standard for metabolites of interest) may allow identification of subtle heterogeneity between each population. Improvements in CE–ESI-MS sensitivity would facilitate detection of minor metabolites. An interesting observation was the presence of dopamine in all α and β cells (Figure 4.10). Previously, endogenous dopamine has been detected in single islets via an enzyme-linked immunosorbent assay (ELISA) assay,[40] but to our knowledge, not in single cells. β cells are known to have the required enzymes for synthesis, metabolism, and storage of dopamine, such as tyrosine hydroxylase[44] and vesicular monoamine transporter type 2;[45] thus, it is generally accepted

that dopamine is produced in β cells.[39] Dopamine within α cells is less studied, and whether dopamine is endogenous to α cells has not yet been investigated. We report direct detection of dopamine in single α and β cells, illustrating the unique capabilities of the presented methodology and small-scale analyses.

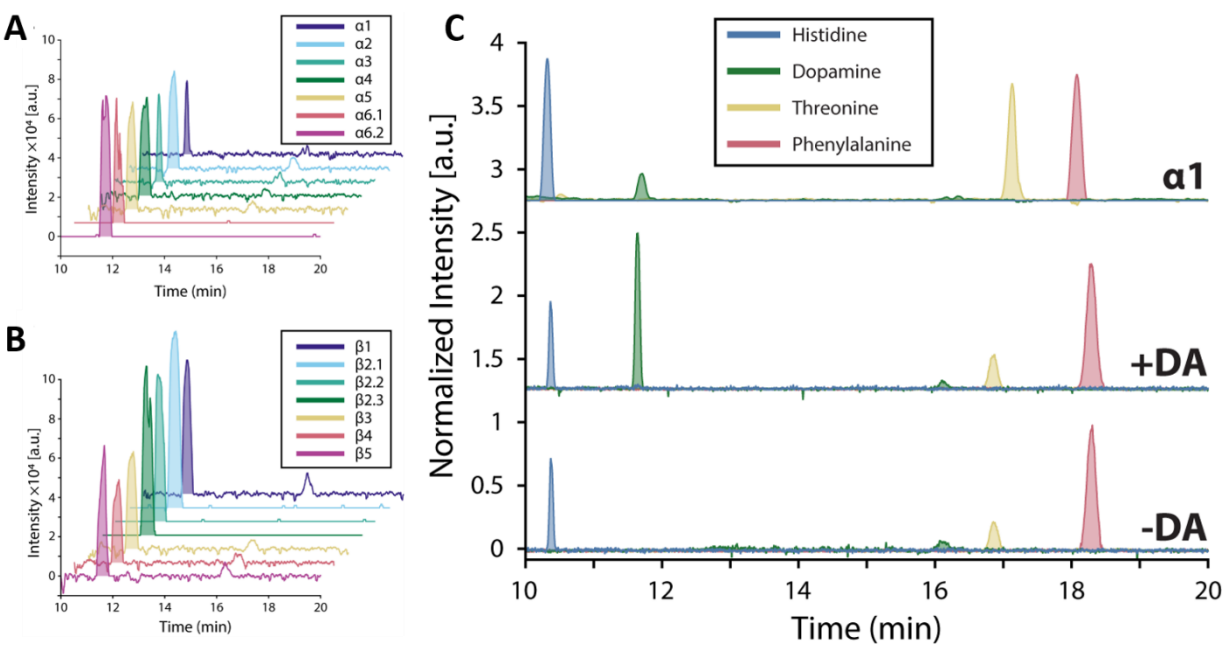

Figure 4.10. Extracted ion electropherograms for m/z 154.09 ± 0.01. The peak with m/z and migration time matching dopamine standard is shaded in each electropherogram: (A) α cells; (B) β cells. Dopamine was detectable in every cell analyzed. The peak at ~16 min is attributed to sodiated leucine. Single-cell samples analyzed with technical replicates are annotated with decimals, e.g., α6.1. (C) EIEs for dopamine and amino acid standards compared with extracted ion electropherograms obtained from α-cell #1. Signal intensities of all ions are normalized to the signal intensity of phenylalanine in each sample. The peak with migration time at ~12 min is identified as dopamine.

4.4 CONCLUSIONS

We developed a semiautomated method that couples high-throughput single-cell chemical profiling with MALDI-MS, followed by in-depth analyses of representative cellular types with CE–ESI-MS metabolomics. The approach leverages the low sample consumption of MALDI-MS, which enables the follow-up analysis of the same sample by CE–ESI-MS. By hyphenating the two

methods, we identified cell types by their peptide profiles, and detected most amino acids and the signaling molecule dopamine, a difficult task for either technique alone. While pancreatic islet cell types were the focus of this study, the methodology is suitable for a broad range of single-cell analyses of dissociated tissues. Future work will leverage the unique capabilities to examine heterogeneity within the nervous and endocrine systems.

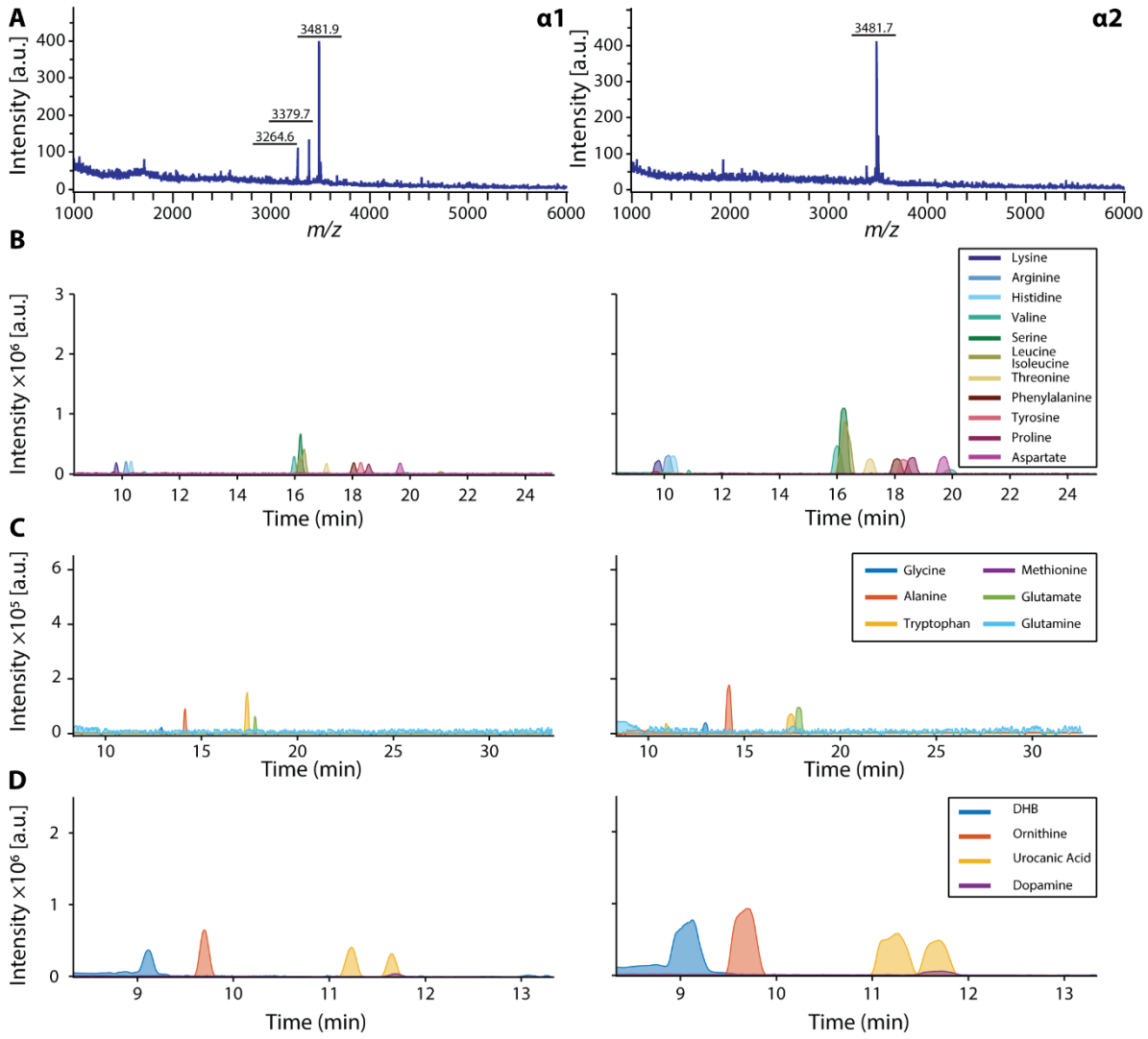

Figure 4.11. Results of single cell MALDI-MS and CE–ESI-MS analysis. MALDI mass spectra and corresponding extracted ion electropherograms (EIEs) are presented for each of the presented cells. (A) Single cell MALDI mass spectra, (B) EIEs for amino acids with high signal intensity, (C) EIEs for amino acids with lower signal intensity, and (D) EIEs for selected metabolites and background signals. The cell identities are displayed in panel (A) and match the annotated points in Figure 1 of the main text. In the following panels, each cell assayed is given a number; for some, technical replicates of CE–ESI-MS, where cell extracts were analyzed repeatedly, are indicated as decimals after the cell identity, e.g., α6.1 and α6.2.

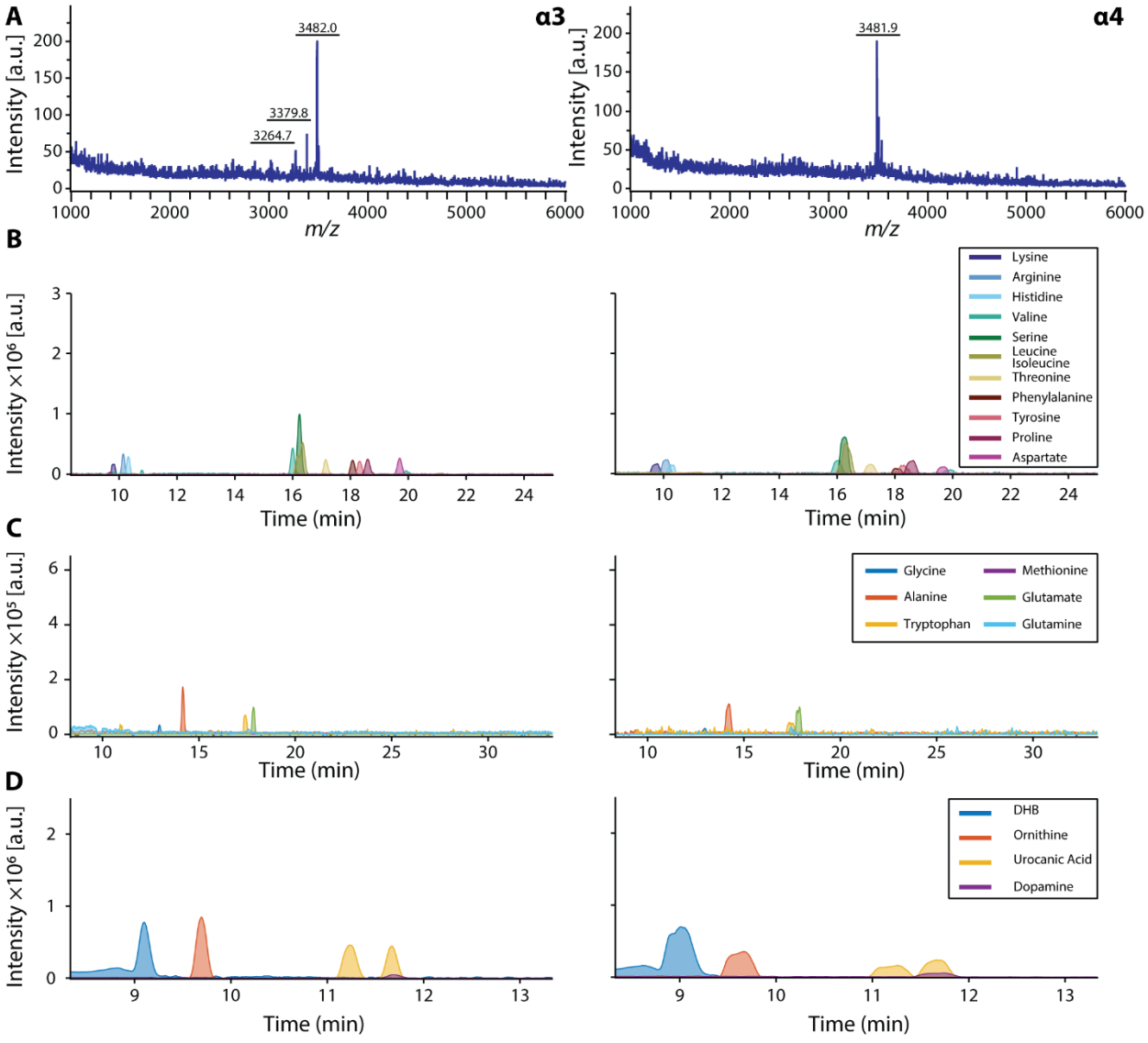

Figure 4.11. (Continued)

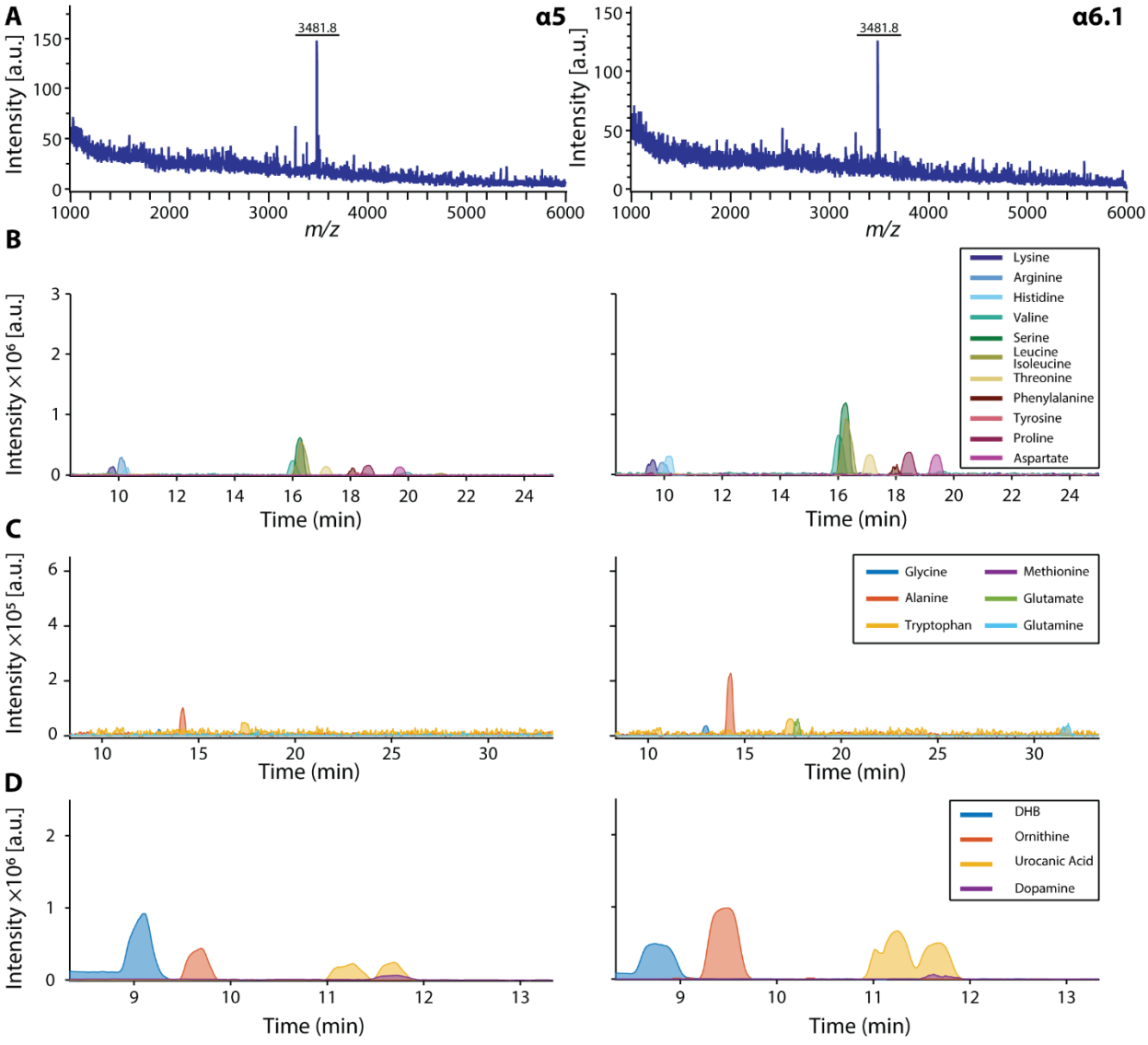

Figure 4.11. (Continued)

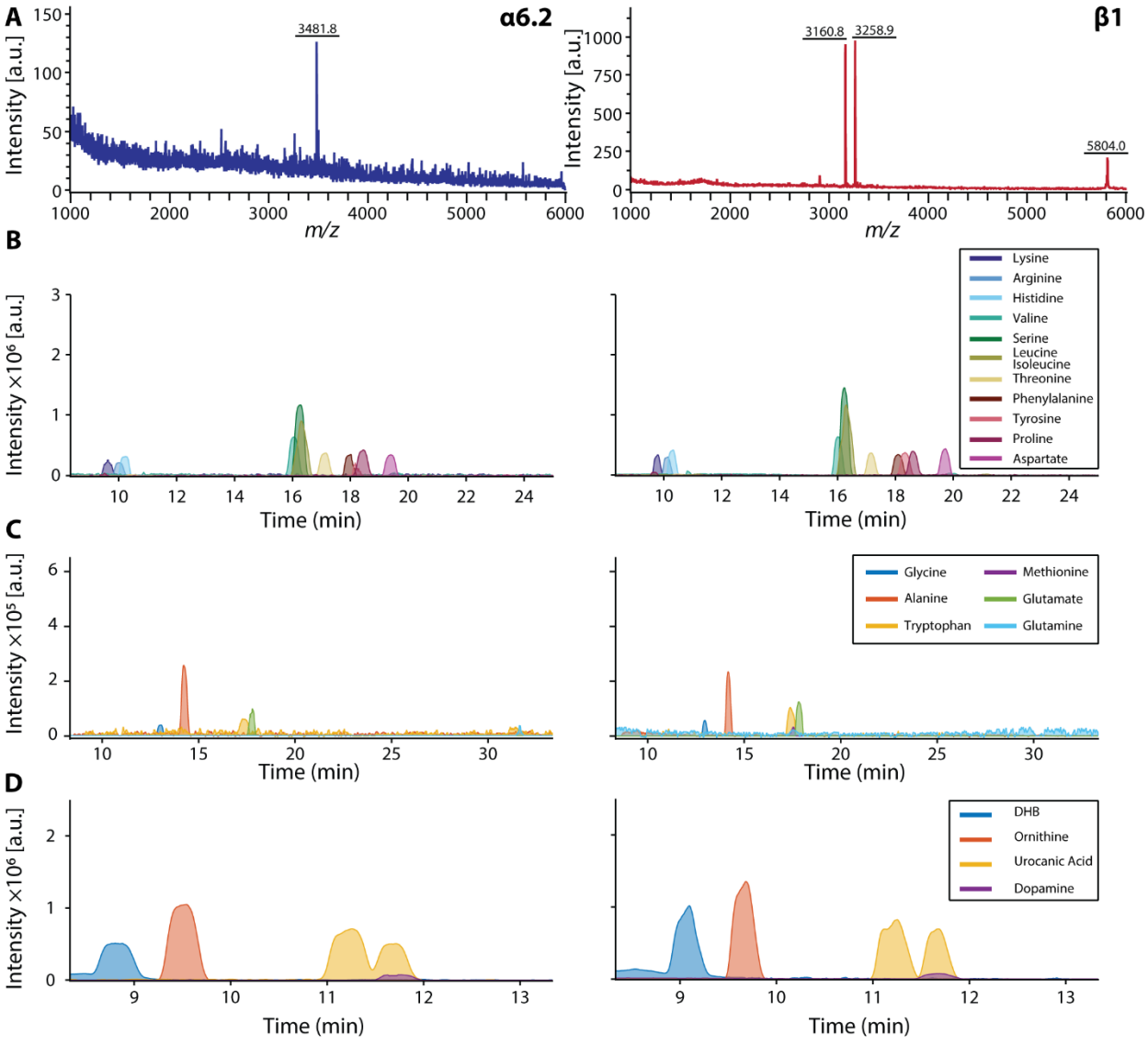

Figure 4.11. (Continued)

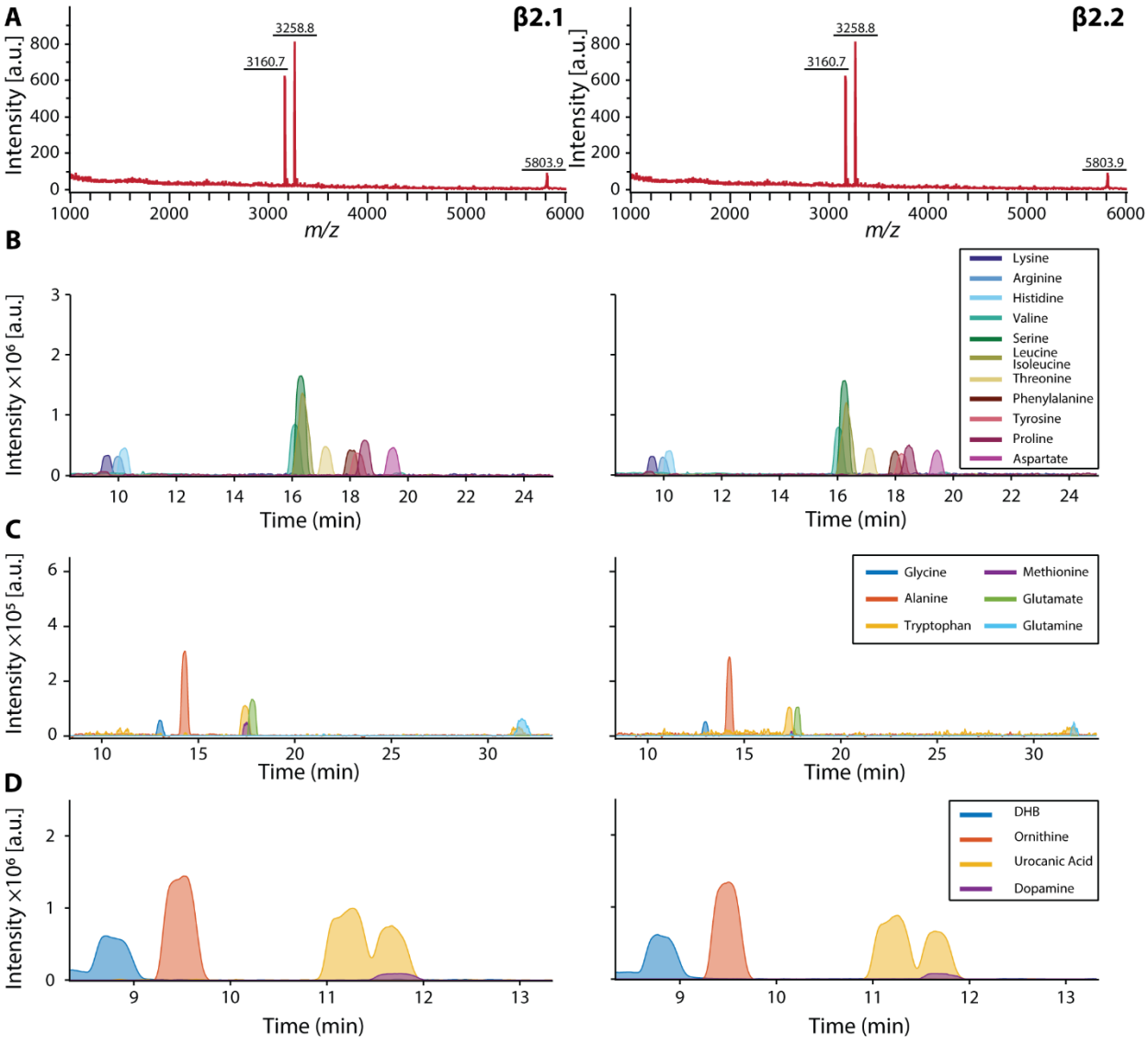

Figure 4.11. (Continued)

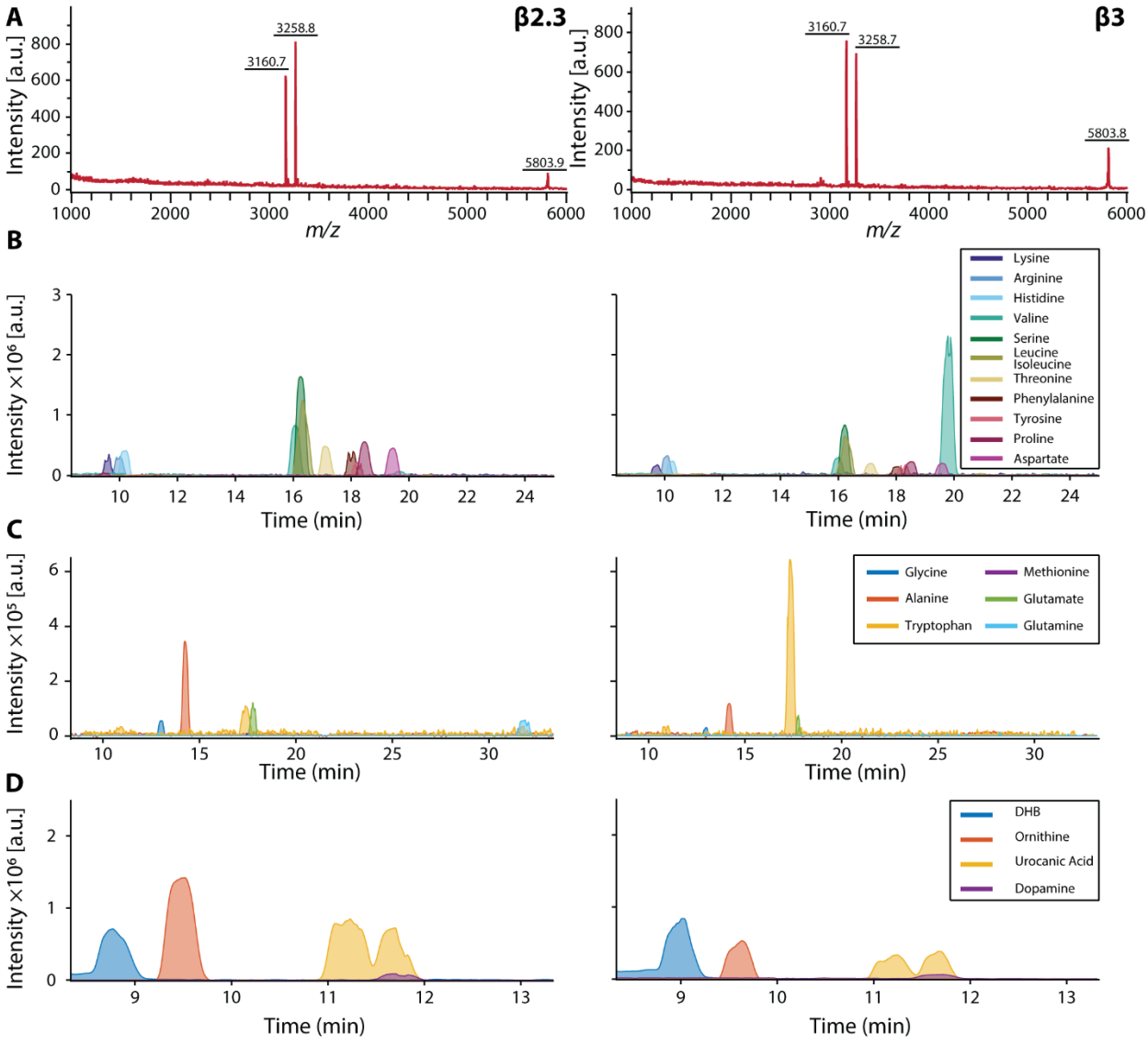

Figure 4.11. (Continued)

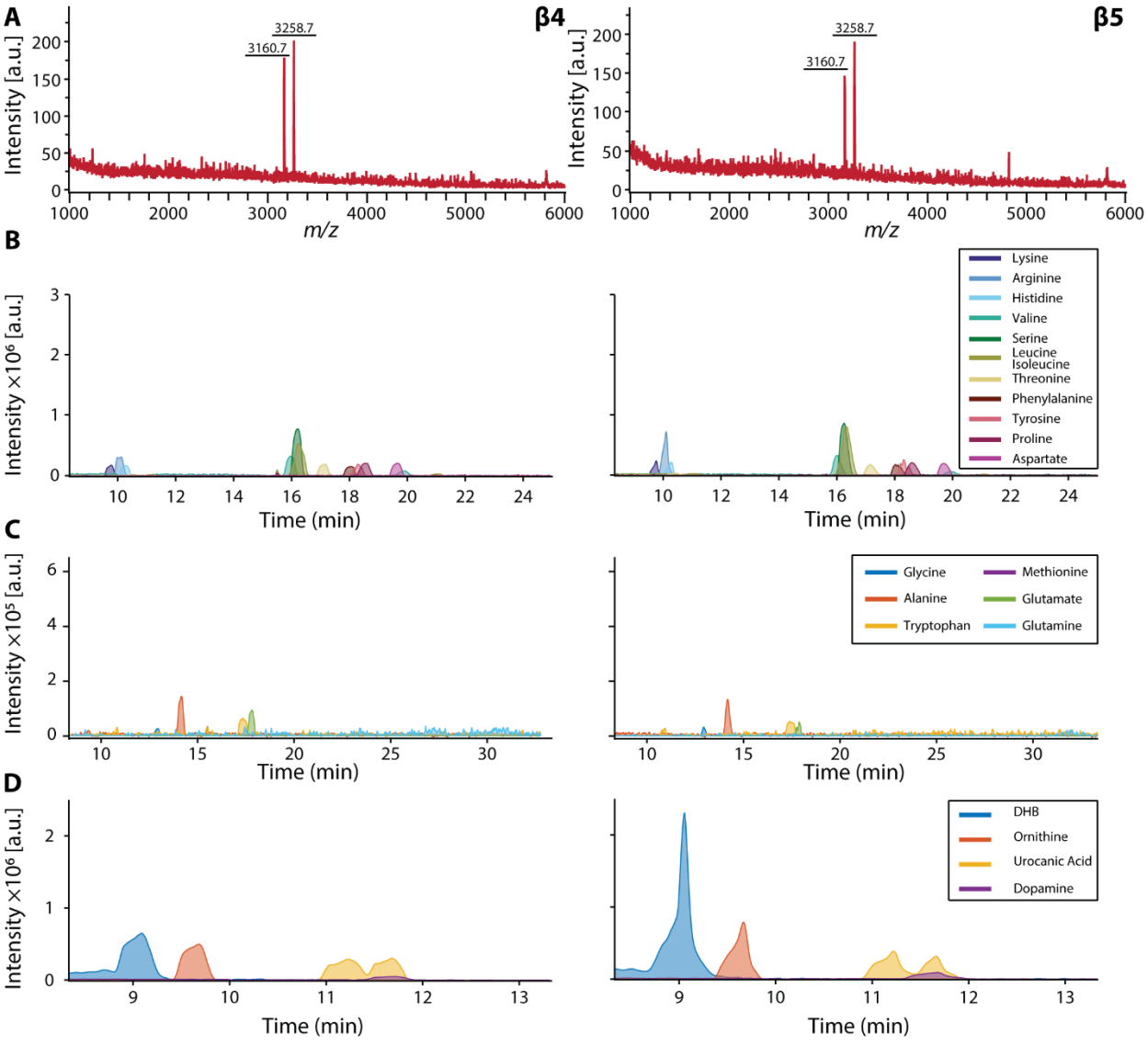

Figure 4.11. (Continued)

4.6 REFERENCES

(1) Onjiko, R. M.; Moody, S. A.; Nemes, P. Single-Cell Mass Spectrometry Reveals Small Molecules That Affect Cell Fates in the 16-Cell Embryo. *PNAS* **2015**, *112* (21), 6545–6550. https://doi.org/10.1073/pnas.1423682112.

(2) Armbrecht, L.; Dittrich, P. S. Recent Advances in the Analysis of Single Cells. *Anal. Chem.* **2017**, *89* (1), 2–21. https://doi.org/10.1021/acs.analchem.6b04255.

(3) Malucelli, E.; Fratini, M.; Notargiacomo, A.; Gianoncelli, A.; Merolle, L.; Sargenti, A.; Cappadone, C.; Farruggia, G.; Lagomarsino, S.; Iotti, S. Where Is It and How Much? Mapping and Quantifying Elements in Single Cells. *Analyst* **2016**, *141* (18), 5221–5235. https://doi.org/10.1039/C6AN01091A.

(4) Zenobi, R. Single-Cell Metabolomics: Analytical and Biological Perspectives. *Science* **2013**, *342* (6163), 1243259. https://doi.org/10.1126/science.1243259.

(5) Altschuler, S. J.; Wu, L. F. Cellular Heterogeneity: Do Differences Make a Difference? *Cell* **2010**, *141* (4), 559–563. https://doi.org/10.1016/j.cell.2010.04.033.

(6) Lawson, D. A.; Bhakta, N. R.; Kessenbrock, K.; Prummel, K. D.; Yu, Y.; Takai, K.; Zhou, A.; Eyob, H.; Balakrishnan, S.; Wang, C.-Y.; et al. Single-Cell Analysis Reveals a Stem-Cell Program in Human Metastatic Breast Cancer Cells. *Nature* **2015**, *526* (7571), 131–135. https://doi.org/10.1038/nature15260.

(7) Powell, A. A.; Talasaz, A. H.; Zhang, H.; Coram, M. A.; Reddy, A.; Deng, G.; Telli, M. L.; Advani, R. H.; Carlson, R. W.; Mollick, J. A.; et al. Single Cell Profiling of Circulating Tumor Cells: Transcriptional Heterogeneity and Diversity from Breast Cancer Cell Lines. *PLOS ONE* **2012**, *7* (5), e33788. https://doi.org/10.1371/journal.pone.0033788.

(8) Ibáñez, A. J.; Fagerer, S. R.; Schmidt, A. M.; Urban, P. L.; Jefimovs, K.; Geiger, P.;

Dechant, R.; Heinemann, M.; Zenobi, R. Mass Spectrometry-Based Metabolomics of Single Yeast Cells. *PNAS* **2013**, *110* (22), 8790–8794. https://doi.org/10.1073/pnas.1209302110.

(9) Rubakhin, S. S.; Romanova, E. V.; Nemes, P.; Sweedler, J. V. Profiling Metabolites and Peptides in Single Cells. *Nat Methods* **2011**, *8* (4), S20–S29. https://doi.org/10.1038/nmeth.1549.

(10) Ong, T.-H.; Tillmaand, E. G.; Makurath, M.; Rubakhin, S. S.; Sweedler, J. V. Mass Spectrometry-Based Characterization of Endogenous Peptides and Metabolites in Small Volume Samples. *Biochimica et Biophysica Acta (BBA) - Proteins and Proteomics* **2015**, *1854* (7), 732–740. https://doi.org/10.1016/j.bbapap.2015.01.008.

(11) Nemes, P.; Knolhoff, A. M.; Rubakhin, S. S.; Sweedler, J. V. Metabolic Differentiation of Neuronal Phenotypes by Single-Cell Capillary Electrophoresis–Electrospray Ionization-Mass Spectrometry. *Anal. Chem.* **2011**, *83* (17), 6810–6817. https://doi.org/10.1021/ac2015855.

(12) Lombard-Banek, C.; Moody, S. A.; Nemes, P. Single-Cell Mass Spectrometry for Discovery Proteomics: Quantifying Translational Cell Heterogeneity in the 16-Cell Frog (Xenopus) Embryo. *Angewandte Chemie International Edition* **2016**, *55* (7), 2454–2458. https://doi.org/10.1002/anie.201510411.

(13) Mizuno, H.; Tsuyama, N.; Harada, T.; Masujima, T. Live Single-Cell Video-Mass Spectrometry for Cellular and Subcellular Molecular Detection and Cell Classification. *Journal of Mass Spectrometry* **2008**, *43* (12), 1692–1700. https://doi.org/10.1002/jms.1460.

(14) Ostrowski, S. G.; Kurczy, M. E.; Roddy, T. P.; Winograd, N.; Ewing, A. G. Secondary Ion MS Imaging To Relatively Quantify Cholesterol in the Membranes of Individual Cells from Differentially Treated Populations. *Anal. Chem.* **2007**, *79* (10), 3554–3560. https://doi.org/10.1021/ac061825f.

(15) Passarelli, M. K.; Ewing, A. G.; Winograd, N. Single-Cell Lipidomics: Characterizing and

Imaging Lipids on the Surface of Individual Aplysia Californica Neurons with Cluster Secondary Ion Mass Spectrometry. *Anal. Chem.* **2013**, *85* (4), 2231–2238. https://doi.org/10.1021/ac303038j.

(16) Chandra, S. Quantitative Imaging of Chemical Composition in Single Cells by Secondary Ion Mass Spectrometry: Cisplatin Affects Calcium Stores in Renal Epithelial Cells. In *Mass Spectrometry Imaging: Principles and Protocols*; Rubakhin, S. S., Sweedler, J. V., Eds.; Methods in Molecular Biology; Humana Press: Totowa, NJ, 2010; pp 113–130. https://doi.org/10.1007/978-1-60761-746-4_6.

(17) Lanni, E. J.; Dunham, S. J. B.; Nemes, P.; Rubakhin, S. S.; Sweedler, J. V. Biomolecular Imaging with a C60-SIMS/MALDI Dual Ion Source Hybrid Mass Spectrometer: Instrumentation, Matrix Enhancement, and Single Cell Analysis. *J. Am. Soc. Mass Spectrom.* **2014**, *25* (11), 1897–1907. https://doi.org/10.1007/s13361-014-0978-9.

(18) Li, L.; Garden, R. W.; Sweedler, J. V. Single-Cell MALDI: A New Tool for Direct Peptide Profiling. *Trends in Biotechnology* **2000**, *18* (4), 151–160. https://doi.org/10.1016/S0167-7799(00)01427-X.

(19) Page, J. S.; Sweedler, J. V. Sample Depletion of the Matrix-Assisted Laser Desorption Process Monitored Using Radionuclide Detection. *Anal. Chem.* **2002**, *74* (24), 6200–6204. https://doi.org/10.1021/ac025898k.

(20) Comi, T. J.; Do, T. D.; Rubakhin, S. S.; Sweedler, J. V. Categorizing Cells on the Basis of Their Chemical Profiles: Progress in Single-Cell Mass Spectrometry. *J. Am. Chem. Soc.* **2017**, *139* (11), 3920–3929. https://doi.org/10.1021/jacs.6b12822.

(21) Ong, T.-H.; Kissick, D. J.; Jansson, E. T.; Comi, T. J.; Romanova, E. V.; Rubakhin, S. S.; Sweedler, J. V. Classification of Large Cellular Populations and Discovery of Rare Cells Using Single Cell Matrix-Assisted Laser Desorption/Ionization Time-of-Flight Mass Spectrometry.

Anal. Chem. **2015**, *87* (14), 7036–7042. https://doi.org/10.1021/acs.analchem.5b01557.

(22) Jansson, E. T.; Comi, T. J.; Rubakhin, S. S.; Sweedler, J. V. Single Cell Peptide Heterogeneity of Rat Islets of Langerhans. *ACS Chem. Biol.* **2016**, *11* (9), 2588–2595. https://doi.org/10.1021/acschembio.6b00602.

(23) Dorrell, C.; Schug, J.; Canaday, P. S.; Russ, H. A.; Tarlow, B. D.; Grompe, M. T.; Horton, T.; Hebrok, M.; Streeter, P. R.; Kaestner, K. H.; et al. Human Islets Contain Four Distinct Subtypes of β Cells. *Nature Communications* **2016**, *7*, 11756. https://doi.org/10.1038/ncomms11756.

(24) Jankowski, J. A.; Tracht, S.; Sweedler, J. V. Assaying Single Cells with Capillary Electrophoresis. *TrAC Trends in Analytical Chemistry* **1995**, *14* (4), 170–176. https://doi.org/10.1016/0165-9936(95)98315-Y.

(25) Lapainis, T.; Rubakhin, S. S.; Sweedler, J. V. Capillary Electrophoresis with Electrospray Ionization Mass Spectrometric Detection for Single-Cell Metabolomics. *Anal. Chem.* **2009**, *81* (14), 5858–5864. https://doi.org/10.1021/ac900936g.

(26) Aerts, J. T.; Louis, K. R.; Crandall, S. R.; Govindaiah, G.; Cox, C. L.; Sweedler, J. V. Patch Clamp Electrophysiology and Capillary Electrophoresis–Mass Spectrometry Metabolomics for Single Cell Characterization. *Anal. Chem.* **2014**, *86* (6), 3203–3208. https://doi.org/10.1021/ac500168d.

(27) Nemes, P.; Rubakhin, S. S.; Aerts, J. T.; Sweedler, J. V. Qualitative and Quantitative Metabolomic Investigation of Single Neurons by Capillary Electrophoresis Electrospray Ionization Mass Spectrometry. *Nat. Protocols* **2013**, *8* (4), 783–799. https://doi.org/10.1038/nprot.2013.035.

(28) Cecala, C.; Sweedler, J. V. Sampling Techniques for Single-Cell Electrophoresis. *Analyst* **2012**, *137* (13), 2922–2929. https://doi.org/10.1039/C2AN16211C.

(29) Liu, J.; Tseng, K.; Garcia, B.; Lebrilla, C. B.; Mukerjee, E.; Collins, S.; Smith, R. Electrophoresis Separation in Open Microchannels. A Method for Coupling Electrophoresis with MALDI-MS. *Anal. Chem.* **2001**, *73* (9), 2147–2151. https://doi.org/10.1021/ac001326t.

(30) Rejtar, T.; Hu, P.; Juhasz, P.; Campbell, J. M.; Vestal, M. L.; Preisler, J.; Karger, B. L. Off-Line Coupling of High-Resolution Capillary Electrophoresis to MALDI-TOF and TOF/TOF MS. *J. Proteome Res.* **2002**, *1* (2), 171–179. https://doi.org/10.1021/pr015519o.

(31) Page, J. S.; Rubakhin, S. S.; Sweedler, J. V. Single-Neuron Analysis Using CE Combined with MALDI-MS and Radionuclide Detection. *Anal. Chem.* **2002**, *74* (3), 497–503. https://doi.org/10.1021/ac0156621.

(32) Fan, Y.; Young Lee, C.; S. Rubakhin, S.; V. Sweedler, J. Stimulation and Release from Neurons via a Dual Capillary Collection Device Interfaced to Mass Spectrometry. *Analyst* **2013**, *138* (21), 6337–6346. https://doi.org/10.1039/C3AN01010D.

(33) Preisler, J.; Foret, F.; Karger, B. L. On-Line MALDI-TOF MS Using a Continuous Vacuum Deposition Interface. *Anal. Chem.* **1998**, *70* (24), 5278–5287. https://doi.org/10.1021/ac9807823.

(34) Tracht, S. E.; Cruz, L.; Stobba-Wiley, C. M.; Sweedler, J. V. Detection of Radionuclides in Capillary Electrophoresis Using a Phosphor-Imaging Detector. *Anal. Chem.* **1996**, *68* (22), 3922–3927. https://doi.org/10.1021/ac9603901.

(35) Van Berkel, G. J.; Kertesz, V.; King, R. C. High-Throughput Mode Liquid Microjunction Surface Sampling Probe. *Anal. Chem.* **2009**, *81* (16), 7096–7101. https://doi.org/10.1021/ac901098d.

(36) ElNaggar, M. S.; Barbier, C.; Van Berkel, G. J. Liquid Microjunction Surface Sampling Probe Fluid Dynamics: Computational and Experimental Analysis of Coaxial Intercapillary

Positioning Effects on Sample Manipulation. *J. Am. Soc. Mass Spectrom.* **2011**, *22* (7), 1157. https://doi.org/10.1007/s13361-011-0145-5.

(37) Comi, T. J.; Neumann, E. K.; Do, T. D.; Sweedler, J. V. MicroMS: A Python Platform for Image-Guided Mass Spectrometry Profiling. *J. Am. Soc. Mass Spectrom.* **2017**, *28* (9), 1919–1928. https://doi.org/10.1007/s13361-017-1704-1.

(38) Do, T. D.; Comi, T. J.; Dunham, S. J. B.; Rubakhin, S. S.; Sweedler, J. V. Single Cell Profiling Using Ionic Liquid Matrix-Enhanced Secondary Ion Mass Spectrometry for Neuronal Cell Type Differentiation. *Anal. Chem.* **2017**, *89* (5), 3078–3086. https://doi.org/10.1021/acs.analchem.6b04819.

(39) Barrado, M. J. G.; Osma, M. C. I.; Blanco, E. J.; Hernández, M. C.; Robledo, V. S.; Iniesta, L. C.; Carrero, S.; Carretero, J. Dopamine Modulates Insulin Release and Is Involved in the Survival of Rat Pancreatic Beta Cells. *PLOS ONE* **2015**, *10* (4), e0123197. https://doi.org/10.1371/journal.pone.0123197.

(40) Ustione, A.; Piston, D. W. Dopamine Synthesis and D3 Receptor Activation in Pancreatic β-Cells Regulates Insulin Secretion and Intracellular [Ca2+] Oscillations. *Molecular Endocrinology* **2012**, *26* (11), 1928–1940. https://doi.org/10.1210/me.2012-1226.

(41) Tucker, K. R.; Li, Z.; Rubakhin, S. S.; Sweedler, J. V. Secondary Ion Mass Spectrometry Imaging of Molecular Distributions in Cultured Neurons and Their Processes: Comparative Analysis of Sample Preparation. *J. Am. Soc. Mass Spectrom.* **2012**, *23* (11), 1931–1938. https://doi.org/10.1007/s13361-012-0472-1.

(42) Giordano, E.; Cirulli, V.; Bosco, D.; Rouiller, D.; Halban, P.; Meda, P. B-Cell Size Influences Glucose-Stimulated Insulin Secretion. *American Journal of Physiology-Cell Physiology* **1993**, *265* (2), C358–C364. https://doi.org/10.1152/ajpcell.1993.265.2.C358.

(43) Mayer, B. X. How to Increase Precision in Capillary Electrophoresis. *Journal of Chromatography A* **2001**, *907* (1), 21–37. https://doi.org/10.1016/S0021-9673(00)01057-8.

(44) Borelli, M. I.; Rubio, M.; García, M. E.; Flores, L. E.; Gagliardino, J. J. Tyrosine Hydroxylase Activity in the Endocrine Pancreas: Changes Induced by Short-Term Dietary Manipulation. *BMC Endocr Disord* **2003**, *3*, 2. https://doi.org/10.1186/1472-6823-3-2.

(45) Raffo, A.; Hancock, K.; Polito, T.; Xie, Y.; Andan, G.; Witkowski, P.; Hardy, M.; Barba, P.; Ferrara, C.; Maffei, A.; et al. Role of Vesicular Monoamine Transporter Type 2 in Rodent Insulin Secretion and Glucose Metabolism Revealed by Its Specific Antagonist Tetrabenazine. *J Endocrinol* **2008**, *198* (1), 41–49. https://doi.org/10.1677/JOE-07-0632.

CHAPTER 5: HYPHENATION OF IMMUNOCYTOCHEMICAL CELL-TYPE IDENTIFICATION AND CE–ESI-MS CHEMICAL PROFILING

This work was performed in collaboration with Dr. Joanna F. Ellis, Dr. Elizabeth K. Neumann, Prof. Stanislav S. Rubakhin, and Prof. Jonathan V. Sweedler. M.C.P performed extractions, CE–ESI-MS, and data analysis. J.F.E. performed optical imaging, cell-finding with microMS, immunostaining, and wrote MATLAB scripts for data visualization and statistical analysis of data sets. E.K.N performed optical imaging, cell-finding, MALDI-FT-ICR-MS, and immunostaining for section 5.3.3. S.S.R. prepared rat brain samples. This work was supported by the American Diabetes Association Award # 1-18-VSN-19.

5.1 INTRODUCTION

Cell type classification is crucial to single cell analysis – without knowing the identity of a cell of interest, correlating chemical profiles to biological function becomes extremely difficult. This difficulty is compounded as we move toward study of diminishingly small samples, such as single cells. Great strides have been made in single cell analysis and classification, especially in the realm of transcriptomics[1]—but only recently has the field been explored using mass spectrometry (MS).[2,3]

Cell types are in many ways as diverse as the models from which we collect the cells. When selecting a target for single cell analysis, the ease of collecting and classifying the cell of interest can be as important a consideration as the biological question one wishes to answer. Cell size, accessibility, and confident identification are among some of the challenges one must address when choosing and preparing samples.

Many single cell analysis approaches circumvent these challenges by thoughtfully choosing a model in which the cells are relatively easy to identify. In several neurological models,

such as the mollusk *Aplysia californica*, the electrophysiology of many cells in the nervous system are well-characterized.[4] Many of the neurons are also large enough to be identified visually based on size and location.[5] Patch-clamp electrophysiology has also been used to identify cells in rodent models for cell type identification prior to chemical analysis.[6] The developmental model *Xenopus laevis* is another excellent option for single cell chemical analysis because the cells within the embryo are transparent and large (on the order of millimeters). The development of *X. laevis* is well-characterized – each cell in the embryo (which conveniently and predictably differ in color) has a distinct cell fate that can be followed through development.[7,8]

In these instances, whether identifying a cell visually or by patch-clamp electrophysiology, the cell can be identified and collected without loss of chemical content. Of course, not all cell types can be classified visually or with lossless analysis techniques. For most cell type classifications, two methods are the gold-standard in identifying and classifying cells: immunocytochemistry (ICC) and transcriptomics, the latter of which is covered in more detail in Chapter 6.

Immunochemistry is a powerful tool for cell type classification – the antibody targets and fluorescence microscopy detection results in highly specific and sensitive cell identification.[9] Antibodies are versatile for chemical detection and enables targeting of many molecules that can distinguish cell types.[10] Though useful for classification, ICC can detect at most only a few analytes in one experiment. To pair ICC with an untargeted chemically profiling approach would enable the correlation of observed heterogeneity with canonical cell types and possibly the discovery of new cell subtypes.

The process of most ICC experiments, however, precludes MS analysis because tissue must be fixed before antibody incubation. Fixation crosslinks proteins and peptides and permeabilizes

the tissue, causing leeching of small molecules.[11] Thus, proteomics, peptidomics, and metabolomics are difficult to perform following the procedure, though it has been accomplished in a few cases.[12] An ideal hyphenation would perform chemical profiling prior to or simultaneously with ICC.

Our group successfully performed ICC following MALDI-MS analysis.[2] Our goal in this study is to expand this type of hyphenation with solution-phase chemical profiling. Here, we present a method which enables hyphenation of ICC cell-type classification with capillary electrophoresis–electrospray ionization-MS (CE–ESI-MS) chemical profiling using the liquid microjunction (LMJ) extraction probe presented in Chapter 4.

5.2 EXPERIMENTAL

5.2.1 Chemicals

2,5-dihydroxybenzoic acid (DHB), bovine serum albumin (BSA), Tween 20, and ethanol were purchased from MilliporeSigma (St. Louis, MO). 4% paraformaldehyde (PFA) in phosphate buffered solution (PBS) was purchased from Affymetrix (Santa Clara, CA). Anti-GFAP (mouse MAB360) and anti-NF-L chain (rabbit AB9568) were purchased from EMD Millipore (Billerica, MA). Daylight 550 secondary antibody (goat anti-mouse) was purchased from Thermo Scientific (Hudson, NH). Alex Fluor 488 secondary antibody (goat anti-rabbit), PBS, Hoechst 33342, and 10% normal goat serum were purchased from Life Technologies (Gaithersburg, MD).

Solvents for CE–ESI-MS analysis were purchased from Honeywell (Charlotte, NC). All remaining chemicals, including formic acid and metabolite standards, were purchased from Sigma-Aldrich (St. Louis, MO).

5.2.2 Isolation of biological samples

All procedures related to animal handling and euthanasia were performed in accordance with approved by the Illinois Institutional Animal Care and Use Committee protocol as well as local, state, and federal regulations. 2.5–3 month-old Sprague-Dawley outbred male rats (Charles Rivers Laboratories, Wilmington, MA) were euthanized using slow asphyxiation with CO_2. Animal blood was partially removed by brief transcardial perfusion with 60 ml of ice cold mGBSS containing (in mM): 1.5 $CaCl_2$, 4.9 KCl, 0.2 KH_2PO_4, 11 $MgCl_2$, 0.3 $MgSO_4$, 138 NaCl, 27.7 $NaHCO_3$, and 0.8 Na_2HPO_4, and 25 HEPES, pH 7.2. The hippocampal area was surgically dissected and placed in equilibrated with 95% O2:5%CO_2 solution containing 20 units/ml papain and 0.005% DNase (papain dissociation system LK003150, Worthington Biochemical, Lakewood, NJ). 2 hours treatment of tissues at 34° C under 95% O2:5%CO_2 atmosphere followed. Tissues were mechanically dissociated after several washes with mGBSS. Cells were plated onto ITO glass slides in droplets of mGBSS and incubated for 10-20 min. Samples were washed with 33% glycerol in mGBSS with aspiration of most of solution. Boxes filled with nitrogen gas were used as storage of the samples at 23° C until use.

5.2.3 Slide preparation and liquid microjunction extraction

Dissociated tissue was dispersed onto glass slides as described in Chapter 3. Briefly, glass slides were prepared for optically guided single-cell profiling by marking the perimeter of dissociated cells with ∼20 fiducial marks. The locations of fiducials and cells were determined by whole-slide bright-field and fluorescence microscopy using an Axio Imager M2 (Carl Zeiss, Jena, Germany). Images were acquired with a 10× objective and tiled to cover the entire region of interest. Florescence imaging of Hoechst 33342 utilized an X-CITE 120 mercury lamp (Lumen Dynamics, Mississauga, Canada) and a 31000v2 DAPI filter set (Chroma Technology, Irvine, CA).

The liquid microjunction extraction probe described in Chapter 3 was used for extraction of prepared single cells.[13] Modifications of the protocol included an increase in the length of the outer coaxial capillary to 3.5 cm, increase of the extraction solution flow rate to 2 μL/min, and an increase in the aspiration vacuum to 12-15 in Hg. Samples collected by the probe were dried using a Mi-Vac sample concentrator (SP Scientific, Warminster, PA) and stored at −20 °C prior to CE–ESI-MS analysis. The slide was promptly removed after extraction for immunocytochemical staining.

5.2.4 Immunocytochemistry

ICC was performed as described previously.[2] After extraction, cells were fixed in paraformaldehyde for 10 min followed by a 3 min wash in PBS buffer. The slides were then incubated in a blocking buffer (50 mg/mL BSA, 10% (v/v) goat serum, and 0.5% (v/v) Tween-20 in PBS), followed by another 3 min PBS rinse. Antibody controls were isolated with a hydrophobic pen. Fixed cells were immunostained with primary antibodies against GFAP for neurons and/or NF-L for astrocytes for 2 d at 4 °C in antibody buffer (1% BSA and 0.5% Tween-20 in PBS; 1:1000 dilution of each antibody). Cells were then stained over another 2-d incubation period with fluorescently labelled secondary antibodies in antibody buffer at 1:100 dilution. Slides were washed in PBS three times for 3 min after each antibody incubation. Stained samples were imaged using the Axio M2 imager as described above.

5.2.5 CE–ESI-MS profiling

Each cell extract was dried and resuspended in 1 μL of 1% formic acid in liquid chromatography–MS grade water containing 1 μM of a quinine internal standard (for hydrodynamic injection), or 10 uL of a 0.1 μM quinine in 90% methanol, 0.01% formic acid solution (for electrokinetic injections). CE–ESI-MS was performed as reported previously using a maXis Qq-TOF-MS/MSmass spectrometer (Bruker Daltonics).[13,14] Analyses were conducted in positive ion mode using a 72.6 cm long CE fused-silica capillary (Polymicro Technologies) and a separation potential of 20 kV. Two injections types were performed, hydrodynamic and electrokinetic. Hydrodynamic injection was performed by raising the injection platform 13 cm for 90 s and injects ~ 10 nL of material. Electrokinetic injection was performed as described later in Chapter 7, with field-amplified sample injection (FASI), by applying 20 kV of high voltage for 30 s. Extracted ion electropherograms were exported using custom scripts in Bruker DataAnalysis version 4.4. Compounds were identified as described previously.[13]

5.3 RESULTS AND DISCUSSION

5.3.1 Immunocytochemistry following extraction

Prior to performing metabolite profiling, we needed to ensure that enough cell material remained on the slide after extraction to immunostain. Single cells from rat hippocampal tissue dispersed onto a microscope slide were extracted using the LMJ probe. The slide was then immediate immunostained to assess whether immunostaining was successful and to confirm that extraction did not dislocate the cells.

Bright field and fluorescence images were taken before and after LMJ extraction and immunostaining (Figure 5.1). The images show that the cells remained in place after extraction and immunostaining – we can confidently assume that we are analyzing the same cell in each analysis. We also get clear immunostaining of astrocytes after extraction. The extraction solution, 50% methanol, 0.5% acetic acid in water, extracts mobile metabolites via diffusion of soluble analytes. This method of extraction is relatively gentle and preserves the structural integrity of the cell. We hypothesize that what remains is the lipid membrane, transmembrane proteins, and insoluble structural proteins. The success of a post-extraction ICC experiment depends upon the extraction solution used and the selection of a structural or transmembrane marker.

5.3.2 Hyphenating ICC to CE–ESI-MS

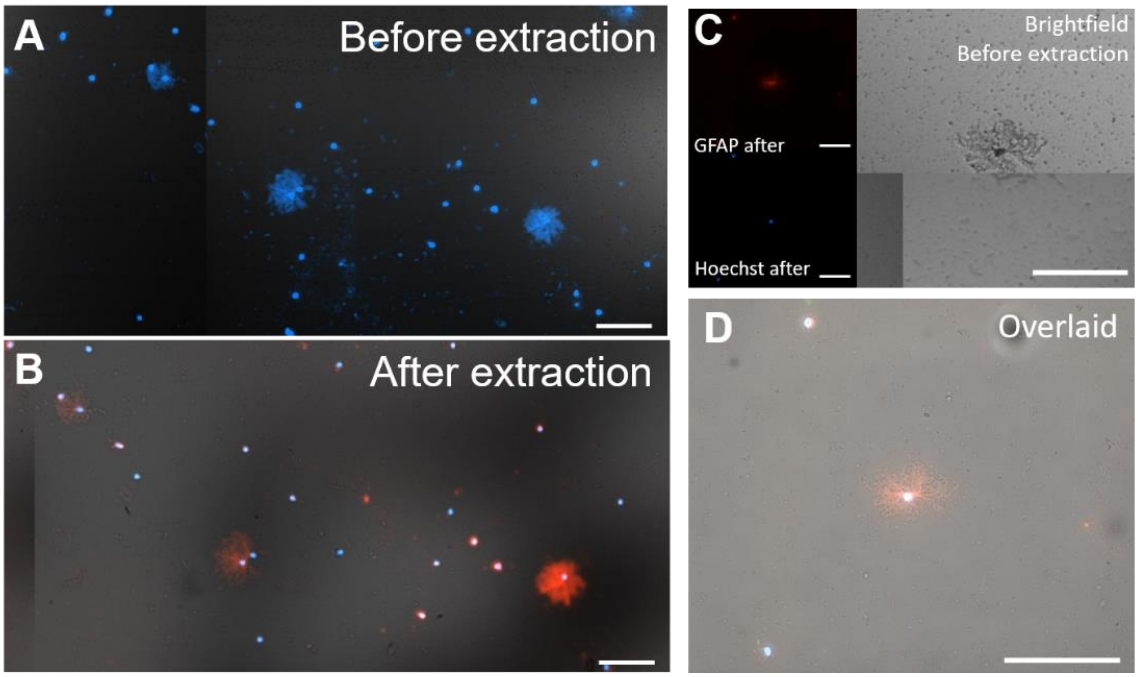

Figure 5.1. Immunostaining of rat hippocampal astrocytes before and after extraction. Cells were stained with nuclear dye Hoechst 33342 (blue) and imaged for registration of cell locations. Following extraction, cells were immunostained for GFAP (red) and imaged again. (A) Hoechst 33342 before extraction. (B) Hoechst 33342 and GFAP after extraction. (C) GFAP and Hoechst 33342 staining separately after extraction, and brightfield image of the same cell before extraction. (D) overlaid image of images in C, demonstrating that cells are not dislocated during extraction or immunostaining. Scale bar denotes 10 µm.

We performed LMJ extraction of single cells as described previously.[13] After tissue dissociation and staining with Hoechst 33342, cells were subject to a 250 μm distance filter in microMS, then manually selected for shape and size quality and visual similarity to astrocytes (a star-like shape with radial processes) or neurons (a linear shape with bidirectional processes). We modified the LMJ probe to have a 3.5 cm outer capillary, which provided more give to the capillary when positioning the probe to contact the slide. The flow rate and vacuum aspiration were increased to maximize extraction of content from the cells.

We experimented with CE–ESI-MS protocols to maximize signal from the single cell content. We performed both hydrodynamic injections and electrokinetic injections. Electrokinetic injections (which additionally employed field-amplified sample stacking as described in Chapter 7) were performed to increase signal, but this method biases injection toward more highly charged metabolites and can cause unwanted chemistries where sample buffer contacts the stainless-steel injection vials. With this method it is also prohibitively difficult to calculate the absolute amount of each metabolite injected. Though hydrodynamic injection does not bias injection of material, less material is injected overall, limiting signal. We noted that, unlike experiments performed on single cells from pancreatic islets of Langerhans,[13] signal of even common metabolite such as amino acids was limited with hydrodynamic injection (Figure 5.2). We hypothesize that this is due to the smaller size of the cells, where even a few μm difference in diameter (as is the case between islet cells and cerebral cells) amounts to an order of magnitude difference in volume and total cell material.

From the samples with which we performed FASI, we detected approximately 50 metabolites per cell, whereas with hydrodynamic injection we detected half as many metabolites

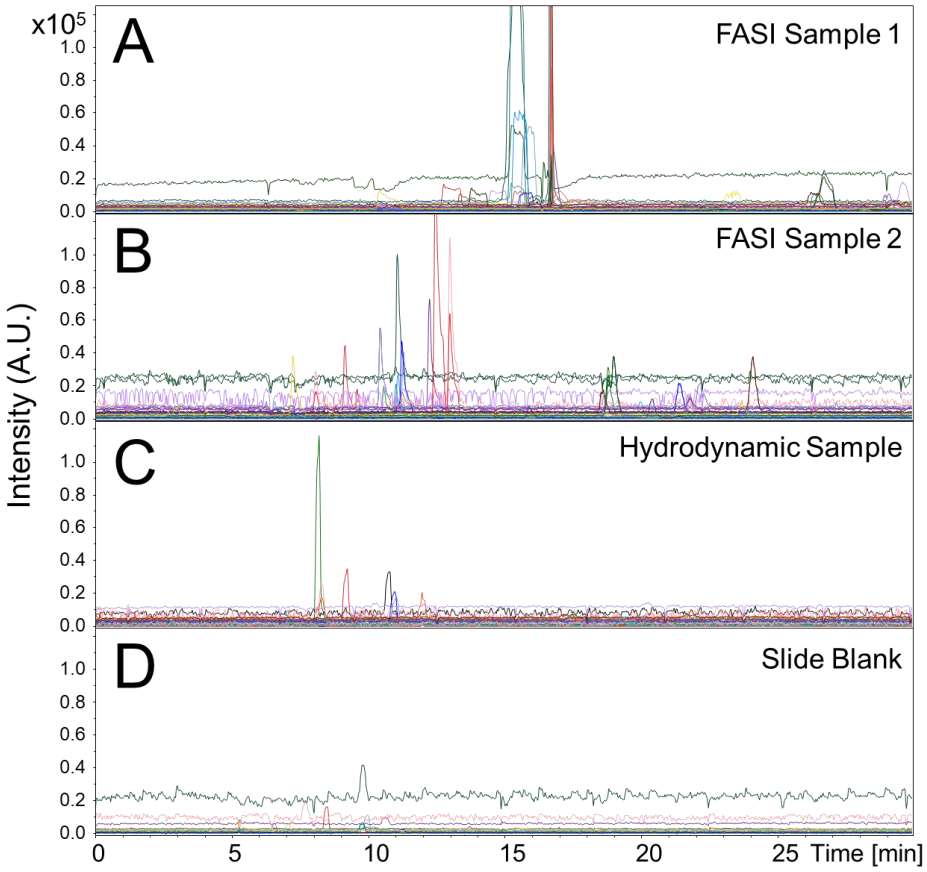

Figure 5.2. Representative electropherograms of single cell samples. (A) A cell analyzed with FASI injection. Though many metabolites were detected, separation was poor, with many coeluting peaks. (B) A cell analyzed with FASI injection. A similar number of analytes was detected with better separation. (C) A cell analyzed with hydrodynamic injection. About half as many metabolites were detected, and with much poorer signal. (D) A blank collected from a clean portion of the microscope slide. The presence of some metabolites indicate contamination; however, cell samples produced more metabolites with higher signal.

with lower signal. However, we confirmed via both injection methods that we successfully extracted metabolite content from single cells by comparing electropherograms with blanks. Though some metabolites signals appear in the blanks, we detected multiple metabolites that did not appear in the blanks, such as the amino acids arginine, valine, serine, leucine/isoleucine, threonine, phenylalanine, tyrosine, proline, and glutamic acid, which we expect to appear in every cell.

We experience several issues when applying FASI to this system, despite the signal enhancement. As demonstrated in Figures 5.2A and 5.2B, we could not consistently separate metabolites under high voltage. We also observed band broadening and poor peak shapes for some metabolites, possibly due to salt interference. Further work is being performed in the Sweedler lab to improve the use of FASI for this application and adapt the method to an automated microfabricated instrument.

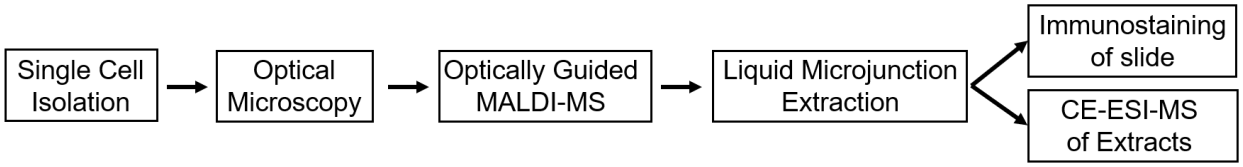

Scheme 5.1. Overview of the hyphenation of MALDI-MS, CE–ESI-MS, and ICC. Rat cerebral tissue was dissected and dissociated onto an ITO-coated glass slide. MALDI-MS is used to assay the lipid profile of individual cells. The liquid microjunction probe collects cell contents from specified locations on the ITO-coated glass slide for follow-up CE–ESI-MS analysis and simultaneous ICC for astrocytes and neurons.

5.3.3 Incorporating MALDI-MS analysis

Incorporating MALDI-MS into the LMJ workflow for ICC is straightforward as MALDI-MS and LMJ hyphenation was previously established as described in Chapter 4, and MALDI-MS and immunostaining have been performed on the same samples in previous work.[2] In this case, we demonstrated the method presented in Scheme 5.1 as a successful hyphenation of MALDI-MS, CE–ESI-MS, and ICC for analysis of the same single cell.

The results are presented in Figure 5.3, where a single rat hippocampal neuron was profiled for lipids using Fourier transform-ion cyclotron resonance (FT-ICR)-MS, profiled for metabolites with CE–ESI-MS, and immunostained for NF-L with ICC.

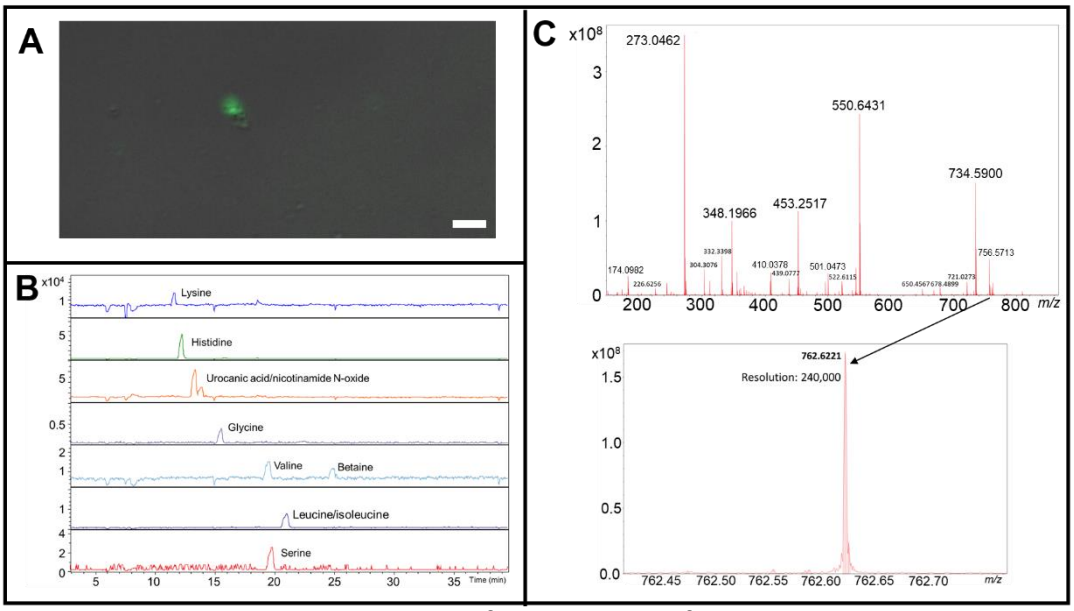

Figure 5.3. Representative results from analysis of a single rat cerebral neuron with hyphenated MALDI-MS, CE–ESI-MS, and immunocytochemistry. (A) Fluorescence image of cell stained with NF-L, a neuron marker. (B) CE–ESI-MS metabolite profile. (C) High-resolution MALDI-FT-ICR-MS profiling of lipids performed prior to LMJ extraction. Arrow indicates zoomed profile of 762.6221 *m/z* peak, likely a phosphatidylcholine, illustrating high mass resolution of 240,000. Scale bar denotes 10 µm.

5.4 CONCLUSIONS

We have successfully applied the liquid microjunction extraction probe to the extraction of single rat cerebral cells and demonstrated our ability to hyphenate CE–ESI-MS, MALDI-MS, and immunocytochemistry on the same single cell. Introducing ICC into mass spectrometry experiments enables positive cell type classification in biological analyses, which widens pool of model systems for chemical analysis to those for which the standard of cell type identification and classification is destructive, such as ICC. Comparing the profiles of astrocytes and neurons will lead to insight into the differing functions of these neighboring cell types. Importantly, this technology will enable further exploration into astrocyte heterogeneity and their biological role beyond serving as support for neurons. This work is still ongoing with continuing members of the Sweedler lab who will optimize the analysis conditions for successful FASI and increase

throughput for CE–ESI-MS analysis with a commercial instrument. This technology will enable investigation into the interplay between biological and chemical function in single cells.

5.5 REFERENCES

(1) Morales, M.; Margolis, E. B. Ventral Tegmental Area: Cellular Heterogeneity, Connectivity and Behaviour. *Nat Rev Neurosci* **2017**, *18* (2), 73–85. https://doi.org/10.1038/nrn.2016.165.

(2) Neumann, E. K.; Comi, T. J.; Rubakhin, S. S.; Sweedler, J. V. Lipid Heterogeneity between Astrocytes and Neurons Revealed by Single-Cell MALDI-MS Combined with Immunocytochemical Classification. *Angewandte Chemie International Edition* **2019**, *58* (18), 5910–5914. https://doi.org/10.1002/anie.201812892.

(3) Comi, T. J.; Do, T. D.; Rubakhin, S. S.; Sweedler, J. V. Categorizing Cells on the Basis of Their Chemical Profiles: Progress in Single-Cell Mass Spectrometry. *J. Am. Chem. Soc.* **2017**, *139* (11), 3920–3929. https://doi.org/10.1021/jacs.6b12822.

(4) Moroz, L. L.; Edwards, J. R.; Puthanveettil, S. V.; Kohn, A. B.; Ha, T.; Heyland, A.; Knudsen, B.; Sahni, A.; Yu, F.; Liu, L.; Jezzini, S.; Lovell, P.; Iannucculli, W.; Chen, M.; Nguyen, T.; Sheng, H.; Shaw, R.; Kalachikov, S.; Panchin, Y. V.; Farmerie, W.; Russo, J. J.; Ju, J.; Kandel, E. R. Neuronal Transcriptome of Aplysia: Neuronal Compartments and Circuitry. *Cell* **2006**, *127* (7), 1453–1467. https://doi.org/10.1016/j.cell.2006.09.052.

(5) Akhmedov, K.; Kadakkuzha, B. M.; Puthanveettil, S. V. Aplysia Ganglia Preparation for Electrophysiological and Molecular Analyses of Single Neurons. *JoVE (Journal of Visualized Experiments)* **2014**, No. 83, e51075. https://doi.org/10.3791/51075.

(6) Aerts, J. T.; Louis, K. R.; Crandall, S. R.; Govindaiah, G.; Cox, C. L.; Sweedler, J. V. Patch Clamp Electrophysiology and Capillary Electrophoresis–Mass Spectrometry Metabolomics for

Single Cell Characterization. *Anal. Chem.* **2014**, *86* (6), 3203–3208. https://doi.org/10.1021/ac500168d.

(7) Moody, S. A. Fates of the Blastomeres of the 16-Cell Stage Xenopus Embryo. *Developmental Biology* **1987**, *119* (2), 560–578. https://doi.org/10.1016/0012-1606(87)90059-5.

(8) Moody, S. A. Fates of the Blastomeres of the 32-Cell-Stage Xenopus Embryo. *Developmental Biology* **1987**, *122* (2), 300–319. https://doi.org/10.1016/0012-1606(87)90296-X.

(9) Van Noorden, S.; Polak, J. M. 2 - Immunocytochemistry Today: Techniques and Practice. In *Immunocytochemistry*; Polak, J. M., Van Noorden, S., Eds.; Butterworth-Heinemann, 1983; pp 11–42. https://doi.org/10.1016/B978-0-7236-0669-7.50009-X.

(10) Doetsch, F.; Caillé, I.; Lim, D. A.; García-Verdugo, J. M.; Alvarez-Buylla, A. Subventricular Zone Astrocytes Are Neural Stem Cells in the Adult Mammalian Brain. *Cell* **1999**, *97* (6), 703–716. https://doi.org/10.1016/S0092-8674(00)80783-7.

(11) Howat, W. J.; Wilson, B. A. Tissue Fixation and the Effect of Molecular Fixatives on Downstream Staining Procedures. *Methods* **2014**, *70* (1), 12–19. https://doi.org/10.1016/j.ymeth.2014.01.022.

(12) Neupert, S.; Rubakhin, S. S.; Sweedler, J. V. Targeted Single-Cell Microchemical Analysis: MS-Based Peptidomics of Individual Paraformaldehyde-Fixed and Immunolabeled Neurons. *Chemistry & Biology* **2012**, *19* (8), 1010–1019. https://doi.org/10.1016/j.chembiol.2012.05.023.

(13) Comi, T. J.; Makurath, M. A.; Philip, M. C.; Rubakhin, S. S.; Sweedler, J. V. MALDI-MS Guided Liquid Microjunction Extraction for Capillary Electrophoresis–Electrospray Ionization MS Analysis of Single Pancreatic Islet Cells. *Anal. Chem.* **2017**, *89* (14), 7765–7772. https://doi.org/10.1021/acs.analchem.7b01782.

(14) Nemes, P.; Rubakhin, S. S.; Aerts, J. T.; Sweedler, J. V. Qualitative and Quantitative Metabolomic Investigation of Single Neurons by Capillary Electrophoresis Electrospray Ionization Mass Spectrometry. *Nat Protoc* **2013**, *8* (4), 783–799. https://doi.org/10.1038/nprot.2013.035.

CHAPTER 6: LIQUID MICROJUNCTION EXTRACTION OF RNA FOR MASS SPECTROMETRY AND TRANSCRIPTOMICS ANALYSIS

The work in this chapter was done in collaboration with Dr. Kevin D. Clark. M.C.P. developed the biphasic extraction modification and initial extraction protocol. K.D.C. prepared *A. californica* samples, optimized extraction for RNA isolation, and performed subsequent chemical analyses including spectrophotometry and LC-MS. This work was supported by the American Diabetes Association Award # 1-18-VSN-19 and the National Institute on Drug Abuse Award # P30 DA018310.

6.1 INTRODUCTION

Besides immunochemistry, transcriptomics has become a gold-standard technique for cell type classification and identification.[1] Not only does transcriptomics not require cell fixation, it is capable of profiling thousands of transcripts to build multidimensional cell-type classification as opposed to basing identification on at most a handful of antibody targets. Performing orthogonal transcriptomics with mass spectrometry (MS)-based chemical measurements can expand our ability to probe biochemical pathways by connecting genetic data with metabolic profiles, which has been previously demonstrated by the Sweedler group in bulk analyses.[2] Scaling these measurements to the single cell level will yield more detailed information on cellular heterogeneity and enable correlation of transcriptional changes to cellular neurochemistry.

The scope of RNA analysis extends beyond transcriptomics. An expanding field of study is interested in exploring modified nucleic acids, which do not change DNA or RNA sequences but do play a significant role in the biochemical function of nucleic acids.[3] Well-known and characterized examples of DNA chemical modifications include cysteine methylation, for instance, which contributes to gene expression.[4] However, more than 150 nucleic acid

modifications in DNA and RNA are known to exist, and the number continues to grow.[5] Chemical modification are not often characterized with traditional amplification-based techniques for nucleic acid analysis (though some features of nucleic acid amplification have been smartly utilized to detect individual modifications[6]), so attention has turned to MS as a label-free strategy to profile many nucleic acid modifications in a single experiment.[5,7,8] We are interested in using liquid chromatography (LC)-MS analysis to study RNA nucleoside modifications in small volume samples and single cells. These small samples pose an interesting analytical challenge in sample preparation and RNA extraction. The methods presented here will also serve as a useful strategy to apply orthogonal transcriptomics to single cell chemical analyses.

Isolation of RNA from biological samples is typically accomplished using a series of liquid processing and extraction steps. The most common liquid-liquid extraction (LLE) protocol for RNA employs a phase separation between an aqueous and organic phase.[9] Specifically, RNA is suspended in an aqueous solution with TRIzol (a phenol-based reagent) and guanidine hydrochloride, which solubilizes biological material and halts enzymatic activity through protein denaturization.[10] Upon the addition of chloroform, RNA remains in the aqueous phase, protein is extracted into the organic phase, and DNA accumulates at the interface. These liquid manipulations typically occur on the milliliter-scale for analysis of bulk samples (tissues or biological fluids, for example). Sample loss during LLE is expected and negligible in most cases with such large sample volumes – whereas sample loss becomes a significant challenge when scaling down to single cells and other small volume samples.

Adapting an LLE protocol to a liquid microjunction (LMJ) extraction procedure benefits small volume analyses of RNA two-fold: first, a simultaneous biphasic extraction will reduce the number of pre-processing steps and thus reduce sample loss, and second, semi-automation of the

extraction procedure will streamline the otherwise burdensome task of isolating and processing single cell and small volume samples. With these goals in mind, we developed a biphasic extraction protocol for the LMJ probe, which we applied to RNA extraction from buccal ganglia from *Aplysia californica*.

6.2 DESIGN OF BIPHASIC LIQUID MICROJUNCTION EXTRACTION PROBE FOR RNA

The LMJ probe was operated as described previously[11] with modifications described in Chapter 5 and an additional modification designed for biphasic extraction with an aqueous and organic phase. The modification uses an IDEX MicroTee fluidic connection (IDEX Health & Science, Part # P-890) to combine the aqueous and organic phases into a single fluid line into the LMJ probe (Figure 6.1A). Using the same syringe pump, differing syringe sizes can be used to adjust phase proportions (eg. a 1 mL syringe for aqueous and a 0.5 mL syringe for organic to achieve a 2:1 ratio of aqueous to organic).

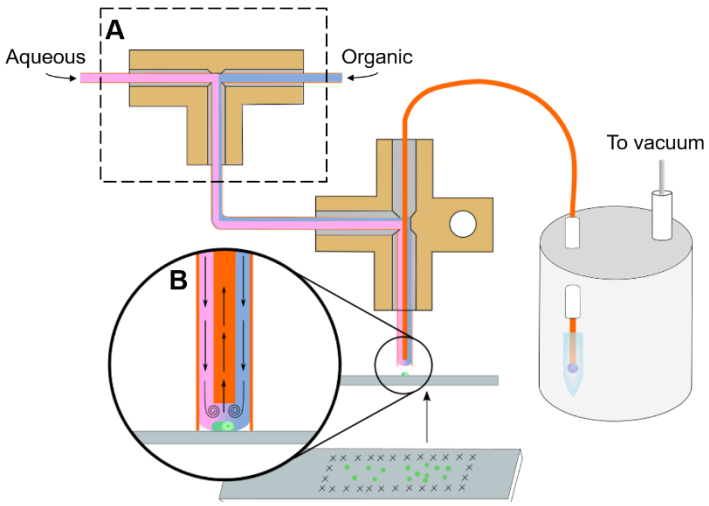

Figure 6.1. Biphasic extraction diagram. The LMJ probe operates as described previously,[11] with the addition of (A) modification to LMJ system which enables biphasic extraction. The two extraction phases are pumped via syringe into a T-junction, where they combine to flow into the LMJ probe for extraction. The phases exhibit laminar flow and do not combine. (B) Diagram illustrating flow profile at probe tip, where both phases extract from the sample simultaneously and experience slight mixing due to vacuum aspiration.

The flow profile of two joining solutions via a T-junction is laminar[12,13] and thus unlikely to mix to any significant degree within the LMJ system. Slight mixing will occur at the probe tip, where both phases will interact with the sample simultaneously (Figure 6.1B). This coinciding contact with the sample will

simultaneously halt any remaining enzymatic activity, extract proteins into the organic chloroform phase, and extract RNA into the aqueous phase.

Typical LLE of RNA uses a TRIzol and guanidine-HCl solution as the aqueous phase for RNA extraction.[10] In preliminary experiments, we noted precipitation of guanidine-HCl crystals which clogged the fused silica capillaries (Figure 6.2A). Additionally, use of TRIzol prevented UV-Vis confirmation of RNA extraction because the phenol-based reagent absorption overlaps with that of RNA (Figure 6.2B).

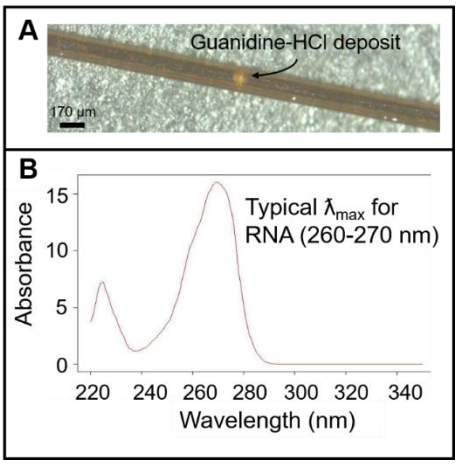

Figure 6.2. Limitations of adapting conventional liquid-liquid RNA extraction to an LMJ protocol. (A) Microscope image of precipitated guanidine hydrochloride in a portion of the LMJ probe, blocking fluid transfer. (B) UV spectrum for TRIzol reagent taken with a Nanodrop spectrophotometer. The absorbance of TRIzol between 240 – 290 nm overlaps with typical RNA absorbance at 260 – 270 nm.

Tests of alternative aqueous phases were performed on spotted tRNA standards to determine an optimal extraction solution which (a) is immiscible with chloroform, (b) dissolves RNA, (c) halts enzymatic activity, (d) does not clog the probe, (e) is UV-transparent, and (f) is compatible with LC-MS analysis. Results are presented in Table 6.1, in which a 10%

Table 6.1. Investigation of RNA extraction solvents. All extractions were performed with a 1:1 ratio of aqueous phase to chloroform. [a] Not applicable due to capillary clogging, [b] No RNA detected by Nanodrop UV spectrophotometry.

Solvent	tRNA recovered (µg)	% Recovery	tRNA carryover	Extractions before clogging
6 M GuHCl	na[a]	na	na[a]	0
1 M GuHCl	na[a]	na	na[a]	0
Milli Q water	5.1 ± 0.4	37.8 ± 2.8	nd[b]	>9
10% MeOH	4.2 ± 0.6	31.1 ± 4.4	nd[b]	>9
20% MeOH	2.7 ± 0.8	20 ± 5.9	0.3±0.4	>9

methanol solution adequately denatured proteins while extracting an optimal amount of RNA without clogging the capillaries or causing sample carryover between extractions.

6.3 LC-MS ANALYSIS OF NEURONAL CELL CLUSTERS

6.3.1 Experimental

A. californica weighing ~150g were purchased from the National Institutes of Health/University of Miami National Resource for Aplysia and maintained at 14 °C in an aquarium filled with Instant Ocean (Aquarium Systems Inc.). Before being dissected, animals were injected (40% volume/body weight) with a solution of 74 g/L $MgCl_2 \cdot 6H_2O$ to anesthetize, after which the buccal ganglia were dissected. One ganglion was reserved for conventional LLE and one buccal ganglion was deposited on a microscope slide. Spots for LMJ extraction were manually selected. Conventional LLE was performed as directed in the user guide of Invitrogen TRIzol Reagent (Catalog Numbers 15596026 and 15596018).

For extraction, two 1 mL syringes were filled with 10% methanol and chloroform, respectively, and delivered into fused silica capillaries at a rate of 1.5 µL/min using a syringe pump. Flow of the immiscible solvents was directed into the LMJ probe as described in Chapter 5. Vacuum pressure of ca. 10-16 in Hg was drawn through the inner capillary to aspirate the extraction solvents into a collection tube. Samples were extracted for 120 s then washed for 30s with 10% methanol. Collected RNA was quantified usinga NanoDrop UV spectrophotometer and subsequently digested for LC-MS analysis.

LC was carried out on an Ultimate 3000 Nano-RSLC system (Thermo Fisher Scientific) coupled to a Bruker Impact quadrupole time-of-flight mass spectrometer operated in positive ionization mode.

6.3.2 Results and Discussion

The developed LMJ extraction protocol was compared to conventional LLE protocol for RNA extraction from buccal ganglia from *A. californica*. The methods were evaluated on their ability to extract and detect RNA modifications. Preliminary results from the comparative LC-MS analyses are presented in Figure 6.3. Not only does the LMJ extraction protocol successfully extract suitable amounts of modified RNA for LC-MS analysis, it appears to result in extraction of a greater number of detectable RNA modifications. The conventional LLE protocol used resulted in the detection of unmodified nucleosides and 2 ± 0 modified nucleosides across 6 samples. The LMJ extraction demonstrated detection of unmodified nucleosides and 6 ± 1

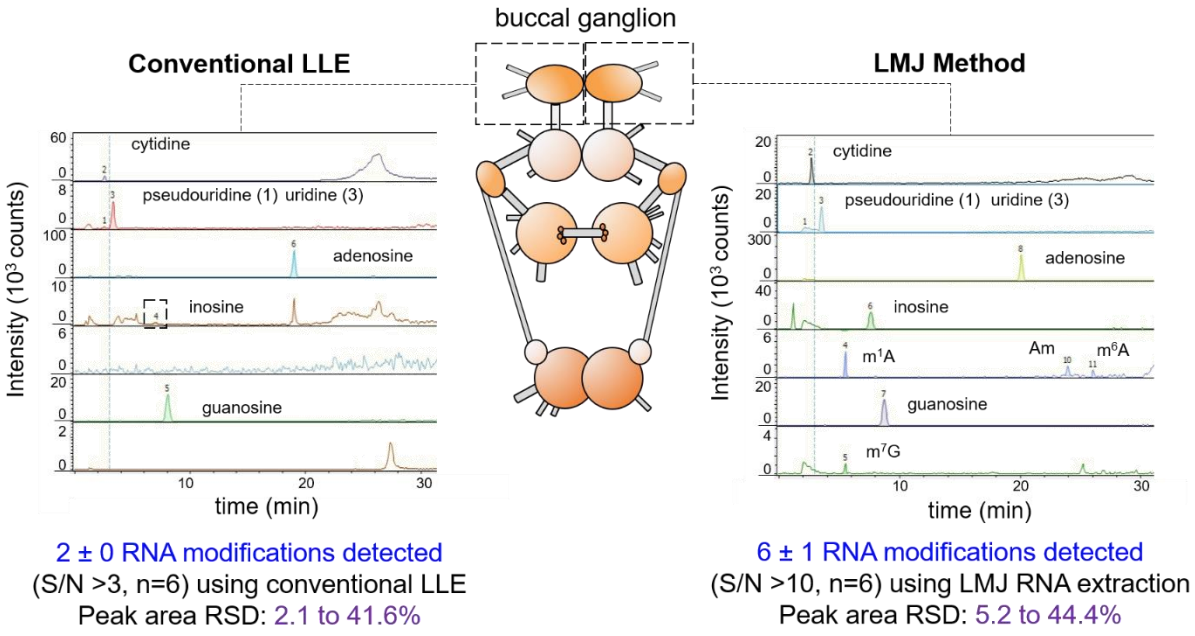

Figure 6.3. LC-MS analysis of RNA extracts from *A. californica* buccal ganglia using conventional liquid-liquid extraction and liquid microjunction extraction. LMJ extraction produced a greater number of identified RNA modifications.

modified nucleosides across the same 6 samples, all with a comparatively higher signal-to-noise ratio. Specifically, the LMJ extraction enabled detection of three different methylated adenosine bases and one methylated guanosine that were not detected using conventional LLE. The increased S/N for all detected RNA bases implies that this method will work well for smaller samples such as single cells. The amount of extracted RNA is suitable for tandem MS analysis of these detected nucleosides (Figure 6.4), enabling confident assignment of structures especially for isomeric modified RNA bases.

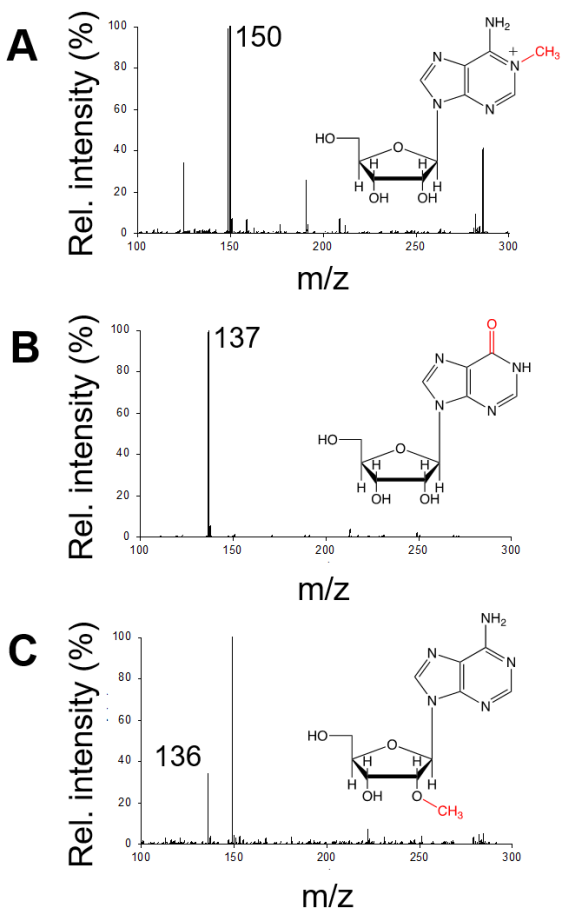

Figure 6.4. Representative MS/MS spectra of 3 modified nucleosides. (A) MS^2 of 1-methyladenosine (m^1A), observed parent mass *m/z* 282.1240, mass error = 13.5 ppm. (B) MS^2 of inosine, observed parent mass *m/z* 269.0925, mass error = 14.5 ppm. (C) MS^2 of 2'-*O*-methyladenosine (Am), observed parent mass observed *m/z* 282.1257, mass error = 20.2 ppm.

6.4 CONCLUSIONS

We have developed a biphasic protocol for extraction of RNA from small volume samples for subsequent LC-MS analysis using our liquid microjunction extraction system. We have demonstrated our protocol to achieve superior detection ability of modified nucleosides compared to conventional liquid-liquid extraction from *A. californica* buccal ganglia. This protocol will be used to study and quantify biologically and functionally relevant RNA modifications in animal models, eventually scaling the protocol to single cell samples. The tree-fold increase in detected modified RNA bases demonstrates the importance of using an optimized sampling approach.

Preliminary experiments have also shown the collected samples to be suitable for polymerase chain reaction (PCR) amplification of the extracts (data not shown), which is a promising sign of this method's applicability to transcriptomic analysis. These experiments are being passed on to future group members in collaboration with the Eberwine laboratory; these early experiments demonstrate the utility of the LMJ probe in hyphenating MALDI-MS to transcriptomics on the same cells. The overarching goal of this work is to correlate transcriptomics to peptide, protein, and metabolite profiles. Our use of the LMJ device across multiple extraction protocols and for varying biomolecules demonstrates this technology's potential for more streamlined, user-friendly, and orthogonal chemical analyses of small volume samples.

6.5 REFERENCES

(1) Poulin, J.-F.; Tasic, B.; Hjerling-Leffler, J.; Trimarchi, J. M.; Awatramani, R. Disentangling Neural Cell Diversity Using Single-Cell Transcriptomics. *Nat Neurosci* **2016**, *19* (9), 1131–1141. https://doi.org/10.1038/nn.4366.

(2) Knolhoff, A. M.; Nautiyal, K. M.; Nemes, P.; Kalachikov, S.; Morozova, I.; Silver, R.; Sweedler, J. V. Combining Small-Volume Metabolomic and Transcriptomic Approaches for Assessing Brain Chemistry. *Anal. Chem.* **2013**, *85* (6), 3136–3143. https://doi.org/10.1021/ac3032959.

(3) Li, S.; Mason, C. E. The Pivotal Regulatory Landscape of RNA Modifications. *Annu. Rev. Genom. Hum. Genet.* **2014**, *15* (1), 127–150. https://doi.org/10.1146/annurev-genom-090413-025405.

(4) Handy, D. E.; Castro, R.; Loscalzo, J. Epigenetic Modifications: Basic Mechanisms and Role in Cardiovascular Disease. *Circulation* **2011**, *123* (19), 2145–2156. https://doi.org/10.1161/CIRCULATIONAHA.110.956839.

(5) Chen, B.; Yuan, B.-F.; Feng, Y.-Q. Analytical Methods for Deciphering RNA Modifications. *Anal. Chem.* **2019**, *91* (1), 743–756. https://doi.org/10.1021/acs.analchem.8b04078.

(6) Eremeeva, E.; Herdewijn, P. PCR Amplification of Base-Modified DNA. *Current Protocols in Chemical Biology* **2018**, *10* (1), 18–48. https://doi.org/10.1002/cpch.33.

(7) Lan, M.-D.; Yuan, B.-F.; Feng, Y.-Q. Deciphering Nucleic Acid Modifications by Chemical Derivatization-Mass Spectrometry Analysis. *Chinese Chemical Letters* **2019**, *30* (1), 1–6. https://doi.org/10.1016/j.cclet.2018.04.021.

(8) Li, Q.-Y.; Yuan, B.-F.; Feng, Y.-Q. Mass Spectrometry-Based Nucleic Acid Modification Analysis. *Chem. Lett.* **2018**, *47* (12), 1453–1459. https://doi.org/10.1246/cl.180736.

(9) Patel, R.; Kvach, J. T.; Mounts, P. Isolation and Restriction Endonuclease Analysis of Mycobacterial DNA. *J. Gen. Microbiol.* **1986**, *132* (2), 541–551. https://doi.org/10.1099/00221287-132-2-541.

(10) Rio, D. C.; Ares, M.; Hannon, G. J.; Nilsen, T. W. Purification of RNA Using TRIzol (TRI Reagent). *Cold Spring Harb Protoc* **2010**, *2010* (6), pdb.prot5439. https://doi.org/10.1101/pdb.prot5439.

(11) Comi, T. J.; Makurath, M. A.; Philip, M. C.; Rubakhin, S. S.; Sweedler, J. V. MALDI-MS Guided Liquid Microjunction Extraction for Capillary Electrophoresis–Electrospray Ionization MS Analysis of Single Pancreatic Islet Cells. *Anal. Chem.* **2017**, *89* (14), 7765–7772. https://doi.org/10.1021/acs.analchem.7b01782.

(12) Gravesen, P.; Branebjerg, J.; Jensen, O. S. Microfluidics-a Review. *J. Micromech. Microeng.* **1993**, *3* (4), 168–182. https://doi.org/10.1088/0960-1317/3/4/002.

(13) Ait Mouheb, N.; Montillet, A.; Solliec, C.; Havlica, J.; Legentilhomme, P.; Comiti, J.; Tihon, J. Flow Characterization in T-Shaped and Cross-Shaped Micromixers. *Microfluid Nanofluid* **2011**, *10* (6), 1185–1197. https://doi.org/10.1007/s10404-010-0746-5.

CHAPTER 7: ENHANCED SIGNAL IN SINGLE CELL CE–ESI-MS METABOLOMICS WITH FIELD AMPLIFIED SAMPLE INJECTION

This chapter is adapted with permission from an original research article published in *Analytica Chimica Acta*, **2020**, DOI: 10.1016/j.aca.2020.04.028 with coauthors H.W. Liao, S.S. Rubakhin, and J.V. Sweedler. H.W.L. performed most of the conceptualization, experimental work, and data analysis. M.C.P. contributed to development of the methodology, data analysis, and data presentation. S.S.R. performed biological sample isolation and preparation. Funding was provided by the National Science Foundation by Award No. CHE-1606791 and the National Institute on Drug Abuse by Award No. P30 DA018310. This study was also supported by the Ministry of Science and Technology of Taiwan (MOST 106-2917-I-564-054). The National Resource for Aplysia (Miami, FL) is funded by PHS grant No. P40 OD010952.

7.1 INTRODUCTION

Despite significant advances in single cell chemical analysis, signal enhancement remains a challenge. In single cell metabolomics with CE–ESI-MS, improved signal will provide more molecular features, greater ability to identify metabolites, and improved quantitation of low-abundance metabolites. Though CE–ESI-MS is a powerful and sensitive analytical technique, some figures of merit are limited by MS detection. CE with different detection strategies, such as laser-induced fluorescence (LIF) and electrochemical detection, tend to be more versatile in employing various separation conditions. As an example, surfactants are often used in CE to adjust separation between analytes.[14] Such strategies preclude MS detection as surfactants often impede ESI performance, contaminate MS sample inlets, and have even been known to damage mass spectrometers.

CE analyses often employ on-line sample concentration for signal enhancement, including pH junctions,[15] sweeping,[16] isotachophoresis,[17] and the combination of different on-line concentration methods.[18] Stacking is an approach that utilizes the difference of an analyte's electrophoretic velocities in different environments, leading to its accumulation at the boundary of the sample matrix and a separation buffer.[19] With the optimization of the conductivities of sample matrix and buffer, analytes can be stacked, resulting in improved detection sensitivity.[20] Large volume sample stacking (LVSS) and field amplified sample injection (FASI) are two common techniques used in CE.[21] Sensitivity enhancements of 100-fold have been reported with LVSS CE–ESI-MS,[22] and it has successfully been applied to both untargeted and targeted single-cell metabolomics.[21,23] FASI has also demonstrated similar enhancements up to 1000-fold[24] and has been previously applied with CE–ESI-MS for targeted analysis.[25]

Here we report efficient and sensitive FASI CE-MS, sample desalting, and low-volume manipulations that combine to optimize the measurements of single-cell metabolites. The described approach successfully addresses several classic FASI-associated issues, including salt interference, leading to migration time shifts and analyte competition during sample loading. To demonstrate the capabilities of the FASI CE-MS approach, metabolites in small pleural sensory neurons of the sea slug *Aplysia californica* have been detected, characterized, and quantified.

7.2 EXPERIMENTAL

7.2.1 Chemicals

Stock solutions (25–100 mM) of metabolite standards were prepared using LC-MS grade water and methanol and stored at –20 °C until use. Most chemicals were purchased from MilliporeSigma (St. Louis, MO) unless otherwise specified. Methanol, isopropanol, formic acid

(FA), and acetonitrile (ACN) were obtained from Thermo Fisher Scientific (Waltham, MA). Sample extracts were kept in polymerase chain reaction tubes from MidSci (St. Louis, MO).

7.2.2 Animals and single-neuron isolation

Adult *Aplysia californica* (180–250 g) were purchased from the National Resource for Aplysia (Rosenstiel School of Marine & Atmospheric Science, University of Miami, FL), and kept at 14 °C in continuously circulated and aerated aquarium filled with sea water prepared in house using Instant Ocean Sea Salt (Instant Ocean Spectrum Brands, Blacksburg, VA). Before dissection, animals were anesthetized by injecting 390 mM $MgCl_2$ solution into the vascular cavity. The injection volume of the $MgCl_2$ solution was equal to approximately one-third of each animal's body weight. The central nervous system was surgically isolated and placed into artificial seawater (ASW) comprising: 460 mM NaCl, 10 mM KCl, 10 mM $CaCl_2$, 22 mM $MgCl_2$, 26 mM $MgSO_4$, and 10 mM 4-(2-hydroxyethyl)-1-piperazineethane-sulfonic acid, and supplemented with 100 U/mL penicillin G, 100 µg/mL streptomycin and 100 µg/mL gentamicin, pH 7.8. Ganglia and adjacent nerves were dissected and treated in 1% protease type IX in ASW-antibiotic solution for 60–100 min (depending on animal size) at 34 °C. After treatment and wash in fresh ASW-antibiotic solution, the sensory neurons were manually isolated from the pleural ganglia using sharp tungsten needles (World Precision Instruments, Inc., Sarasota, FL). The isolated single neurons were quickly (2–5 s) washed with deionized water to minimize transfer of extracellular inorganic salts from the ASW into final samples. Washed single neurons were placed into 10 µL of methanol to facilitate analyte extraction and quench enzymatic processes occurring *ex vivo*. The samples were stored in the solution at –20 °C until analysis. Before analysis, the samples were dried in a SpeedVac vacuum concentrator (Genevac, Ipswich, Suffolk, UK) and resuspended in 50 µL of a mixture containing isopropanol and ACN (0.8:0.2, v:v) providing analyte solubilization as

well as further extraction of metabolites. The samples were centrifuged for 5 min at 16000 × g, and the supernatant was further dried in the SpeedVac vacuum concentrator. Finally, the samples were reconstituted in 50 μL of a solution containing 95% methanol, 5% water, and 0.01% FA.

7.2.3 FASI-CE-MS platform and single-neuron analysis

Standard- and single cell-containing samples were assayed using an in-house assembled CE platform hyphenated to a high-resolution mass spectrometer (qTOF maXis 4G, Bruker Corp., Billerica, MA) through a custom-built coaxial sheath-flow ESI source.[26–28] The ESI source consisted of a micro-tee assembly (part P-875, IDEX Health & Science, Oak Harbor, WA) with a platinum alloy emitter (10% iridium, 0.0055" ID × 0.003'' wall × 1'' length, part 29910E, Johnson Matthey Inc., Wayne, PA). The sheath liquid (50% methanol in water solution with 0.1% FA) was supplied through the emitter at a 750 nL/min flow rate using a syringe pump (Pump 11 Elite, Harvard Apparatus, Holliston, MA) and a fused silica delivery capillary for the sheath flow (75 μm ID, 363 μm OD, Polymicro Technologies, Phoenix, AZ). The CE separation was performed on 75–80 cm, 40 μm ID, and 105 μm OD fused silica capillary (part TSP040105, Polymicro Technologies,) with a separation voltage of 20 kV. The background solution was 1.0% FA in water. FASI was performed by electrokinetic injection of the sample solution at 20 kV for 30 s. The emitter was grounded, and the capillary voltage of the mass spectrometer was set at 2000 V to establish the cone-jet spray. The dry gas was set at 180 ºC with a flow rate of 3 L min^{-1}. The mass spectrometer was calibrated regularly in the mass range of m/z 50–500 by infusing sodium formate (15 mM) via the ESI source. Recalibration of acquired data sets was performed offline with endogenous sodium formate clusters. Migration time was corrected in reference to two dipeptide internal standards, alanine-alanine and proline-leucine.

Tandem MS experiments were accomplished with 20 to 40 eV collision energies to facilitate the molecular identifications. To determine the molecular features, the obtained data were first processed by the XCMS[29] package written in R[30] using the following settings: 30 ppm mass error, signal-to-noise ratio equal to 3, and filtered with an arbitrary threshold of 1000 counts. Signals related to the analyte's isotopic distribution and background interference were manually eliminated. The detected accurate molecular masses were matched to data available at online metabolite databases (METLIN,[31] the Human Metabolome Database,[32] and MycompoundID[33]) with an allowed error of 5 ppm. Identified molecular features are presented in Table 7.1.

Quantification was based on metabolite standards with a dynamic range of approximately 5 nM to 1000 nM. The repeatability of our measurements was evaluated using fresh 10 nM standard mixtures examined on four consecutive days. These experiments revealed that the analytical repeatability of the method had an RSD of 15±2 %.

7.3 RESULTS AND DISCUSSION

7.3.1 FASI

Qualitative and quantitative measurements of low amounts of metabolites in a single cell are challenging. Cell diameters span the range of a few micrometers to hundreds of micrometers and corresponding cell volumes vary from fL to nL, which is a million-fold volume range. The wide range of analyte concentrations in different cells adds to the technical demands of the analysis. Therefore, single-cell measurements require a sensitive analytical approach that offers a wide dynamic range.

Here, we optimized FASI to improve the detection limits in single-cell ESI-MS analysis. Because analyte stacking efficiency is determined by the conductivity difference between the background solution and sample matrix, the percent composition of organic solvents and FA in

the solutions differ.[34–36] Generally, increasing the organic solvent percentage and decreasing the FA content improves detection sensitivity because this reduces conductivity. However, this also leads to increased Joule heating, and an increased likelihood of air bubble formation. After method optimization, we found that a 0.01% FA, 4.99% water, and 95% methanol solution was the most effective. This solution was used in experiments comparing the FASI approach to the classic hydrodynamic sample injection method. In these measurements, ~6 nL of a standard mixture containing lysine, histidine, and arginine (all at 100 nM) was loaded onto a CE column by a 60 s hydrodynamic injection and analyzed. The standard mixture, diluted to 10 nM for all analytes, was loaded during 60 s by FASI. We observed that 307-, 191-, and 215-fold detection sensitivity enhancement was achieved for lysine, histidine, and arginine, respectively, by FASI CE-ESI analysis of the more diluted samples (Figure 7.1).

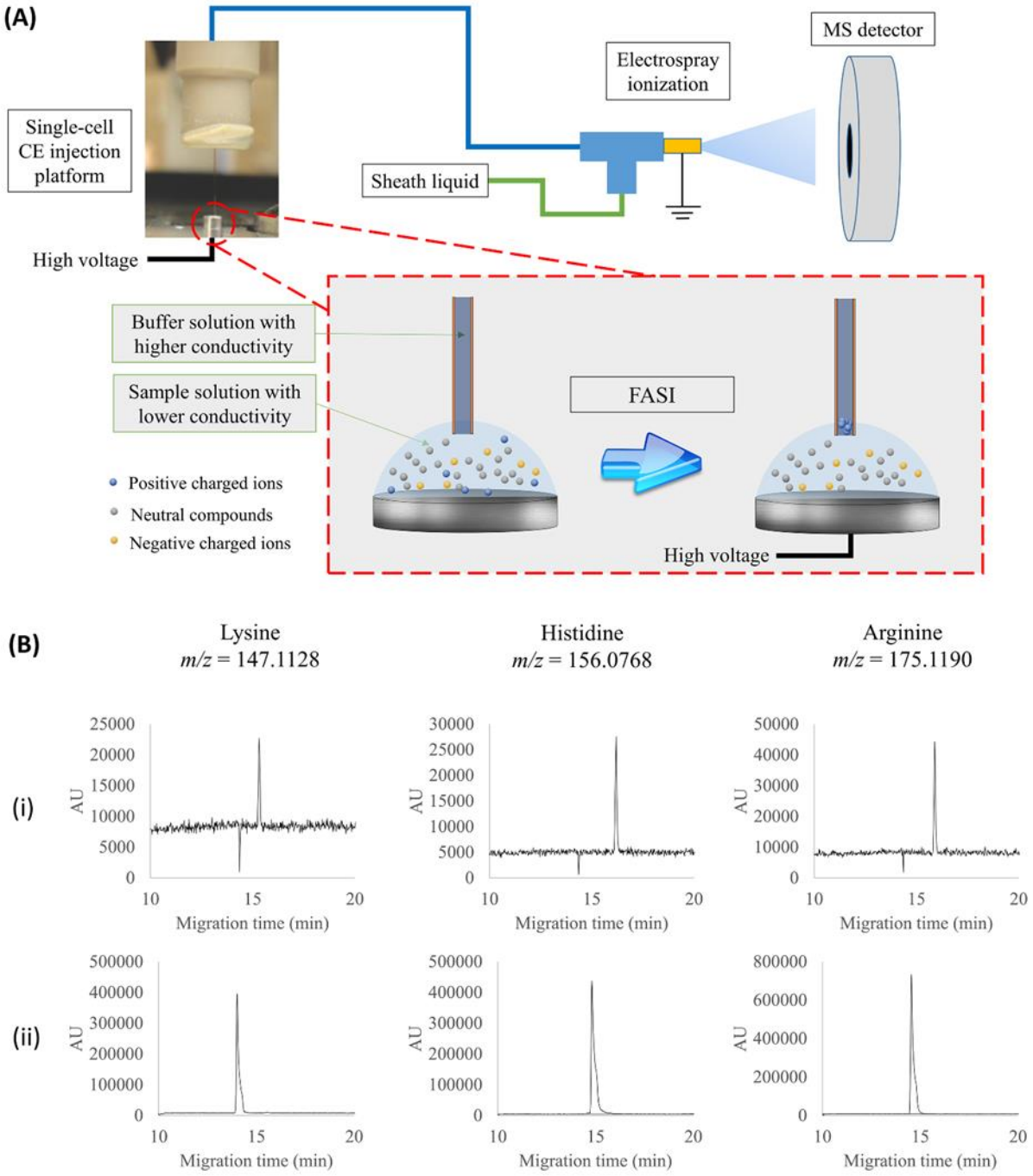

Figure 7.1. Comparison of hydrodynamic injection and FASI for CE-MS analysis of a lysine, histidine, and arginine mixture. (A) System schematic. (B) The extracted ion electropherograms of lysine, histidine, and arginine standards with (i) 6 nL of 100 nM lysine, histidine, and arginine solution injected via the hydrodynamic approach and (ii) 10 nM lysine, histidine, and arginine standard solution with FASI.

7.3.2 Inorganic salt interference in single-cell CE-MS analysis

Inorganic salts present inside single cells and the associated extracellular physiological saline solutions impact FASI performance, especially when working with cells collected from a marine organism with cation concentrations reaching ~500 mM. Sodium and potassium can be at concentrations greater than 100 mM, are found both inside and outside the cell, and impact sample stacking, ionization efficiency, and metabolite detection.[37] A quick wash of the single cell with deionized water is helpful in reducing sample salt content, and accordingly, ion competition during electrokinetic injection.[26] Because the volume of the extracellular liquid depends on the operator's skills during cell isolation, washing is an important step that helps increase the repeatability of measurements between cells. Cell membrane stability should be considered during this quick hypoosmotic washing step to prevent cell lysis. However, because the FASI approach requires high sample purity, without salts, which cannot

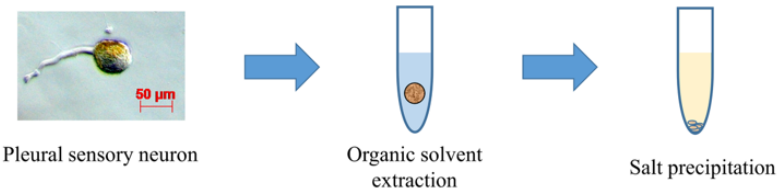

Scheme 7.1. Salt precipitation of a single pleural sensory neuron approximately 50 µm in diameter.

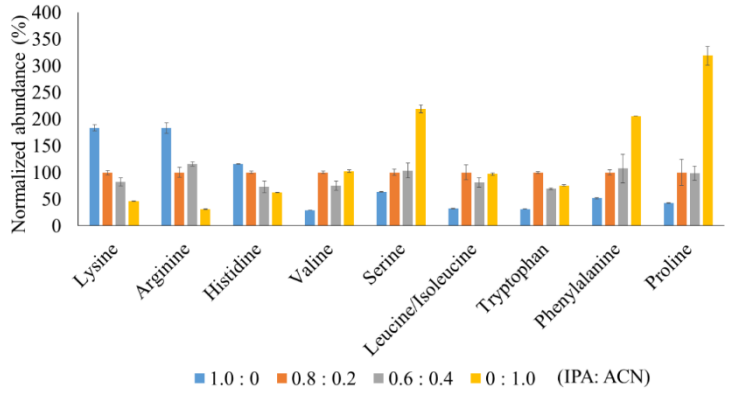

Figure 7.2. The normalized signal abundances for 100 nM standards of 10 amino acids in 2 mM sodium chloride solution, and analyzed after extraction using different organic solvent mixtures. Mixtures of IPA to ACN are used as extraction solution and their ratios are listed. Data for each amino acid are normalized to signal abundance values for the same amino acid compared to IPA with a 0.8 : 0.2 ratio.

be achieved by the cell rinse alone, we introduced a salt precipitation step (Scheme 7.1). The solubility of sodium chloride differs with the solvents used.[38] For example, isopropanol (IPA) and ACN are poor solvents for NaCl;[38] therefore, IPA and ACN were tested as analyte extraction solvents that can also precipitate and remove inorganic salts. Generally, inorganic salt solubility in ACN is lower than in IPA, resulting in improved detection sensitivity for metabolites with lower mobility. However, a decrease in detection sensitivity for some polar metabolites with higher mobility, such as lysine, arginine, and histidine, was observed (Figure 7.2), likely due to their poor solubility in ACN. Considering these results and the solubility of the amino acids and inorganic salts, as well as salt-related analyte injection competition, a 4:1 mixture of IPA to ACN was chosen. To evaluate the effect of salt precipitation on the detection of endogenous lysine, histidine, and arginine, we used samples containing single pleural sensory neurons. As a result of incorporating this step, the signal intensity of these metabolites increased 4.5- to 6-fold (Figure 7.3).

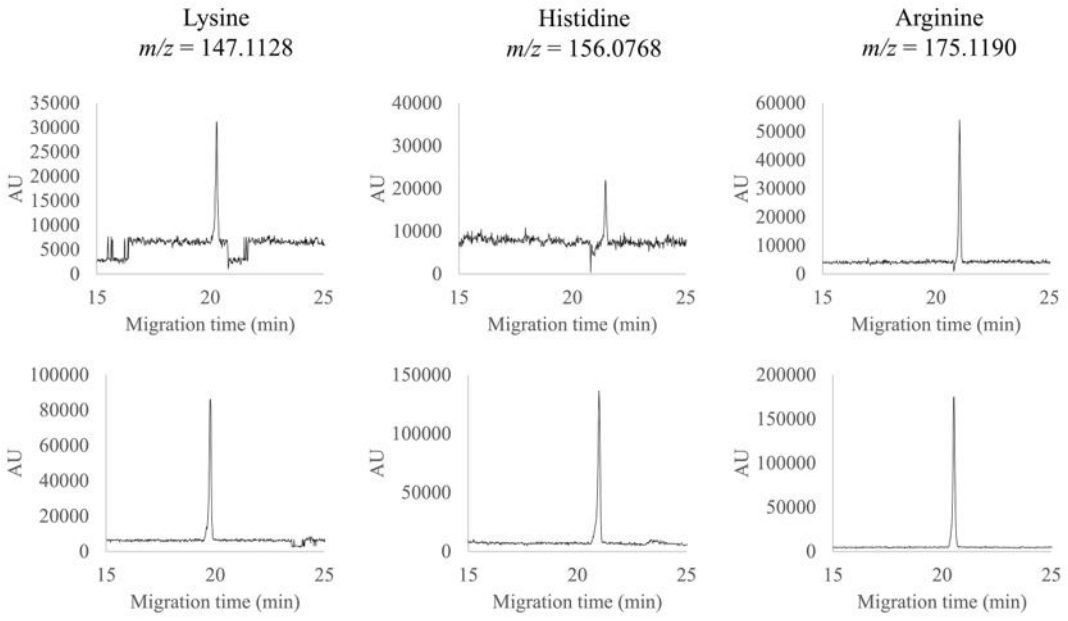

Figure 7.3. The extracted ion electropherograms of lysine, histidine, and arginine detected from the same pleural sensory neuron: (top row) without salt precipitation, and (bottom row) with salt precipitation.

7.3.3 FASI CE-MS metabolite detection and quantification in single-cell samples

To demonstrate the FASI CE-MS system's capabilities for the analysis of endogenous metabolites, isolated sensory neurons from the *Aplysia* nervous system were characterized. Neurons with a cell body diameter of ~50 µm were randomly isolated from the pleural sensory cluster. These neurons have 10- to 1000-fold less cell body volume compared to *A. californica* left pleural 1 (LPl1) and R2 neurons exhibiting diameters of somata ranging between 150 to 500 µm, previously analyzed and characterized by CE-MS.[27] We detected and identified 37 metabolites in the sensory pleural neurons (Figure 7.4).

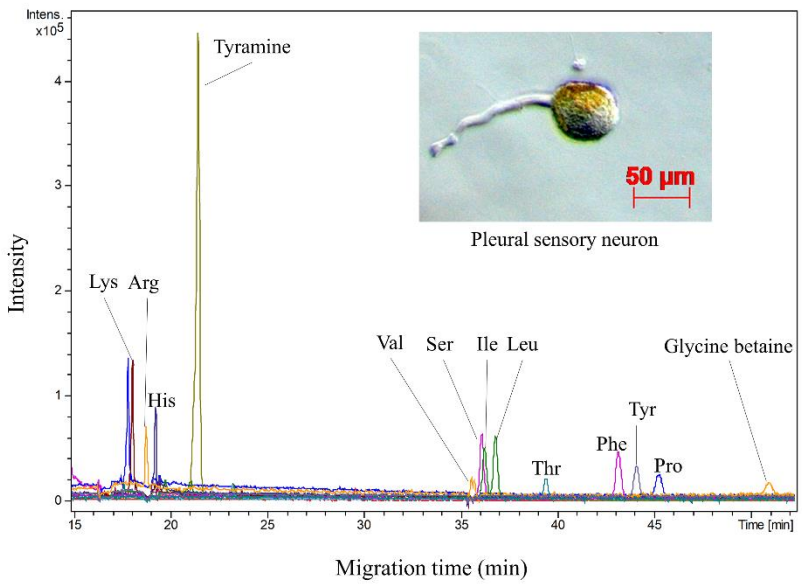

Figure 7.4. FASI CE-MS analysis of individual pleural sensory neurons. Extracted ion electropherograms of several detected metabolites. Inset: pleural sensory neuron with a ~50 µm diameter cell body.

We used FASI CE-MS to quantify selected metabolites inside individual neurons (Figure 7.5). Among these metabolites, tyramine is a neuromodulator in *A. californica*,[39] and it showed a surprisingly high concentration of 67 ± 25 mM, higher than others we measured. The results of the product ion scan for tyramine are shown in Figure S3. Dopamine was also detected in several neurons at 3 ± 1 mM. Both tyramine and dopamine are important neurotransmitters / modulators in *A. californica*.[40,41] Neither automated or manual examination of the electropherograms revealed other transmitters / neuromodulators, such as γ-aminobutyric acid (GABA), and serotonin (Figure

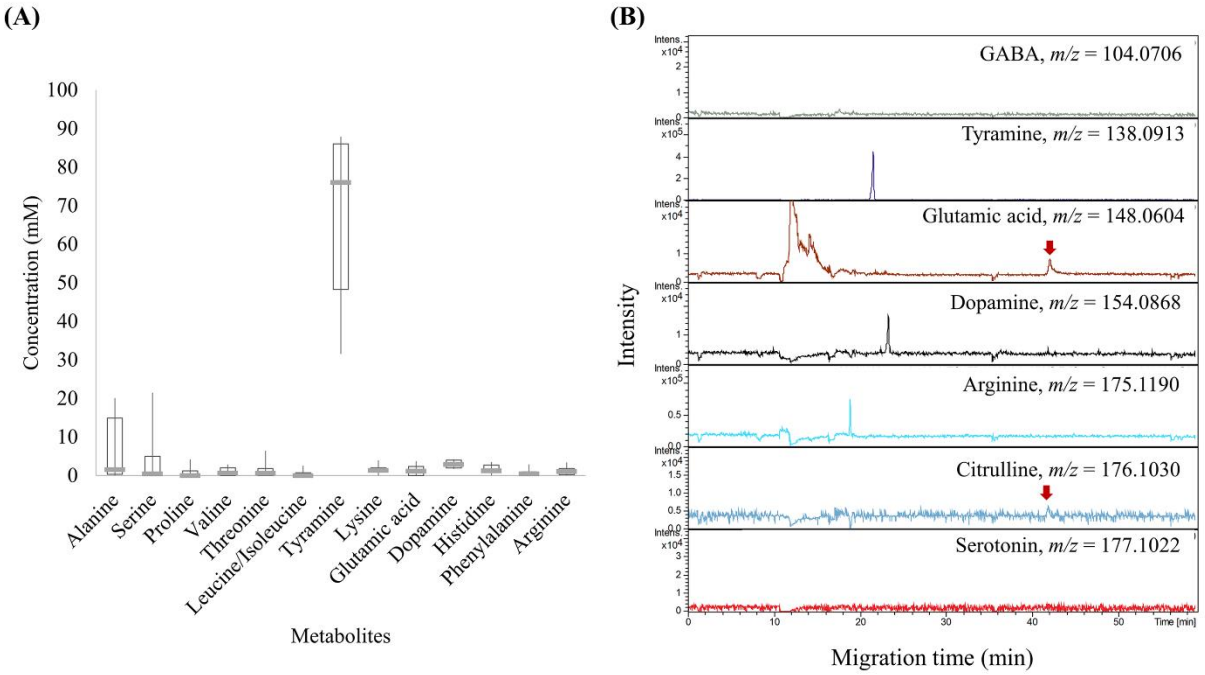

Figure 7.5. Quantitative FASI CE-MS analysis of metabolites in individual pleural sensory neurons. (A) Box plot demonstrating absolute concentrations of different metabolites in 6 pleural sensory neurons. (B) Representative extracted mass electropherograms of common neurotransmitters and metabolites detected in studied neurons. Red arrows indicate localization of metabolite signal matching by migration time and accurate m/z to signal of corresponding standard. The EICs showed no serotonin or GABA signals.

7.5B). Arginine (1.2 ± 1.3 mM) and citrulline (<LOQ) were also detected in some of the pleural sensory neurons (Figure 7.5A). Similar results were obtained using other approaches for an entire pleural sensory cluster previously characterized.[42–44] These findings corroborate with data demonstrating the presence of the nitric oxide synthase pathway in the pleural sensory neurons.[42–44]

7.4 CONCLUSIONS

We created a robust and reproducible FASI CE-MS approach to characterize and quantify the cationic metabolites present in neurons. The use of FASI in CE–ESI-MS analysis improves metabolite detection, providing enhanced sensitivity (100- to 300-fold) and repeatability. Additionally, with the introduction of a sample pretreatment using a 0.8:0.2 IPA:ACN solvent

mixture the negative impact of inorganic salts on analyte detection and characterization was reduced. These experimental advances were further enhanced by two IS normalization of analyte migration times occurring due to run-to-run changes in analyte electrophoretic mobilities. FASI CE-MS was applied to the detection, characterization, and quantification of metabolites in single neurons from *A. californica*. The observation of several functionally important metabolites, such as the tyramine, arginine, and citrulline, in the pleural sensory neurons demonstrate the capabilities of this microanalysis approach.

Because the number of detected signals in a single cell could not be identified with reasonable confidence, further improvement in the sensitivity of the FASI CE-MS system is needed for analyte fragmentation and identification in smaller and more chemically complex neuron samples. We anticipate that an optimized FASI CE-MS approach can be applied to analysis of other cell types, including mammalian and insect neurons. Future advances in cell sampling, e.g., microjunction analyte extraction as well as automated sample injection, are expected to further enhance the throughput and accuracy of single-cell FASI CE-MS analysis.

7.5 SUPPLEMENTARY INFORMATION

Table 7.1. Structural characterization and, in some cases, identification of molecular features detected in the pleural sensory neurons. * 1: Identified by matching accurate molecular masses and migration times of endogenous analyte and its standard. 2: Identified by matching detected endogenous analyte's accurate molecular masse and fragmentation pattern to information available in METLIN (https://metlin.scripps.edu). 3: Identification by matching detected and reported in METLIN accurate molecular masses. 4: Identified using information present in literature.

No.	Name	Formula	Charged form	Identification*	Theoretical *m/z*	Measured *m/z*	ppm error	Migration time (min)	MS/MS fragments
1	DEA/Butylamine	C4H11N	[M+H]+	3	74.0964	74.0962	-2.70	15.0	
2	Glycine	C2H5NO2	[M+H]+	1	76.0393	76.0391	-2.63	22.0	
3	Fragment of histidine			3	83.0604	83.0603	-1.20	16.8	
4	Fragment of lysine			3	84.0809	84.0806	-3.57	15.8	
5	Piperidine	C5H11N	[M+H]+	2	86.0964	86.0962	-2.32	14.8	69.0699

Table 7.1. (con't)

6	Fragment of isoleucine			3	86.0964	86.0962	-2.32	29.5	
7	Fragment of leucine			3	86.0964	86.0962	-2.32	29.9	
8	Fragment of acetylcholine			3	87.0448	87.0439	-10.34	16.4	
9		C4H9NO	[M+H]+	3	88.0757	88.0757	0.00	13.8	
10	Fragment of diethanolamine			3	88.0757	88.0755	-2.27	16.5	
11		C4H9NO	[M+H]+	3	88.0757	88.0756	-1.14	18.2	
12	Sarcosine	C3H7NO2	[M+H]+	3	90.0550	90.0549	-1.11	15.8	
13	Fragment of Ala-Ala (IS)			3	90.0550	90.0547	-3.33	21.9	
14	Alanine	C3H7NO2	[M+H]+	1	90.0550	90.0549	-1.11	24.5	
15		C4H11NO	[M+H]+	3	90.0913	90.0915	2.22	14.6	
16		C4H11NO	[M+H]+	3	90.0913	90.0912	-1.11	15.8	
17		C4H11NO	[M+H]+	3	90.0913	90.0913	0.00	17.0	
18	Fragment of histidine			3	93.0451	93.0447	-4.30	16.8	
19	Fragment of urocanic acid			3	93.0451	93.0447	-4.30	18.5	
20	Fragment of urocanic acid			3	93.0451	93.0448	-3.22	19.4	
21	Fragment of Histidine			3	95.0605	95.0600	-5.26	16.8	
22	Fragment of urocanic acid			3	95.0605	95.0600	-5.26	18.5	
23		C6H9N	[M+H]+	3	96.0808	96.0807	-1.04	13.5	
24		C6H11N	[M+H]+	3	98.0964	98.0964	0.00	13.5	
25		C6H11N	[M+H]+	3	98.0964	98.0964	0.00	15.9	
26		C6H11N	[M+H]+	3	98.0964	98.0963	-1.02	18.0	
27		C6H11N	[M+H]+	3	98.0964	98.0964	0.00	19.4	
28		C6H11N	[M+H]+	3	98.0964	98.0962	-2.04	21.9	
29		C6H11N	[M+H]+	3	98.0964	98.0959	-5.10	41.3	
30	Cyclohexylammonium	C6H13N	[M+H]+	2	100.1121	100.1120	-1.00	16.8	83.0854
31	Triethylamine	C6H15N	[M+H]+	2	102.1277	102.1275	-1.96	16.4	74.0962
32	Fragment of carnitine			3	103.0395	103.0388	-6.79	19.1	
33	γ-Aminobutyric acid	C4H9NO2	[M+H]+	3	104.0706	104.0706	0.00	16.7	
34		C4H9NO2	[M+H]+	3	104.0706	104.0706	0.00	17.5	
35		C4H9NO2	[M+H]+	3	104.0706	104.0704	-1.92	27.5	
36	Choline	C5H13NO	[M+H]+	3	104.1070	104.1070	0.00	14.4	
37	Serine	C3H7NO3	[M+H]+	1	106.0499	106.0497	-1.89	29.6	

Table 7.1. (con't)

38	Diethanolamine	C4H11NO2	[M+H]+	2	106.0863	106.0861	-1.89	16.5	88.0759
39	Fragment of histidine			3	110.0711	110.0712	0.91	16.8	
40		C6H10N2	[M+H]+	3	111.0917	111.0917	0.00	13.5	
41	Fragment of lysine			3	112.0757	112.0758	0.89	15.8	
42		C6H9NO	[M+H]+	3	112.0757	112.0755	-1.78	21.6	
43	Histamine	C5H9N3	[M+H]+	2	112.0869	112.0863	-5.35	9.1	95.0605
44	2-Imino-4-methylpiperidine	C6H12N2	[M+H]+	2	113.1073	113.1072	-0.88	13.5	96.0807
45		C6H12N2	[M+H]+	3	113.1073	113.1074	0.88	15.2	
46	Creatinine	C4H7N3O	[M+H]+	3	114.0662	114.0661	-0.88	15.6	
47	Fragment of arginine			3	115.0851	115.0864	11.30	16.4	
48	Fragment of ornithine			3	115.0866	115.0864	-1.74	15.6	
49	Fragment of ornithine			3	116.0706	116.0706	0.00	15.6	
50	Fragment of arginine			3	116.0706	116.0705	-0.86	16.4	
51	Proline	C5H9NO2	[M+H]+	1	116.0706	116.0706	0.00	35.9	
52		C4H9N3O	[M+H]+	3	116.0818	116.0808	-8.61	15.4	
53	Trimethylaminoacetone	C6H13NO	[M+H]+	2	116.1070	116.1069	-0.86	13.5	98.0964, 100.0753
54	N-(2-Methylpropyl)acetamide	C6H13NO	[M+H]+	2	116.1070	116.1071	0.86	14.9	74.0965
55	Trimethylaminoacetone	C6H13NO	[M+H]+	3	116.1070	116.1070	0.00	15.9	98.0964, 100.0753
56		C7H17N	[M+H]+	3	116.1434	116.1433	-0.86	18.0	
57		C7H17N	[M+H]+	3	116.1434	116.1433	-0.86	18.4	
58	Fragment of tryptophan			3	118.0643	118.0647	3.39	32.6	
59		C8H7N	[M+H]+	3	118.0643	118.0647	3.39	34.4	
60		C8H7N	[M+H]+	3	118.0643	118.0647	3.39	35.0	
61	Valine	C5H11NO2	[M+H]+	1	118.0863	118.0860	-2.54	29.1	
62	Glycine betaine	C5H11NO2	[M+H]+	3	118.0863	118.0860	-2.54	40.1	
63	2-Diethylaminoethanol	C6H15NO	[M+H]+	2	118.1226	118.1228	1.69	13.5	100.1124, 86.0966
64		C6H15NO	[M+H]+	3	118.1226	118.1227	0.85	17.4	
65	Fragment of tyrosine			3	119.0494	119.0487	-5.88	35.0	

Table 7.1. (con't)

66	Threonine	C4H9NO3	[M+H]+	1	120.0653	120.0653	0.00	31.8	
67	Fragment of phenylalanine			3	120.0806	120.0804	-1.67	34.4	
68	Fragment of urocanic acid			3	121.0395	121.0395	0.00	18.5	
69	Fragment of urocanic acid			3	121.0395	121.0395	0.00	19.4	
70		C8H8O	[M+H]+	3	121.0648	121.0645	-2.48	35.0	
71	Fragment of tyramine			3	121.0666	121.0648	-14.87	18.5	
72		C5H12OS	[M+H]+	3	121.0682	121.0684	1.65	31.8	
73		C5H13FSi	[M+H]+	3	121.0843	121.0839	-3.30	34.4	
74	Fragment of thiamine			3	122.0715	122.0712	-2.46	13.5	
75	Tromethamine (Tris)	C4H11NO3	[M+H]+	2	122.0812	122.0810	-1.64	18.5	104.071
76		C8H11N	[M+H]+	3	122.0964	122.0963	-0.82	17.1	
77	Fragment of tyrosine			3	123.0444	123.0438	-4.88	44.0	
78		C6H8N2O2	[M+H]+	3	123.0550	123.0552	1.63	18.5	
79		C6H8N2O2	[M+H]+	3	123.0550	123.0550	0.00	19.4	
80		C6H9N3	[M+H]+	3	124.0869	124.0868	-0.81	13.5	
81		C6H9N3	[M+H]+	3	124.0869	124.0868	-0.81	17.3	
82	Melamine	C3H6N6	[M+H]+	3	127.0727	127.0729	1.57	16.3	
83	Fragment of lysine			3	129.1007	129.1020	10.07	15.8	
84		C6H12N2O	[M+H]+	3	129.1022	129.1020	-1.55	15.2	
85	Fragment of lysine			3	130.0861	130.0865	3.07	15.8	
86		C6H11NO2	[M+H]+	3	130.0863	130.0861	-1.54	30.9	
87		C8H19N	[M+H]+	3	130.1590	130.1589	-0.77	18.8	
88		C8H19N	[M+H]+	3	130.1590	130.1588	-1.54	20.0	
89	N-Acetylputrescine	C6H14N2O	[M+H]+	2	131.1179	131.1178	-0.76	9.5	114.0912
90		C5H9NO3	[M+H]+	3	132.0655	132.0653	-1.51	43.0	
91	Creatine	C4H9N3O2	[M+H]+	3	132.0768	132.0767	-0.76	22.4	
92	Fragment of tryptophan			3	132.0805	132.0806	0.76	32.6	
93		C6H13NO2	[M+H]+	3	132.1019	132.1020	0.76	14.9	
94		C6H13NO2	[M+H]+	3	132.1019	132.1020	0.76	15.6	
95		C6H13NO2	[M+H]+	3	132.1019	132.1020	0.76	17.8	
96	Fragment of trolamine			3	132.1019	132.1020	0.76	18.2	
97		C6H13NO2	[M+H]+	3	132.1019	132.1020	0.76	19.9	

Table 7.1. (con't)

98	Isoleucine	C6H13NO2	[M+H]+	1	132.1019	132.1017	-1.51	29.5	
99	Leucine	C6H13NO2	[M+H]+	1	132.1019	132.1017	-1.51	29.9	
100	β-Alanine betaine	C6H13NO2	[M+H]+	3	132.1019	132.1018	-0.76	46.2	
101		C7H17NO	[M+H]+	3	132.1383	132.1384	0.76	18.2	
102		C7H17NO	[M+H]+	3	132.1383	132.1384	0.76	18.4	
103		C2H4N4O3	[M+H]+	3	133.0356	133.0343	-9.77	11.1	
104	Asparagine	C4H8N2O3	[M+H]+	1	133.0608	133.0607	-0.75	31.9	
105	Ornithine	C5H12N2O2	[M+H]+	2	133.0972	133.0971	-0.75	15.7	115.0863, 116.0705
106		C15H27N3O	[M+2H]2+	3	133.6150	133.6151	0.75	17.3	
107	Aspartic acid	C4H7NO4	[M+H]+	1	134.0448	134.0443	-3.73	49.5	
108		C5H11NO3	[M+H]+	3	134.0812	134.0809	-2.24	33.8	
109		C6H15NO2	[M+H]+	3	134.1176	134.1176	0.00	16.3	
110		C6H15NO2	[M+H]+	3	134.1176	134.1176	0.00	17.8	
111		C6H15NO2	[M+H]+	3	134.1176	134.1176	0.00	19.4	
112		C5H10O2S	[M+H]+	3	135.0474	135.0474	0.00	17.8	
113	Fragment of tyrosine			3	136.0747	136.0754	5.14	35.0	
114		C9H13N	[M+H]+	3	136.1121	136.1118	-2.20	34.3	
115	Proline	C5H9NO2	[M+Na]+	3	138.0525	138.0531	4.35	35.9	
116	Tyramine	C8H11NO	[M+H]+	1	138.0913	138.0913	0.00	18.5	
117	cis-urocanic acid	C6H6N2O2	[M+H]+	4	139.0502	139.0502	0.00	18.5	121.0395
118	trans-urocanic acid	C6H6N2O2	[M+H]+	4	139.0502	139.0503	0.72	19.4	121.0395, 95.0605
119	Valine	C5H11NO2	[M+Na]+	3	140.0682	140.0679	-2.14	29.1	
120	Glycine betaine	C5H11NO2	[M+Na]+	3	140.0682	140.0679	-2.14	40.1	
121		C6H8N2O2	[M+H]+	3	141.0659	141.0658	-0.71	18.5	
122		C6H8N2O2	[M+H]+	3	141.0659	141.0658	-0.71	19.4	
123	Fragment of tryptophan			3	144.0808	144.0805	-2.08	32.6	
124	1-Aminocyclohexanecarboxylic acid	C7H13NO2	[M+H]+	3	144.1019	144.1019	0.00	18.3	
125	Proline betaine	C7H13NO2	[M+H]+	3	144.1019	144.1019	0.00	41.4	

Table 7.1. (con't)

126	Fragment of tryptophan			3	146.0589	146.0598	6.16	32.6	
127		C5H11N3O2	[M+H]+	3	146.0924	146.0922	-1.37	18.4	
128	Acetylcholine	C7H15NO2	[M+H]+	1	146.1176	146.1174	-1.37	16.4	87.044
129		C7H15NO2	[M+H]+	3	146.1176	146.1174	-1.37	17.9	
130		C7H15NO2	[M+H]+	3	146.1176	146.1174	-1.37	18.8	
131		C7H15NO2	[M+H]+	3	146.1176	146.1174	-1.37	19.5	
132		C7H15NO2	[M+H]+	3	146.1176	146.1174	-1.37	20.3	
133		C8H19NO	[M+H]+	3	146.1539	146.1542	2.05	14.7	
134	Fragment of tyrosine			3	147.0429	147.0438	6.12	35.0	
135	Glutamine	C5H10N2O3	[M+H]+	1	147.0764	147.0764	0.00	33.0	
136	Lysine	C6H14N2O2	[M+H]+	1	147.1128	147.1127	-0.68	15.8	
137	Glutamic acid		[M+H]+	1	148.0604	148.0603	-0.68	33.7	
138		C6H13NO3	[M+H]+	3	148.0968	148.0968	0.00	51.7	
139		C5H11NO2S	[M+H]+	3	150.0583	150.0581	-1.33	26.1	
140	Methionine	C5H11NO2S	[M+H]+	1	150.0583	150.0581	-1.33	32.8	133.0337, 104.0524
141	Trolamine	C6H15NO3	[M+H]+	2	150.1125	150.1124	-0.67	18.2	132.102, 114.0915
142		C9H13NO	[M+H]+	3	152.1075	152.1069	-3.94	34.3	
143	N-Methyltyramine	C9H13NO	[M+H]+	3	152.1075	152.1068	-4.60	35.1	121.0645
144	β-Alanine betaine	C6H13NO2	[M+Na]+	3	154.0838	154.0837	-0.65	46.2	
145	Dopamine	C8H11NO2	[M+H]+	1	154.0868	154.0863	-3.24	19.8	
146	Octopamine	C8H11NO2	[M+H]+	1	154.0868	154.0863	-3.24	19.8	
147	Glycine betaine	C5H11NO2	[M+K]+	3	156.0421	156.0417	-2.56	40.1	
148	Histidine	C6H9N3O2	[M+H]+	1	156.0768	156.0767	-0.64	16.8	
149		C9H17NO	[M+H]+	3	156.1383	156.1381	-1.28	19.6	
150		C9H17NO	[M+H]+	3	156.1383	156.1381	-1.28	21.9	
151	2,2,6,6-Tetramethylpiperidin-4-amine	C9H20N2	[M+H]+	2	157.1699	157.1700	0.64	12.9	140.1434, 84.0808
152	Fragment of citrulline			3	159.0764	159.0763	-0.63	33.5	
153	Fragment of tryptophan			3	159.0927	159.0914	-8.17	32.6	
154		C7H13NO3	[M+H]+	3	160.0968	160.0967	-0.62	19.5	

Table 7.1. (con't)

155		C7H13NO3	[M+H]+	3	160.0968	160.0967	-0.62	20.2	
156		C7H13NO3	[M+H]+	3	160.0968	160.0967	-0.62	24.5	
157		C7H13NO3	[M+H]+	3	160.0968	160.0967	-0.62	44.0	
158		C7H13NO3	[M+H]+	3	160.0968	160.0967	-0.62	49.7	
159		C7H13NO3	[M+H]+	3	160.0968	160.0967	-0.62	51.5	
160		C7H13NO3	[M+H]+	3	160.0968	160.0967	-0.62	52.6	
161	Ala-Ala (IS1)	C6H12N2O3	[M+H]+	1	161.0921	161.0919	-1.24	21.9	
162	Tryptamine	C10H12N2	[M+H]+	1	161.1073	161.1086	8.07	18.0	
163	Carnitine	C7H15NO3	[M+H]+	2	162.1125	162.1122	-1.85	19.1	85.0285, 103.0394
164		C19H38N4	[M+2H]2+	3	162.1621	162.1623	1.23	12.6	
165	Fragment of tyrosine			3	165.0533	165.0547	8.48	35.0	
166	Proline betaine	C7H13NO2	[M+Na]+	3	166.0838	166.0835	-1.81	41.4	
167	Phenylalanine	C9H11NO2	[M+H]+	1	166.0863	166.0861	-1.20	34.4	
168		C9H13NO2	[M+H]+	3	168.1019	168.1017	-1.19	35.1	
169	Fragment of C10H20N2O			3	168.1383	168.1379	-2.38	21.6	
170	1-methylhistidine	C7H11N3O2	[M+H]+	2	170.0924	170.0924	0.00	17.3	96.0679, 109.0758
171	1,3-Bis(2,2,6,6-tetramethyl-4-piperidyl)urea	C19H38N4O	[M+2H]2+	3	170.1596	170.1597	0.59	17.3	
172	3-Acrylamidopropyl trimethylammonium	C9H18N2O	[M+H]+	2	171.1492	171.1486	-3.51	24.4	112.0752
173	Fragment of C9H21NO3			3	174.1488	174.1485	-1.72	21.9	
174	Arginine	C6H14N4O2	[M+H]+	1	175.1190	175.1189	-0.57	16.4	
175	Citrulline	C6H13N3O3	[M+H]+	1	176.1030	176.1029	-0.57	33.5	
176	Serotonin	C10H12N2O	[M+H]+	1	177.1022	177.1022	0.00	19.7	
177		C10H15N3	[M+H]+	3	178.1339	178.1338	-0.56	18.6	
178	Tyrosine	C9H11NO3	[M+H]+	3	182.0812	182.0809	-1.65	35.0	
179	Ala-Ala (IS1)	C6H12N2O3	[M+Na]+	3	183.0737	183.0738	0.55	21.9	
180		C10H20N2O	[M+H]+	3	185.1648	185.1646	-1.08	21.6	
181		C12H27N	[M+H]+	3	186.2216	186.2214	-1.07	23.6	
182	Phenylalanine	C9H11NO2	[M+Na]+	3	188.0682	188.0677	-2.66	34.4	

Table 7.1. (con't)

183	Fragment of tryptophan			3	188.0706	188.0704	-1.06	32.6	170.0602, 118.0643
184		C7H16N4O2	[M+H]+	3	189.1345	189.1346	0.53	12.0	
185	N6,N6,N6-trimethyl-lysine	C9H20N2O2	[M+H]+	4	189.1598	189.1599	0.53	16.7	
186		C9H19NO3	[M+H]+	3	190.1438	190.1434	-2.10	21.7	
187		C21H38N4O2	[M+2H]2+	3	190.1570	190.1570	0.00	17.5	
188		C6H10N2O5	[M+H]+	3	191.0662	191.0660	-1.05	40.3	
189		C9H21NO3	[M+H]+	3	192.1594	192.1592	-1.04	21.5	
190		C9H21NO3	[M+H]+	3	192.1594	192.1592	-1.04	21.9	
191		C9H21NO3	[M+H]+	3	192.1594	192.1592	-1.04	22.6	
192		C10H13NO3	[M+H]+	3	196.0968	196.0967	-0.51	21.4	
193		C9H15N3O2	[M+H]+	3	198.1237	198.1233	-2.02	19.3	
194		C9H15N3O2	[M+H]+	3	198.1237	198.1235	-1.01	24.5	
195		C26H38N2O	[M+2H]2+	3	198.1565	198.1548	-8.58	17.8	
196		C22H42N4O2	[M+2H]2+	3	198.1727	198.1729	1.01	18.4	
197		C11H22N2O	[M+H]+	3	199.1805	199.1803	-1.00	23.2	
198		C10H21N3O	[M+H]+	3	200.1757	200.1753	-2.00	22.3	
199		C11H23NO2	[M+H]+	3	202.1802	202.1801	-0.49	21.5	
200	Ala Leu	C9H18N2O3	[M+H]+	2	203.1390	203.1391	0.49	22.4	132.0767
201		C9H18N2O3	[M+H]+	3	203.1390	203.1391	0.49	24.4	
202	Spermine	C10H26N4	[M+H]+	2	203.2235	203.2232	-1.48	10.0	129.1385
203	Acetylcarnitine	C9H17NO4	[M+H]+	2	204.1230	204.1234	1.96	20.9	85.0288, 145.05
204	Tryptophan	C11H12N2O2	[M+H]+	1	205.0972	205.0969	-1.46	32.6	
205		C9H21NO4	[M+H]+	3	208.1543	208.1541	-0.96	22.6	
206	Kynurenine	C10H12N2O3	[M+H]+	1	209.0921	209.0920	-0.48	28.7	
207		C12H24N2O	[M+H]+	3	213.1961	213.1961	0.00	24.1	
208		C11H22N2O2	[M+H]+	3	215.1754	215.1753	-0.46	17.8	
209		C11H22N2O2	[M+H]+	3	215.1754	215.1753	-0.46	20.1	
210		C11H22N2O2	[M+H]+	3	215.1754	215.1750	-1.86	22.7	
211		C11H22N2O2	[M+H]+	3	215.1754	215.1750	-1.86	23.4	

Table 7.1. (con't)

212	Propionylcarnitine	C10H19NO4	[M+H]+	2	218.1387	218.1385	-0.92	21.8	85.03, 159.064
213		C12H27NO2	[M+H]+	3	218.2115	218.2111	-1.83	23.3	
214		C12H27NO2	[M+H]+	3	218.2115	218.2111	-1.83	23.9	
215		C13H19NO2	[M+H]+	3	222.1485	222.1486	0.45	21.5	
216	Cys Thr	C7H14N2O4S1	[M+H]+	3	223.0747	223.0741	-2.69	30.2	
217	Sodium formate			1	226.9534	226.9534	0.00	10.2	
218	Fragmentation of valerylcarnitine			3	228.1702	228.1702	0.00	23.4	
219		C11H21N3O2	[M+H]+	3	228.1707	228.1701	-2.63	17.8	
220		C11H20N2O3	[M+H]+	3	229.1547	229.1544	-1.31	23.1	
221	Pro-Leu (IS2)	C11H20N2O3	[M+H]+	1	229.1547	229.1547	0.00	24.5	
222	Butyryl-L-carnitine/Isobutyryl carnitine	C11H21NO4	[M+H]+	2	232.1543	232.1540	-1.29	22.3	85.0285, 173.0813
223	Butyryl-L-carnitine/Isobutyryl carnitine	C11H21NO4	[M+H]+	2	232.1543	232.1540	-1.29	22.6	85.0285, 173.0813
224	Dimer of glycine betaine			3	235.1647	235.1647	0.00	40.1	
225	HEPES	C8H18N2O4S	[M+H]+	4	239.1060	239.1061	0.42	23.9	
226	Cytidine	C9H13N3O5	[M+H]+	1	244.0928	244.0926	-0.82	22.6	
227	Valerylcarnitine/2-Methylbutyroylcarnitine	C12H23NO4	[M+H]+	2	246.1700	246.1699	-0.41	23.1	
228	Valerylcarnitine/2-Methylbutyroylcarnitine	C12H23NO4	[M+H]+	2	246.1700	246.1699	-0.41	23.4	85.0285, 187.0969
229		C13H24N2O3	[M+H]+	3	257.1860	257.1862	0.78	24.5	
230	Hexanoylcarnitine	C13H25NO4	[M+H]+	3	260.1856	260.1853	-1.15	24.2	
231	Thiamine	C12H16N4OS	[M+H]+	2	265.1118	265.1119	0.38	14.2	144.0476, 122.0711
232	Heptanoylcarnitine	C14H27NO4	[M+H]+	3	274.2012	274.2010	-0.73	24.5	
233		C16H35NO2	[M+H]+	3	274.2741	274.2735	-2.19	32.4	
234		C16H15N3O2	[M+H]+	3	282.1237	282.1227	-3.54	23.7	
235	Dimer of proline betaine			3	287.1965	287.1957	-2.79	41.3	
236	Potassium formate			1	290.8500	290.8477	-7.91	7.3	

Table 7.1. (con't)

237	Argininosuccinic acid	C10H18N4O6	[M+H]+	4	291.1299	291.1291	-2.75	26.3	
238		C10H18N4O7	[M+H]+	3	307.1248	307.1226	-7.16	24.3	
239		C12H12N2O9	[M+H]+	3	329.0616	329.0605	-3.34	24.5	
240		C19H38N4O	[M+H]+	3	339.3118	339.3121	0.88	18.8	
241		C17H35N9O4	[M+H]+	3	430.2885	430.2907	5.11	41.3	
242		C20H35N5O6	[M+H]+	3	442.2660	442.2691	7.01	39.8	
243		C22H37N5O6	[M+H]+	3	468.2817	468.2846	6.19	41.0	
244		C19H31N9O7S	[M+H]+	3	530.2140	530.2132	-1.51	41.3	

7.6 REFERENCES

(1) Kremser, L.; Bilek, G.; Kenndler, E. Effect of Detergent on Electromigration of Proteins: CE of Very Low Density Lipoprotein Receptor Modules and Viral Proteins. *ELECTROPHORESIS* **2007**, *28* (20), 3684–3690. https://doi.org/10.1002/elps.200700168.

(2) Britz-McKibbin, P.; Chen, D. D. Y. Selective Focusing of Catecholamines and Weakly Acidic Compounds by Capillary Electrophoresis Using a Dynamic PH Junction. *Anal. Chem.* **2000**, *72* (6), 1242–1252. https://doi.org/10.1021/ac990898e.

(3) Markuszewski, M. J.; Britz-McKibbin, P.; Terabe, S.; Matsuda, K.; Nishioka, T. Determination of Pyridine and Adenine Nucleotide Metabolites in Bacillus Subtilis Cell Extract by Sweeping Borate Complexation Capillary Electrophoresis. *Journal of Chromatography A* **2003**, *989* (2), 293–301. https://doi.org/10.1016/S0021-9673(03)00031-1.

(4) Phung, S. C.; Nai, Y. H.; Powell, S. M.; Macka, M.; Breadmore, M. C. Rapid and Sensitive Microbial Analysis by Capillary Isotachophoresis with Continuous Electrokinetic Injection under Field Amplified Conditions. *ELECTROPHORESIS* **2013**, *34* (11), 1657–1662. https://doi.org/10.1002/elps.201200479.

(5) Osbourn, D. M.; Weiss, D. J.; Lunte, C. E. On-Line Preconcentration Methods for Capillary Electrophoresis. *Electrophoresis* **2000**, *21* (14), 2768–2779. https://doi.org/10.1002/1522-2683(20000801)21:14<2768::AID-ELPS2768>3.0.CO;2-P.

(6) Chien, R.-L.; Burgi, D. S. Field Amplified Sample Injection in High-Performance Capillary Electrophoresis. *Journal of Chromatography A* **1991**, *559* (1), 141–152. https://doi.org/10.1016/0021-9673(91)80066-P.

(7) Hempel, G. Strategies to Improve the Sensitivity in Capillary Electrophoresis for the Analysis of Drugs in Biological Fluids. *ELECTROPHORESIS* **2000**, *21* (4), 691–698. https://doi.org/10.1002/(SICI)1522-2683(20000301)21:4<691::AID-ELPS691>3.0.CO;2-U.

(8) Kawai, T.; Ota, N.; Okada, K.; Imasato, A.; Owa, Y.; Morita, M.; Tada, M.; Tanaka, Y. Ultrasensitive Single Cell Metabolomics by Capillary Electrophoresis–Mass Spectrometry with a Thin-Walled Tapered Emitter and Large-Volume Dual Sample Preconcentration. *Anal. Chem.* **2019**, *91* (16), 10564–10572. https://doi.org/10.1021/acs.analchem.9b01578.

(9) Kim, J.; Chun, M.-S.; Choi, K.; Chung, D. S. Large Volume Stacking Using an EOF Pump in NACE-MS. *ELECTROPHORESIS* **2009**, *30* (6), 1046–1051. https://doi.org/10.1002/elps.200800396.

(10) Liu, J.-X.; Aerts, J. T.; Rubakhin, S. S.; Zhang, X.-X.; Sweedler, J. V. Analysis of Endogenous Nucleotides by Single Cell Capillary Electrophoresis-Mass Spectrometry. *The Analyst* **2014**, *139* (22), 5835. https://doi.org/10.1039/c4an01133c.

(11) Jung, B.; Bharadwaj, R.; Santiago, J. G. Thousandfold Signal Increase Using Field-Amplified Sample Stacking for on-Chip Electrophoresis. *ELECTROPHORESIS* **2003**, *24* (19–20), 3476–3483. https://doi.org/10.1002/elps.200305611.

(12) Bermudo, E.; Núñez, O.; Moyano, E.; Puignou, L.; Galceran, M. T. Field Amplified Sample Injection–Capillary Electrophoresis–Tandem Mass Spectrometry for the Analysis of Acrylamide in Foodstuffs. *Journal of Chromatography A* **2007**, *1159* (1), 225–232. https://doi.org/10.1016/j.chroma.2007.03.008.

(13) Nemes, P.; Knolhoff, A. M.; Rubakhin, S. S.; Sweedler, J. V. Metabolic Differentiation of Neuronal Phenotypes by Single-Cell Capillary Electrophoresis–Electrospray Ionization-Mass Spectrometry. *Anal. Chem.* **2011**, *83* (17), 6810–6817. https://doi.org/10.1021/ac2015855.

(14) Nemes, P.; Rubakhin, S. S.; Aerts, J. T.; Sweedler, J. V. Qualitative and Quantitative Metabolomic Investigation of Single Neurons by Capillary Electrophoresis Electrospray Ionization Mass Spectrometry. *Nat. Protocols* **2013**, *8* (4), 783–799. https://doi.org/10.1038/nprot.2013.035.

(15) Lapainis, T.; Rubakhin, S. S.; Sweedler, J. V. Capillary Electrophoresis with Electrospray Ionization Mass Spectrometric Detection for Single-Cell Metabolomics. *Anal. Chem.* **2009**, *81* (14), 5858–5864. https://doi.org/10.1021/ac900936g.

(16) Benton, H. P.; Want, E. J.; Ebbels, T. M. D. Correction of Mass Calibration Gaps in Liquid Chromatography–Mass Spectrometry Metabolomics Data. *Bioinformatics* **2010**, *26* (19), 2488–2489. https://doi.org/10.1093/bioinformatics/btq441.

(17) R: The R Project for Statistical Computing https://www.r-project.org/ (accessed Mar 3, 2020).

(18) Guijas, C.; Montenegro-Burke, J. R.; Domingo-Almenara, X.; Palermo, A.; Warth, B.; Hermann, G.; Koellensperger, G.; Huan, T.; Uritboonthai, W.; Aisporna, A. E.; Wolan, D. W.; Spilker, M. E.; Benton, H. P.; Siuzdak, G. METLIN: A Technology Platform for Identifying

Knowns and Unknowns. *Anal. Chem.* **2018**, *90* (5), 3156–3164. https://doi.org/10.1021/acs.analchem.7b04424.

(19) Wishart, D. S.; Feunang, Y. D.; Marcu, A.; Guo, A. C.; Liang, K.; Vázquez-Fresno, R.; Sajed, T.; Johnson, D.; Li, C.; Karu, N.; Sayeeda, Z.; Lo, E.; Assempour, N.; Berjanskii, M.; Singhal, S.; Arndt, D.; Liang, Y.; Badran, H.; Grant, J.; Serra-Cayuela, A.; Liu, Y.; Mandal, R.; Neveu, V.; Pon, A.; Knox, C.; Wilson, M.; Manach, C.; Scalbert, A. HMDB 4.0: The Human Metabolome Database for 2018. *Nucleic Acids Res* **2018**, *46* (D1), D608–D617. https://doi.org/10.1093/nar/gkx1089.

(20) Huan, T.; Tang, C.; Li, R.; Shi, Y.; Lin, G.; Li, L. MyCompoundID MS/MS Search: Metabolite Identification Using a Library of Predicted Fragment-Ion-Spectra of 383,830 Possible Human Metabolites. *Anal. Chem.* **2015**, *87* (20), 10619–10626. https://doi.org/10.1021/acs.analchem.5b03126.

(21) Burgi, D. S.; Chien, R. Ling. Optimization in Sample Stacking for High-Performance Capillary Electrophoresis. *Anal. Chem.* **1991**, *63* (18), 2042–2047. https://doi.org/10.1021/ac00018a028.

(22) Chien, R. Ling.; Burgi, D. S. Sample Stacking of an Extremely Large Injection Volume in High-Performance Capillary Electrophoresis. *Anal. Chem.* **1992**, *64* (9), 1046–1050. https://doi.org/10.1021/ac00033a015.

(23) Quirino, J. P.; Terabe, S. Sample Stacking of Cationic and Anionic Analytes in Capillary Electrophoresis. *Journal of Chromatography A* **2000**, *902* (1), 119–135. https://doi.org/10.1016/S0021-9673(00)00812-8.

(24) Garcia, L. L.; Shihabi, Z. K. Sample Matrix Effects in Capillary Electrophoresis I. Basic Considerations. **1993**, 5.

(25) Burgess, J. *Metal Ions in Solution*; Ellis Horwood, 1978.

(26) Chang, D.-J.; Li, X.-C.; Lee, Y.-S.; Kim, H.-K.; Kim, U. S.; Cho, N. J.; Lo, X.; Weiss, K. R.; Kandel, E. R.; Kaang, B.-K. Activation of a Heterologously Expressed Octopamine Receptor Coupled Only to Adenylyl Cyclase Produces All the Features of Presynaptic Facilitation in Aplysia Sensory Neurons. *PNAS* **2000**, *97* (4), 1829–1834. https://doi.org/10.1073/pnas.97.4.1829.

(27) Dunn, T. W.; Farah, C. A.; Sossin, W. S. Inhibitory Responses in Aplysia Pleural Sensory Neurons Act to Block Excitability, Transmitter Release, and PKC Apl II Activation. *Journal of Neurophysiology* **2011**, *107* (1), 292–305. https://doi.org/10.1152/jn.00767.2011.

(28) Due, M. R.; Jing, J.; Weiss, K. R. Dopaminergic Contributions to Modulatory Functions of a Dual-Transmitter Interneuron in Aplysia. *Neuroscience Letters* **2004**, *358* (1), 53–57. https://doi.org/10.1016/j.neulet.2003.12.058.

(29) Ye, X.; Xie, F.; Romanova, E. V.; Rubakhin, S. S.; Sweedler, J. V. Production of Nitric Oxide within the Aplysia Californica Nervous System. *ACS Chem. Neurosci.* **2010**, *1* (3), 182–193. https://doi.org/10.1021/cn900016z.

(30) Floyd, P. D.; Moroz, L. L.; Gillette, R.; Sweedler, J. V. Capillary Electrophoresis Analysis of Nitric Oxide Synthase Related Metabolites in Single Identified Neurons. *Anal. Chem.* **1998**, *70* (11), 2243–2247. https://doi.org/10.1021/ac9713013.

(31) Ye, X.; Kim, W.-S.; Rubakhin, S. S.; Sweedler, J. V. Ubiquitous Presence of Argininosuccinate at Millimolar Levels in the Central Nervous System of Aplysia Californica. *Journal of Neurochemistry* **2007**, *101* (3), 632–640. https://doi.org/10.1111/j.1471-4159.2006.04395.x.